Electronic and Mechanical Properties of Collective-mode Conductors

By

Lincoln C. Bourne

B.S. (Andrews University) 1981
M.A. (University of California) 1986

DISSERTATION

Submitted in partial satisfaction of the requirements for the degree of

DOCTOR OF PHILOSOPHY

in

PHYSICS

in the

GRADUATE DIVISION

OF THE

UNIVERSITY OF CALIFORNIA, BERKELEY

Approved: Alex Zettl 4/8/88
Chairman Date

N. Bartlett 04/05/88

Marvin L. Cohen 4/6/88

ELECTRONIC AND MECHANICAL PROPERTIES OF COLLECTIVE-MODE CONDUCTORS

Lincoln C. Bourne

Department of Physics

University of California at Berkeley

ABSTRACT

We have measured the elastic properties of the collective mode conductors $K_{0.3}MoO_3$, URu_2Si_2 and $La_{2-x}Sr_xCuO_4$. $K_{0.3}MoO_3$ has an anisotropic modulus anomaly at the Charge-Density-Wave (CDW) transition temperature that we compare to a theoretical model of CDW formation; we also find no change in elastic properties from CDW depinning. URu_2Si_2 has anomalies in both the modulus and the dissipation near 18 K due to the formation of a Charge- or Spin-Density Wave. $La_{2-x}Sr_xCuO_4$ shows a dramatic lattice softening that may be related to the superconducting mechanism, and a small modulus anomaly at T_c that has been used to predict the corresponding specific heat anomaly.

The elastic properties of the CDW conductors TaS_3 and $NbSe_3$ have been measured in the presence of ac, dc, and combined ac and dc electric fields. For both materials, the application of ac fields E_{ac} in the MHz range softens the crystal lattice, even for values of E_{ac} well below the the dc threshold field E_t for CDW depinning. For combined ac and dc fields, anomalies in the electronic response (such as Shapiro step structure) are reflected also in the modulus and the dissipation. On mode-locked steps,

the elastic properties tend to return to their pinned CDW values, despite the finite CDW drift velocity. We propose that these electroelastic experiments probe directly the internal degrees of freedom of the CDW, and our results are discussed in terms of applicable theoretical models.

We have substituted isotopes of oxygen, barium and copper in the high-T_c superconductor $YBa_2Cu_3O_7$ and isotopes of oxygen in $La_{1.85}Sr_{0.15}CuO_4$. The measured shifts in T_c's are much smaller than those expected from the conventional BCS phonon-induced electron pairing mechanism. We discuss the results of similar experiments and review the current theoretical approaches to the isotope effect.

Alex Zettl

TABLE OF CONTENTS

ACKNOWLEDGMENTS

My primary indebtedness is to my research advisor Alex Zettl. This work was made possible by the excellent research environment that he has fostered in his laboratory and by his substantial involvement in every phase of the work, from the initial conception of projects through to the editing of the final publications.

I have benefited a great deal from interaction with a number of the faculty and students of the Berkeley physics department: Troy Barbee, Gary Bernstein, Kee-Joo Chang, Marvin Cohen, Bill Creager, Mike Crommie, Ken Daly, Leo Falicov, Mats Gustafsson, Rick Hall, Storrs Hoen, Mike Hundley, Doug Lowder, Carl Mears, Richard Packard, Phil Parilla, Bob Phelps, Alan Portis, Mark Sherwin, Ruth Ellen Thompson, Ulrich Walter, Renata Wentzcovitch and Peter Yu. I am also grateful to Don Morris of the Lawrence Berkeley Laboratory and to Karl Amundson, Neil Bartlett, Bill Ham, Hano zur Loye and Angelica Stacy of the Berkeley chemistry department.

I am especially grateful to Al Daft, the supervisor of the student machine shop, who despite his disgust at my quick-and-dirty techniques was an invaluable source of solutions to experimental problems. This work would have been much more difficult without him.

Part of my support for this work was provided by a three year National Science Foundation graduate student fellowship. The research was funded in part by NSF grants DMR 84-00041 and 83-51678, and by contributions from the Alfred P. Sloan Foundation, IBM Corporation, General Motors Research Corporation, AT&T Bell Laboratories, and E.I. DuPont De Nemours and Co.

FOREWORD

This dissertation is an account of a mostly serendipitous pursuit of interesting phenomena in novel electronic materials. I began this work by developing a sensitive technique for measuring the elastic properties of small samples, motivated by the discovery of Brill and Roark that the depinning of a Charge-Density-Wave (CDW) affects the bulk elastic properties of the host crystal. We performed an extensive study of the effects of ac, dc, and combined ac and dc electric fields on the elastic properties of CDW systems, finding among other things the surprising result that the elastic properties of a mode-locked CDW are similar to those of a pinned CDW. The results of this study are presented in chapter two.

Having developed an excellent system for the study of the mechanical properties of materials, we investigated several other interesting systems, as reported in chapter one. The CDW system $K_{0.3}MoO_3$ showed a large, anisotropic modulus anomaly at the CDW critical temperature, and we were able to test a theoretical model of CDW formation with our measurements. The heavy-Fermion superconductor URu_2Si_2 has a transition at 18 K that is probably due to the formation of a Charge- or Spin-Density-Wave; we performed the first study of the elastic anomalies at the transition. The discovery in 1986 of high-temperature superconductivity in copper oxide systems attracted the attention of the entire solid state community; our measurements in the first high-T_c compound $La_{2-x}Sr_xCuO_4$ showed unusual lattice softening that may be related to the as yet unknown high-T_c superconducting mechanism.

One of the other high-T_c projects that I was involved with was the study of the isotope effect. Working at times in collaboration with other groups in the physics and chemistry departments and at the Lawrence Berkeley and the Lawrence Livermore laboratories, we substituted isotopes of oxygen, barium and copper in the 90 K

superconductor $YBa_2Cu_3O_7$ and isotopes of oxygen in the 40 K superconductor $La_{1.85}Sr_{0.15}CuO_4$. We found that the isotope shifts in the superconducting transition temperatures were too small to be accounted for with the conventional BCS calculations involving phonon-mediated electron pairing, indicating that high-T_c superconductivity might be due to a non-phonon mechanism. These measurements have attracted great interest and are being repeated and discussed by many other groups; chapter three contains a description of our work and a review of the current status of the field.

This dissertation deals primarily with the results of our experiments; the first two chapters consist essentially of updated versions of our published papers. An adequate introduction to each of the systems studied in this work would be a futile task in light of the enormous amount of published material on each of these systems. I refer the reader instead to recent reviews of CDWs[1-3] and heavy-Fermions[4,5]. Thousands of papers have already been published on the high-T_c compounds and no general review exists; one of the first substantial collection of papers is that of the 1987 Berkeley conference on novel superconductivity[6].

1. G. Gruner and A. Zettl, Phys. Rep. 119, 117 (1985)

2. "Electronic Properties of Inorganic Quasi-One-Dimensional Materials", ed. P. Monceau (Reidel, Dorcecht, 1985) (2 vols.).

3. "Charge Density Waves in Solids", eds. Gy. Hutiray and J. Solyom (Springer, New York, 1985).

4. G.R. Stewart, Rev. Mod. Phys. 56, 755 (1984).

5. Z. Fisk, D.W. Hess, C.J. Pethick, D. Pines, J.L. Smith, J.D. Thompson and J.O. Willis, Science 239, 33 (1988).

6. "Novel Superconductivity", eds. S.A. Wolf and V.Z. Kresin (Plenum Press, New York, 1987).

CHAPTER 1

ELASTIC ANOMALIES AT ELECTRONICALLY DRIVEN PHASE TRANSITIONS

The bulk elastic properties of a material are generally very sensitive to changes in other properties of the material, particularly at phase transitions. We have developed a version of the vibrating reed technique, as described in the appendix, that allows us to study the Young's modulus and acoustic dissipation of small samples as a function of temperature, magnetic field and ac and dc electric fields. We have used this technique to study of variety of unusual electronic systems: Charge-Density-Wave systems, a heavy-Fermion material and one of the new high-temperature superconductors. This chapter is divided into three self-contained sections that each focus on a material representing one of the above systems, focusing particularly on phase transformations in these systems. Chapter 2 describes a series of studies of the effects of electrical excitations of Charge-Density-Wave materials on the bulk elastic properties of the materials.

Section 1: $K_{0.3}MoO_3$.

Introduction

Of the few low dimensional materials which have been observed to display sliding CDW transport, the blue bronzes $A_{0.3}MoO_3$ (A=K, Rb) form a particularly interesting class[1]. Unlike the transition metal trichalcogenides $NbSe_3$ and TaS_3, for example, $K_{0.3}MoO_3$ is a very cohesive three dimensional crystal despite its quasi one dimensional electronic structure. Below the Peierls transition temperature T_p=180K, $K_{0.3}MoO_3$ displays a host of unusual electronic properties, including nonlinear dc conductivity[2] and enormous low-frequency polarization effects[3,4]. These properties are attributed to excitations of the collective CDW mode.

Studies of layered 2-D and quasi 1-D linear chain CDW systems have demonstrated that CDW formation is often associated with anomalies in the elastic properties of the host crystal[5-7]. More recent experiments have revealed a sensitivity of the elastic properties to the dynamic state of the CDW condensate, for example dc depinning, ac excitation, or electronic mode locking induced by combined ac and dc electric fields[8-10]; some of this work is presented in chapter 2.

This section is concerned with measurements of the elastic properties of $K_{0.3}MoO_3$. The Young's modulus Y has been measured both parallel to the highly conducting b axis (denoted $Y_{||}$) and perpendicular to this axis, in the (102) direction (denoted $Y_{\perp}$). At room temperature, the elastic constants are anisotropic, and there are well defined, non-hysteretic anomalies in Y at T_p=180K. Somewhat surprisingly, no changes are observed in $Y_{||}$ or δ upon CDW depinning, making this the first system in which these effects are not known to occur. Much of the work in this section has been reported in the literature[11].

Experiments and Results

Single crystals of $K_{0.3}MoO_3$ were grown by electrolytic reduction of a K_2MoO_4 - MoO_3 melt[12]. The crystals were cleaved into thin plates of typical dimensions 1mm x 0.3mm x .05mm, with the long dimension corresponding to the direction in which the elastic properties were measured. Indium pads were evaporated onto the ends of the sample to ensure good electrical contacts. The sample was clamped at one end with silver paint, and a roughly spherical blob of silver paint was attached to the free end of the sample, giving resonant frequencies in the KHZ range. A fine gold wire was usually attached to the weighted end of the sample to allow for electrical measurements. When the sample was thermally cycled, it would occasionally break partially free from the silver paint at around 60K, causing irreversible drops in the resonance frequency. These effects could be prevented by placing stycast epoxy around the fixed end of the

sample.

At room temperature, The Young's modulus for $K_{0.3}MoO_3$ was determined from eq. (A-3) to be $Y_{||} = (0.8 - 2.0)x10^{12}$ dyne cm^{-2} and $Y_{||} = (0.4 - 0.8)x10^{12}$ dyne cm^{-2}. The uncertainties reflect difficulties in determining the effective sample geometry. On the average, $Y_{||}/Y_{\perp} \equiv 2$ at room temperature.

Figure 1 shows $Y_{||}$ and $Y_{\perp}$ for $K_{0.3}MoO_3$ as functions of temperature. For both $Y_{||}$ and $Y_{\perp}$, well defined anomalies are apparent at T=180k, corresponding to the Peierls transition temperature as determined by resistivity measurements on the same crystal. Measurements on several other $K_{0.3}MoO_3$ crystals yielded identical results; one crystal from a high impurity concentration growth batch, with a transition temperature of 174K, showed similar modulus anomalies at T=174K. After accounting for the strictly thermal changes in Y, the relative changes in elasticity due to the CDW transition are $\Delta Y_{||}/Y_{||} = 1.6x10^{-3}$ and $\Delta Y_{\perp}/Y_{\perp} = 1.7x10^{-2}$. Hence the anomaly in $Y_{||}$ is nearly an order of magnitude less than the corresponding anomaly in $Y_{\perp}$. The strong anomaly in $Y_{\perp}$ is very similar that previously observed in the CDW material TaS_3 [7,8]. The weaker anomaly in $Y_{||}$ is nearly identical in form, but larger in magnitude, than the corresponding anomaly in $(TaSe_4)_2I$ at T_p[13]. No hysteresis in temperature was observed for these anomalies, and no other anomalies were observed between room temperature and 77K. The detailed behavior of $Y_{||}$ and $Y_{\perp}$ near T_p is shown in Fig. 2.

In the related CDW conductors $NbSe_3$ (both upper and lower CDW states), TaS_3, and $(TaSe_4)_2I$, applied dc electric fields E exceeding the threshold field E_T for the onset of nonlinear conduction have dramatic effects on the elastic properties of the crystal: for $E>E_T$, Y smoothly decreases and eventually saturates, and δ increases and then quickly saturates[7-10]. Fig. 3 shows a graph of the differential resistance dV/dI and Y and δ in $K_{0.3}MoO_3$ as functions of dc bias; no change in the elastic properties is observed at the CDW depinning threshold. The CDW was depinned at several temperatures in the range 50-85K for two different crystals, again with no observed

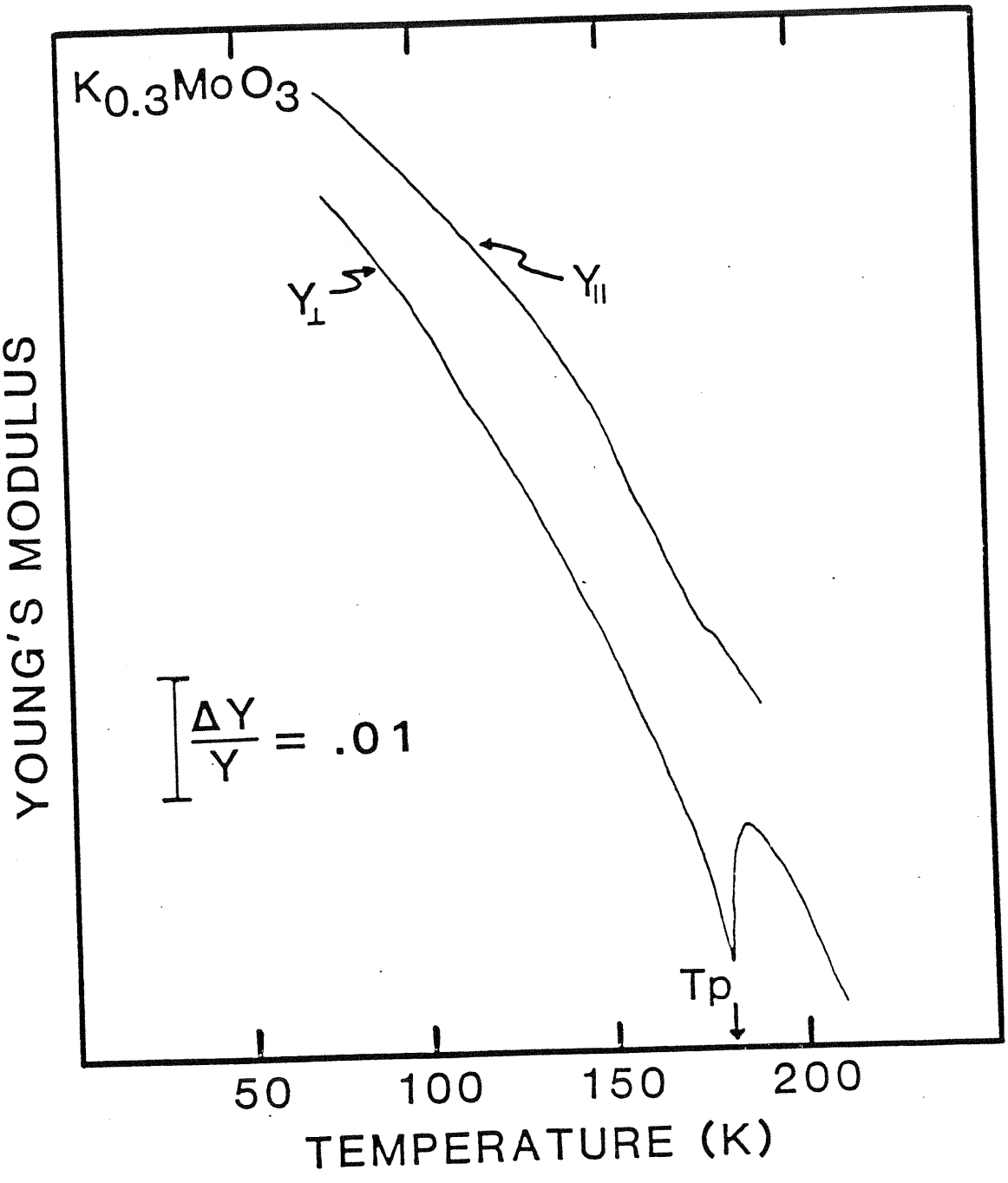

Fig.1 Young's modulus Y measured both parallel and perpendicular to the b axis in $K_{0.3}MoO_3$. The curves have been vertically displaced. The arrow identifies the Peierls transition temperature.

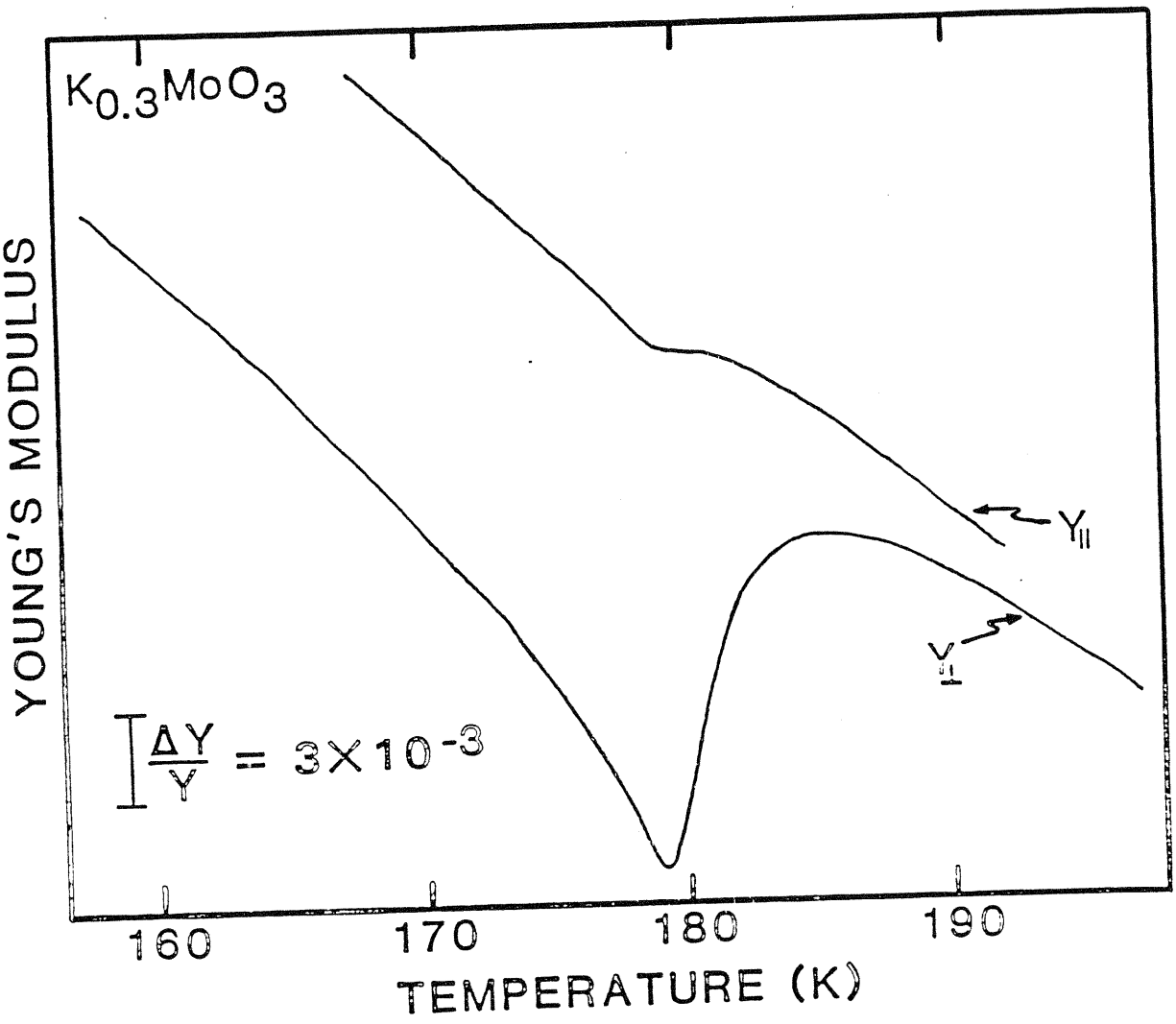

Fig. 2 Detail figure of Young's Modulus near the Peierls transition.

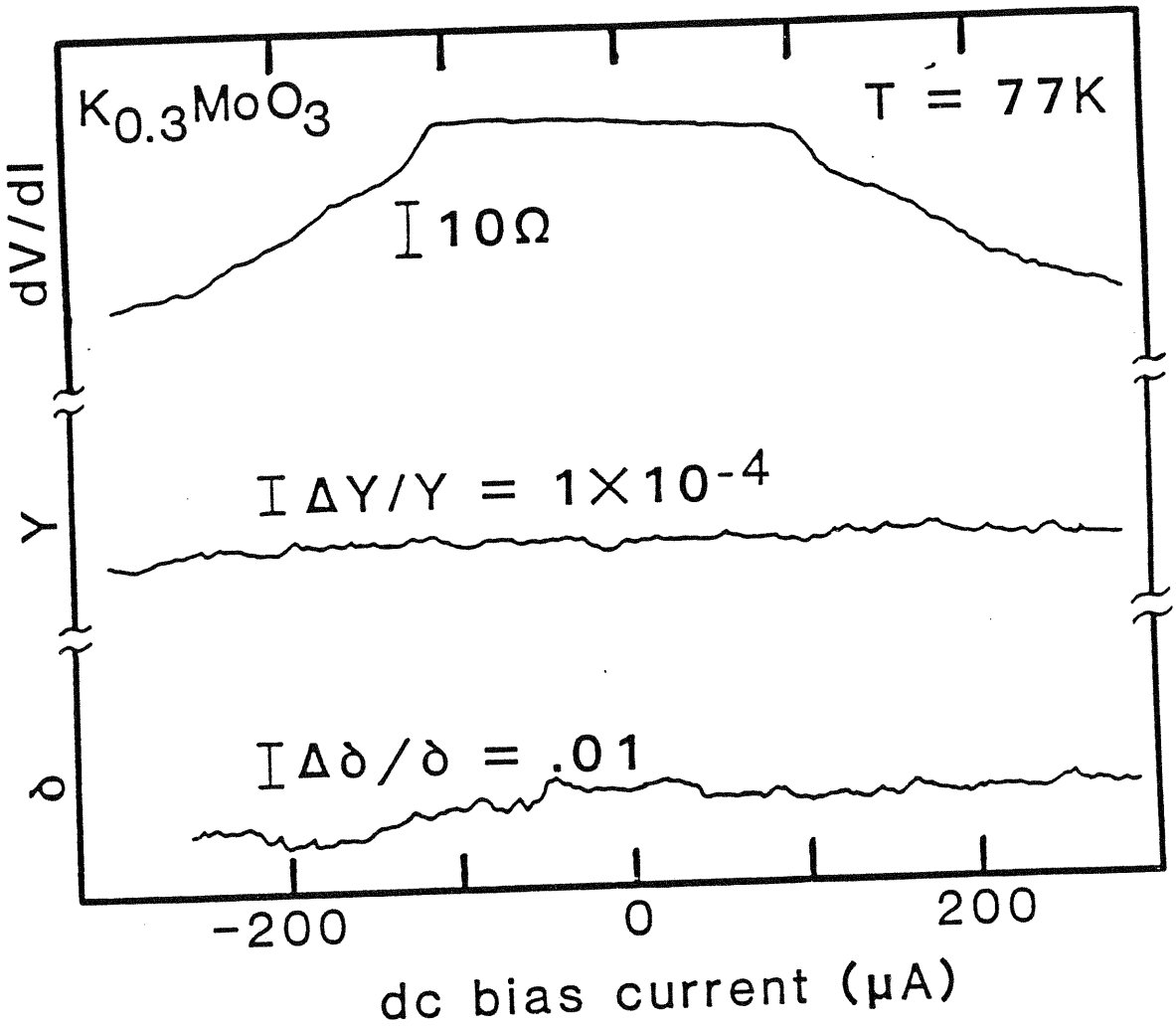

Fig. 3 Differential electrical resistance dV/dI, Young's Modulus $Y_{||}$ and internal friction δ in $K_{0.3}MoO_3$, as functions of dc bias current. CDW depinning has no observable effect on $Y_{||}$ or on δ.

effects in the elastic properties. Careful measurements involving signal averaging at 77K and 57K placed limits on the fractional change of the elastic properties of 5×10^{-5} for $Y_{\|}$ and 2×10^{-3} for δ. We did not measure $Y_{\perp}$ at the depinning threshold because of the experimental difficulties associated with the simultaneous measurement of elastic and electrical properties in perpendicular directions in the same crystal; however, these difficulties should not be intractable and it would be worthwhile to attempt this experiment, as will be discussed below.

Discussion

The non-hysteretic anomaly observed in Y at T_p is consistent with a second order phase transition in $K_{0.3}MoO_3$. The width of the transition as shown in Fig. 2 is in agreement with X-ray and neutron diffraction studies which show superlattice structure above T_p[1,14]. There has been some speculation as to the existence of an incommensurate-commensurate (IC-C) phase transition in $K_{0.3}MoO_3$ near 100K[15]. In the layered CDW compound 2H-$TaSe_2$, the IC-C transition is associated with a giant hysteretic elasticity anomaly, presumably due to the formation and movement of boundaries between IC and C domains[5]. We find no similar behavior in $K_{0.3}MoO_3$, which would suggest the absence of an IC-C transition, in agreement with structural neutron studies[14].

The anomaly in Y at a second order phase transition can be related to the stress dependence of T_p and to the thermal expansivity using thermodynamic considerations:[16]

$$\frac{\partial T_p}{\partial \sigma_i} = \left[\frac{-(\Delta Y/Y)\,T_p}{Y \Delta C_p} \right]^{\frac{1}{2}} \qquad 1\text{-}1$$

$$\Delta\alpha_i = \frac{(\Delta Y/Y)}{Y(\partial T_p/\partial\sigma_i)} \qquad 1\text{-}2$$

where σ_i and α_i are respectively the i^{th} components of the stress and the thermal expansivity, and C_p is the specific heat. An entropy change of 150 mJ/mole K has been observed[1] at the CDW transition in $K_{0.3}MoO_3$, corresponding to a specific heat anomaly of $\Delta C_p = 4.12\times10^4$ dyne/cm^{2}K. The observed values of the elastic anomalies at T_p therefore give calculated stress dependences of $dT_p/d\sigma_\perp = 1.05\times10^{-8}$ K/dyne cm^{-2} and $dT_p/d\sigma_{||} = 2.3\times10^{-9}$ K/dyne cm^{-2}, with expansivity coefficients of $\alpha_\perp = -2.6\times10^{-6}K^{-1}$ and $\alpha_{||} = -5.4\times10^{-7}K^{-1}$. Assuming a small interlayer interaction between planes (201) in $K_{0.3}MoO_3$, the estimated pressure dependence of the the transition temperature is $dT_p/dP \cong 13$K/Kbar. This predicted pressure dependence of T_p is somewhat larger than that observed in $NbSe_3$ (4K/Kbar) or in TaS_3 (1.3K/Kbar)[17,18].

It is interesting to compare the anisotropy of the elastic constants at T_p with the directions of atomic displacements involved in CDW formation. The structure of $K_{0.3}MoO_3$ is monoclinic, with infinite planes of corner-sharing MoO_6 octahedra separated by K ions[19]. There are three inequivalent Mo sites, which undergo differing displacements during CDW formation, with the greatest displacements occurring in the (102) direction[20]. Since the bulk elastic anomaly at T_p is also primarily in the (102) direction, it is reasonable to expect that the dynamical effects of the CDW would couple more strongly to the elastic properties in this direction than along the b axis. The observation of coupled CDW - elastic dynamical effects would allow for an additional probe of the unique electronic properties of the blue bronzes.

The Peierls distortion in $K_{0.3}MoO_3$ is associated with a complete destruction of the Fermi surface, leading to a metal-insulator transition. The loss of normal electrons below T_p should decrease electron screening, thereby stiffening phonon

modes and increasing the sound velocity in the crystal. This effect is apparently observed at the density wave transitions of TTF-TCNQ [6], 2H-$TaSe_2$ [5], and $(TMTSF)_2PF_6$ [21]. On the other hand, the softening of the phonon modes that lead to the atomic displacements of the CDW could possibly result in a softening of the lattice about T_p, as observed in TaS_3 [7], $(TaSe_4)_2I$ [12], 2H-$NbSe_2$ [5], and the upper CDW transition of $NbSe_3$ [7]. A combination of reduced electronic screening and phonon softening may account for the behavior of 2H-$TaSe_2$, in which the Young's modulus decreases slightly just above T_p and then strongly increases below T_p[5].

The data of Figs. 1 and 2 shows that despite the complete loss of the Fermi surface in $K_{0.3}MoO_3$, lattice softening dominates the behavior of Y near T_p in this system. In a recent theoretical investigation of elastic anomalies in CDW systems, Nakane[22] has discussed the dip in Young's modulus at the Peierls transition in terms of coupling between the electrons and the soft phonon. The theory predicts a scaling relation for the elasticity behavior above and below the transition temperature,

$$\frac{\Delta Y}{Y} = C\tau^{-\frac{1}{2}}, \quad (T>T_p) \qquad 1\text{-}3$$

$$\frac{\Delta Y}{Y} = 2C(2\tau)^{-\frac{1}{2}}, \quad (T<T_p) \qquad 1\text{-}4$$

valid for small τ, where $\tau = |(T-T_p)/T_p|$ and C is proportional to T^2. At larger values of τ, where T moves away from T_p, there is a dimensionality crossover of the critical fluctuations from three dimensions to one. In this crossover temperature regime, the scaling relations eqns. 1-3 and 1-4 still hold, but the critical exponent becomes 3/2 instead of 1/2.

The size of the elasticity anomaly in $K_{0.3}MoO_3$ allows for a careful comparison of theory and experiment. Figure 4 shows the large anomaly in $Y_\perp$ of Fig. 2 replotted as a function of log(τ), after the subtraction from $Y_\perp$ of a term that is linear in temperature and represents conventional thermal expansion. The experimental data show remarkable similarities to Nakane's theory: there is an apparent dimensionality crossover at a temperature of 2K from Tp, with a change in the critical exponent from roughly 1/2 to roughly 3/2 as T_p is approached from either direction. The strength of the modulus anomaly differs above and below T_p by a factor of approximately 4, in good agreement with the numerical factor predicted by eqns. 1-3 and 1-4. There are however striking differences between experiment and theory: the critical exponent should change from 3/2 to 1/2 as T approaches T_P, and the modulus anomaly should be stronger below T_p, not above. (If the theoretical prediction is plotted and then rotated by an angle π, there is an excellent match between theory and experiment!) In spite of these differences, this theoretical approach is clearly very promising.

In summary, anisotropic anomalies have been observed in the elastic modulus of $K_{0.3}MoO_3$ at the CDW transition temperature, with no evidence for an additional lock-in transition at 100K. The elasticity anomalies at T_p have been used to predict the stress and expansivity coefficients at T_p, and a detailed study of the behavior of Y near T_p has shown remarkable similarities between experiment and theoretical predictions of elasticity effects at a Peierls transition.

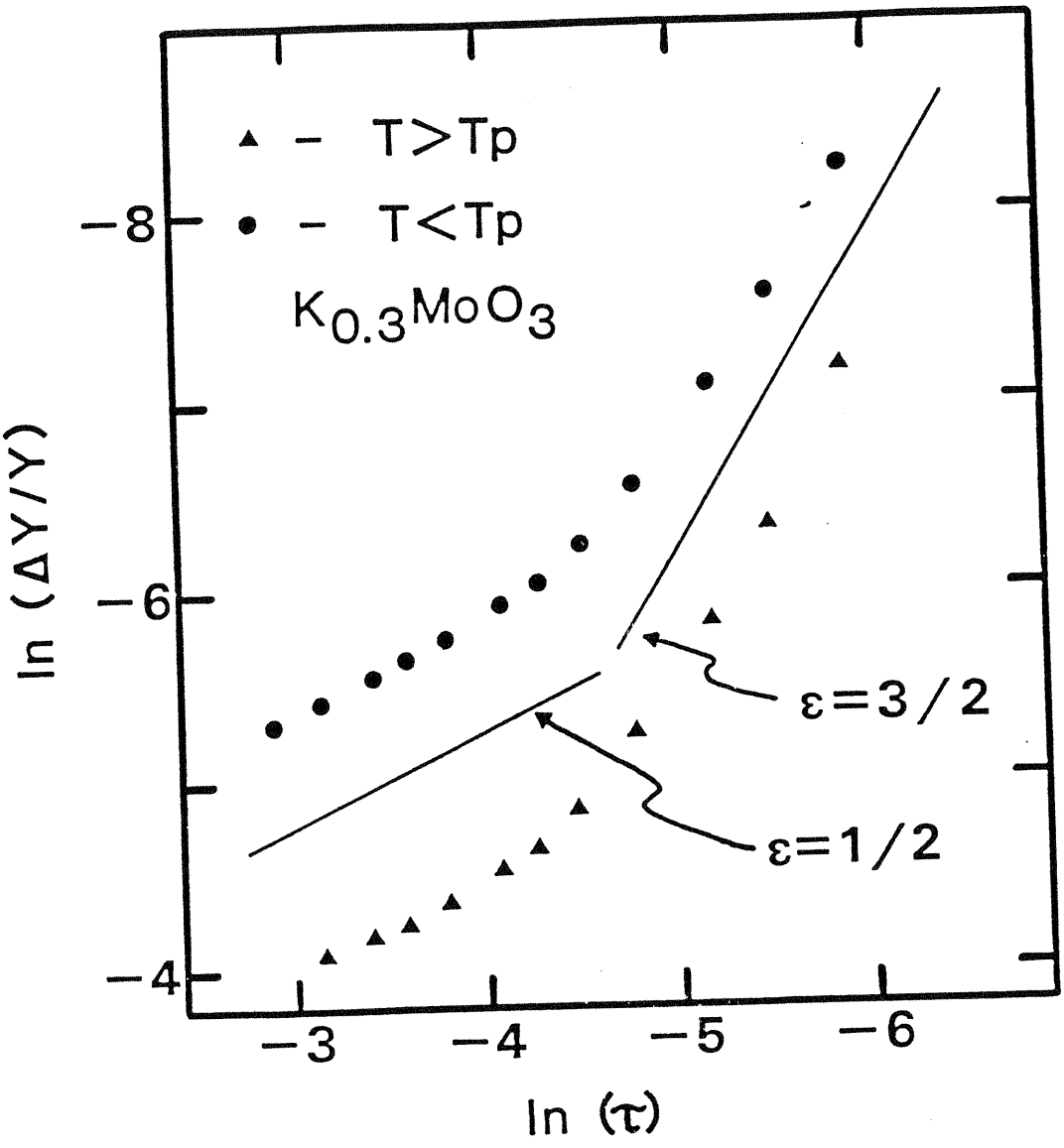

Fig. 4 Scaling behavior of $Y_{||}$ near the CDW transition temperature. The data points at the far right are 0.5K from T_p and at the far left are 10K from T_p. The lines show critical exponents of 3/2 and 1/2.

CHAPTER 1 SECTION 1 REFERENCES

1. C. Schlenker and J. Dumas, in "Crystal Chemistry and Properties of Materials with Quasi One-Dimensional Structures", ed. J. Rouxel (D. Reidel Pub. Comp.) p. 135 (1986).

2. W. Fogle and J. H. Perlstein, Phys. Rev. B6, 1402 (1972); J. Dumas, C. Schlenker, J. Marcus and R. Buder, Phys. Rev. Lett. 50, 757 (1983).

3. R. J. Cava, R. M. Fleming, P. Littlewood, E. A. Rietman, L. F. Schneemeyer and R. F. Dunn, Phys. Rev. B30, 3228 (1984).

4. R. P. Hall, M. S. Sherwin and A. Zettl, Solid State Commun. 54, 683 (1985).

5. M. Barmatz, L. R. Testardi, and F. J. DiSalvo, Phys. Rev. B12, 4367 (1975); P. Prelovsek and T. M. Rice, Phys. Rev. Lett. 51, 903 (1983).

6. T. Tiedje, R. R. Haering, M. H. Jericho, W. A. Roger and A. Simpson, Solid State Commun. 23, 713 (1977).

7. J. W. Brill and N. P. Ong, Solid State Commun. 25, 1075 (1978); J. W. Brill, Mol. Cryst. Liq. Cryst. 81, 107 (1982); J. W. Brill, Solid State Commun. 41, 925 (1982).

8. J. W. Brill and W. Roark, Phys. Rev. Lett. 53, 846 (1984); J. W. Brill, W. Roark and G. Minton, Phys. Rev. B33, 6831 (1986).

9. G. Mozurkewich, P. M. Chaikin, W. G. Clark and G. Gruner, Solid State Commun. 56, 421 (1985).

10. L. C. Bourne, M. S. Sherwin and A. Zettl, Phys. Rev. Lett. 56, 1952 (1986); L. C. Bourne and A. Zettl, Phys. Rev. B36, 2626 (1987).

11. L. C. Bourne and A. Zettl, Solid State Commun. 60, 789 (1986).

12. A. Wold, W. Kunnmann, R. J. Arnott and A. Ferretti, Inorg. Chem. 3, 545 (1964).

13. L. C. Bourne and A. Zettl (unpublished).

14. J. Pouget, S. Kagoshima, C. Schlenker and J. Marcus, J. Phys. Lett. 44, L113 (1983); M. Sato, H. Fujishita and S. Hoshino, J. Phys. C16, L877 (1983); R. M. Fleming, L. F. Schneemeyer and D. E. Moncton, Phys. Rev. B31, 899 (1985); C. Escribe-Filippini, J. P. Pouget, R. Currat, B. Hennion and J. Marcus, in "Charge Density Waves in Solids", ed. Gy. Hutiray and J. Solyom (Springer, 1985).

15. See, for example, R. M. Flemming et. al. in "Charge Density Waves in Solids", ed. Gy. Hutiray and J. Solyom (Springer, 1985).

16. L.R. Testardi, Phys. Rev. B12, 3849 (1975).

17. J. Chaussy, P. Haen, J. C. Lasjaunias, P. Monceau, G. Waysant, A. Waintal, A. Meerschaut, P. Molinie and J. Rouxel, Solid State Commun. 20, 759 (1976).

18. M. Ido, K. Tsutsumi, T. Sambongi and N. Mori, Solid State Commun. 29, 399 (1979).

19. J. Graham and A. D. Wadsley, Acta Cryst. 20, 93 (1966).

20. M. Sato, in Ref. 15.

21. P. M. Chaikin, T. Tiedje and A. N. Bloch, Solid State Commun. 41, 739 (1982).

22. Y. Nakane, J. Phys. Soc. Japan 55, 2235 (1986).

SECTION 2: URu_2Si_2

URu_2Si_2 is a unique member of the rapidly growing class of heavy Fermion compounds with unusual electronic properties, in that it shows evidence for multiple and coexisting Fermi-surface instabilities. Previous work on URu_2Si_2 has demonstrated that in addition to exhibiting a large effective electron mass ($m^* \approx 25 m_e$) and a superconducting ground state below T_c=1.5 K, this material displays anomalous behavior in electrical resistivity, magnetic susceptibility, and specific heat near a "transition" temperature T_p=17.5 K.[2-6] It has been suggested that the anomalous behavior near T_p results from antiferromagnetic ordering,[4,6] or from the formation of a conduction electron Charge Density Wave (CDW) or Spin Density Wave (SDW).[2] Recent neutron scattering experiments on a single crystal of URu_2Si_2 indicate that antiferromagnetic ordering occurs below T_p with an unusually small ordered moment of $\approx 0.03 \mu_B$, and a modulation along the (100) direction.[7] This antiferromagnetically ordered state appears to coexist with the superconducting state below T_c.

The low-field dc electrical resistivity of URu_2Si_2 shows a small peak just below T_p, with a functional form very similar to the resistance anomalies observed below the CDW transition in $ZrTe_3$[8] and below both CDW transitions in $NbSe_3$.[9] The strongest evidence for density wave formation (either CDW or SDW) formation in URu_2Si_2 comes, however, from specific heat measurements which show a BCS-like anomaly near 17.5K, consistent with a 40% destruction in Fermi surface area.[2]

The results of elasticity measurements in URu_2Si_2 are reported in this section. There is an anomaly in the Young's modulus near 17.5 K, with a corresponding anomaly in the internal friction at a slightly lower temperature; these results support the interpretation of the formation of a Charge- or Spin Density Wave below 17.5 K. A quantitative measurement of the modulus anomaly is in good agreement with the value expected from specific heat and pressure data. These results have been reported in the

literature.[1]

The elasticity measurements were performed on polycrystalline samples of URu_2Si_2 prepared by the usual arc melting method. The Young's modulus Y and internal friction δ were measured using the vibrating reed technique as described in detail in the appendix. The elasticity properties were studied in the temperature range 300 K to 4.2 K. At room temperature, the absolute value of the Young's modulus is estimated to be $Y \approx 2.5 \times 10^{11}$ dyne/cm^2, with a large uncertainty due to uncertainties in the geometrical factors associated with the above equation. Between room temperature and 4.2 K, Y increased by a total of 5%. A broad internal friction peak, possibly due to grain boundary motion, was observed at around 216 K.

Fig. 1 shows the detailed behavior of Y and δ near T_p. As is apparent from the figure, both Y and δ show well-defined anomalies near T=18K. There is some uncertainty in the temperature scale; the temperature indicated represents that of the sample holder, not the sample itself. The estimated temperature differential between the sample and the sample holder may be as large as one degree. Nevertheless, it is clear that near T_p there is a dip in Y of magnitude $\Delta Y/Y = -2.2 \times 10^{-4}$, determined by comparing Y at the minimum of the the dip to the value of Y extrapolated from the high temperature behavior. Note that the maximum in δ does not correspond exactly to the minimum in Y, but is offset to a lower temperature by approximately 0.25 K. No thermal hysteresis was observed in the temperature dependences of Y and δ.

Assuming that the hydrostatic pressure dependence of T_p is due primarily to stress along just one of the axes, the published values of $\partial T_p/\partial P$ of 118 mK/kbar[5] and 125 mK/kbar[2] yield values of ΔC_p of respectively 5.4 J/mole K and 4.8 J/mole K, in excellent agreement with the measured discontinuity in C_p of 5.8 J/mole K.[2] The estimated value for the thermal expansivity at T_p is $\Delta\alpha = -7.7 \times 10^{-6}$ K^{-1}. It should of course be recognized that the polycrystalline nature of the samples implies that our measurements probably represent an average over all crystallographic directions.

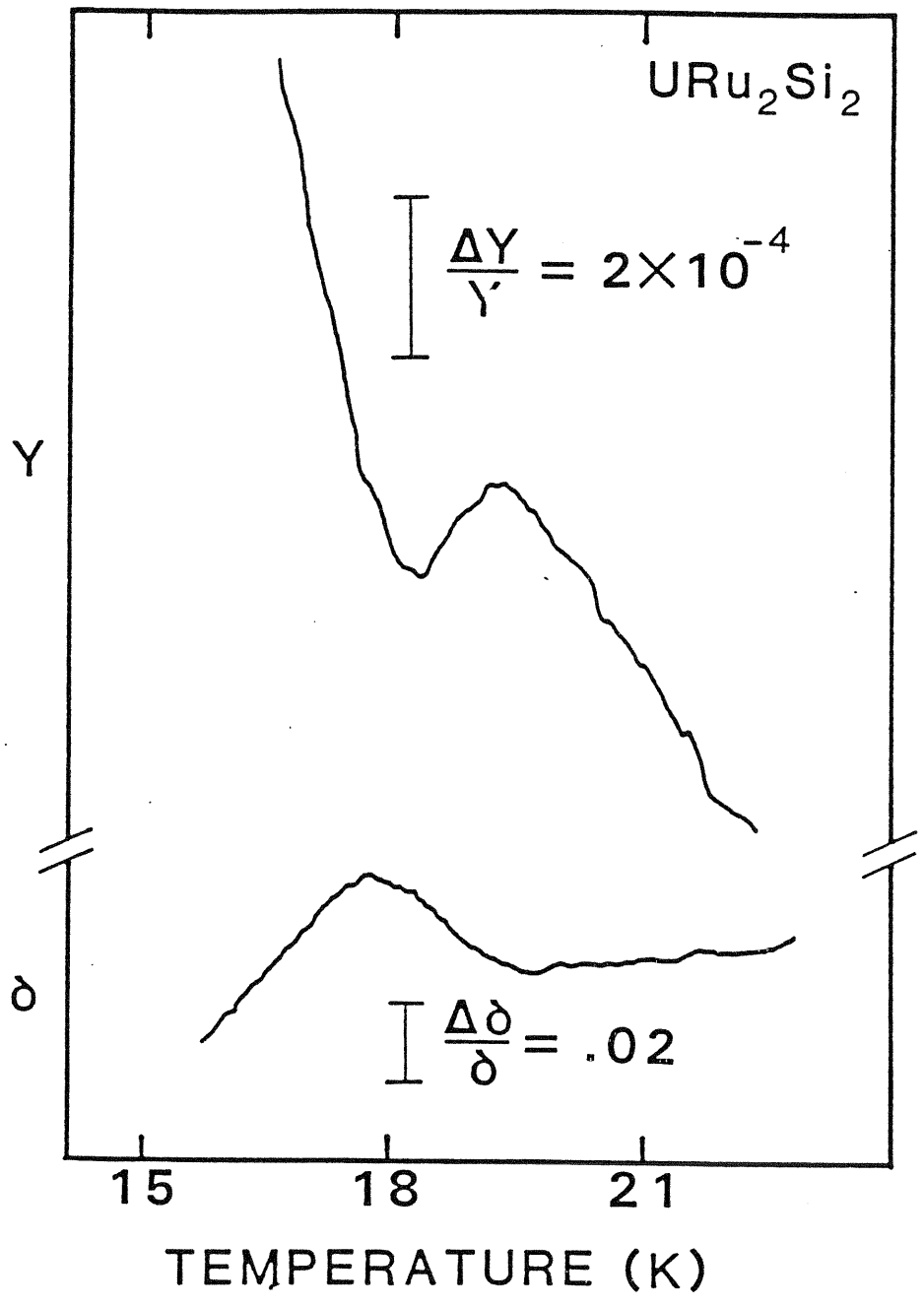

Fig. 1. Young's modulus Y and internal friction δ near T_p=17.5 K in URu_2Si_2. The temperature scale refers to the sample holder temperature (see text).

As observed in Fig. 1, the maximum in the internal friction δ in URu_2Si_2 occurs at a slightly lower temperature than the minimum in Y. This behavior has been previously observed in materials undergoing a phase transition with an associated order parameter.[10] In general, fluctuations in the order parameter lead to an internal friction peak that is symmetric about T_p, but additional processes that occur in the ordered state below T_p tend to shift the peak of the total internal friction to lower temperatures. The peak position of δ in URu_2Si_2 provides evidence for these relaxations in an ordered state below T_p.

The observed behaviors of Y and δ near T_p in URu_2Si_2 are very similar to elastic anomalies associated with the CDW transitions in TaS_3 and $NbSe_3$,[11] $K_{0.3}MoO_3$,[12] and with the SDW transition in Cr.[13] These measurements provide additional evidence for a collective mode CDW or SDW ground state in URu_2Si_2.

CHAPTER 1 SECTION 2 REFERENCES

1. M.F. Hundley, L.C. Bourne, A. Zettl, C. Rossel and M.B. Maple, Solid State Commun. 62, 603 (1987).

2. M.B. Maple, J.W. Chen, Y. Dalichaouch, T. Kohara, C. Rossel, M.S. Torikachvili, M.W. McElfresh and J.D. Thompson, Phys. Rev. Lett. 56,185 (1986).

3. T.T.M. Palstra, A.A. Menovsky, J. van den Berg, A.J. Dirkmaat, P.H. Kes, G.J. Nieuwenhuys and J.A. Mydosh, Phys. Rev. Lett. 55, 2727 (1985).

4. W. Schlabitz, J.Baumann, B. Pollit, U. Rauchschwalbe, H.M. Mayer, U. Ahlheim and C.D. Bredl, Z. Phys. B62, 171 (1986).

5. F.R. Boer, J.J.M. Franse, E. Louis, A.A. Menovsky, J.A. Mydosh, T.T.M. Palstra, U. Rauchschwalbe, W. Schlabitz, F. Steglich and A. de Visser, Physica 138B, 1 (1986).

6. T.T.M. Palstra, A.A. Menovsky and J.A. Mydosh, Phys. Rev. B33, 6527 (1986).

7. C. Broholm, J.K. Kjems, W.J.L. Buyers, P. Matthews, T.T.M. Palstra, A.A. Menovsky and J. Mydosh, Phys. Rev. Lett. 58, 1467 (1987).

8. S. Takahashi, T. Sambongi, J.W. Brill and W. Roark, Solid State Commun. 49, 1031 (1984).

9. P. Monceau, N.P. Ong, A.M. Portis, A. Meerschaut and J. Rouxel, Phys. Rev. Lett. 37, 602 (1976).

10. M. Barmatz, L.R. Testardi and F.J. DiSalvo, Phys. Rev. B12, 4367 (1975).

11. J.W. Brill, Mol. Cryst. Liq. Cryst. 81, 107 (1982).

12. L.C. Bourne and A. Zettl, Solid State Commun. 60, 789 (1986).

13. S.B. Palmer and E.W. Lee, Phil. Mag. 24, 311 (1971); K.W. Katahara, M. Nimalendran, M.H. Manghanani and E.S. Fisher, J. Phys. F: Metal Phys. 9, 2167 (1979)

SECTION 3: $La_{2-X}Sr_XCuO_4$

This section presents a series of elasticity measurements that were performed on $La_{2-X}Sr_XCuO_4$ shortly after its discovery came to the attention of the scientific community[1]; these measurements have been reported in the literature.[2] Anomalous behavior in the Young's modulus Y is observed, behavior that may be related to the presence of relatively high superconducting transition temperatures (T_c's) in these compounds. Careful measurements of the modulus anomaly at T_c in $La_{1.85}Sr_{0.15}CuO_4$, and its dependence on magnetic field, allow for predictions of the specific heat anomaly at T_c and of the dependence of T_c on magnetic field.

High-T_c superconductivity is usually explained in terms of strong electron-phonon interactions[3] or a high density of states at the Fermi energy. The strong electron-phonon coupling is often associated with soft phonon modes which can also induce structural phase transitions. For example, in most A-15 compounds, cubic-to-tetragonal phase transitions[4] are observed, and the soft mode causing the structural changes is considered to be associated with the high-T_c superconducting mechanism. Evidence is presented here for the occurrence of similar behavior in the $La_{2-X}Sr_XCuO_4$ system.

Samples of $La_{2-X}Sr_XCuO_4$ were made by pressing pellets from mixtures of La_2O_3, CuO and $SrCO_3$ prepared either by mechanical mixing or by coprecipitation, and then sintering the pellets in air at 1100° C for 44 h. These polycrystalline samples were characterized by magnetic susceptibility measurements employing a superconducting quantum interference device (SQUID) magnetometer, and with four-probe electrical measurements. The X=0.15 and 0.30 samples showed diamagnetic effects respectively of 100% and 1.5%. Samples with X=0.15 had superconducting transitions with T_c=35-37 K, while those with X=0.3 had transitions near T_c=20 K. These measurements are in agreement with previous studies.[5]

Elasticity measurements were performed using the resonant vibration technique as described in the appendix. Polycrystalline samples with approximate dimensions of 5x0.5x0.5 mm^3 were cut from the sintered pellets with a diamond saw and rigidly clamped at one end, and flexural vibrations were induced in the sample and detected with a capacitive technique. On occasion, a weight (silver paint blob) was attached to the free end of the sample to produce a system with a resonant vibration in the experimentally accessible frequency range. All measurements were performed in the range of 2-7 KHz. Changes in Young's modulus Y are determined directly from changes in vibration frequency, and the internal friction δ is inversely proportional to the vibration amplitude, as described elsewhere in this thesis.

Elasticity data for a $La_{2-X}Sr_XCuO_4$ sample with X=0.15 are shown in Fig. 1. As the sample is cooled from 300 K, the normal increase of Young's modulus from thermal contraction is observed. At about 200 K, Y shows an anomalous turnover and decreases with decreasing temperature until about 100 K, where Y saturates abruptly. The total change in Y from 200 to 100 K is 14%. At lower temperatures, Y begins to rise again, and the internal friction (inverse of the amplitude) shows a strong dip near 25 K. For a given sample, the saturation point in Y (near 100 K in Fig. 1) was found to be very reproducible from run to run, but the location of the peak in Y (near 200 K in Fig. 1) was found to vary by as much as 20 - 30 K with thermal cycling. The inset to Fig. 1 shows the results of a careful measurement of Y and δ near the superconducting transition temperature T_c=35 K (as determined from susceptibility measurements). At T_c there exist well-defined anomalies in both Y and δ; these features will be discussed shortly.

The anomalous high-temperature lattice softening near 200 K in $La_{2-X}Sr_XCuO_4$ was investigated both for different values of X and for fixed X, but with different high-temperature sample annealing conditions. Additional annealing of the sample at 900° C resulted in an increase in T_c to 37 K; the corresponding elastic properties showed

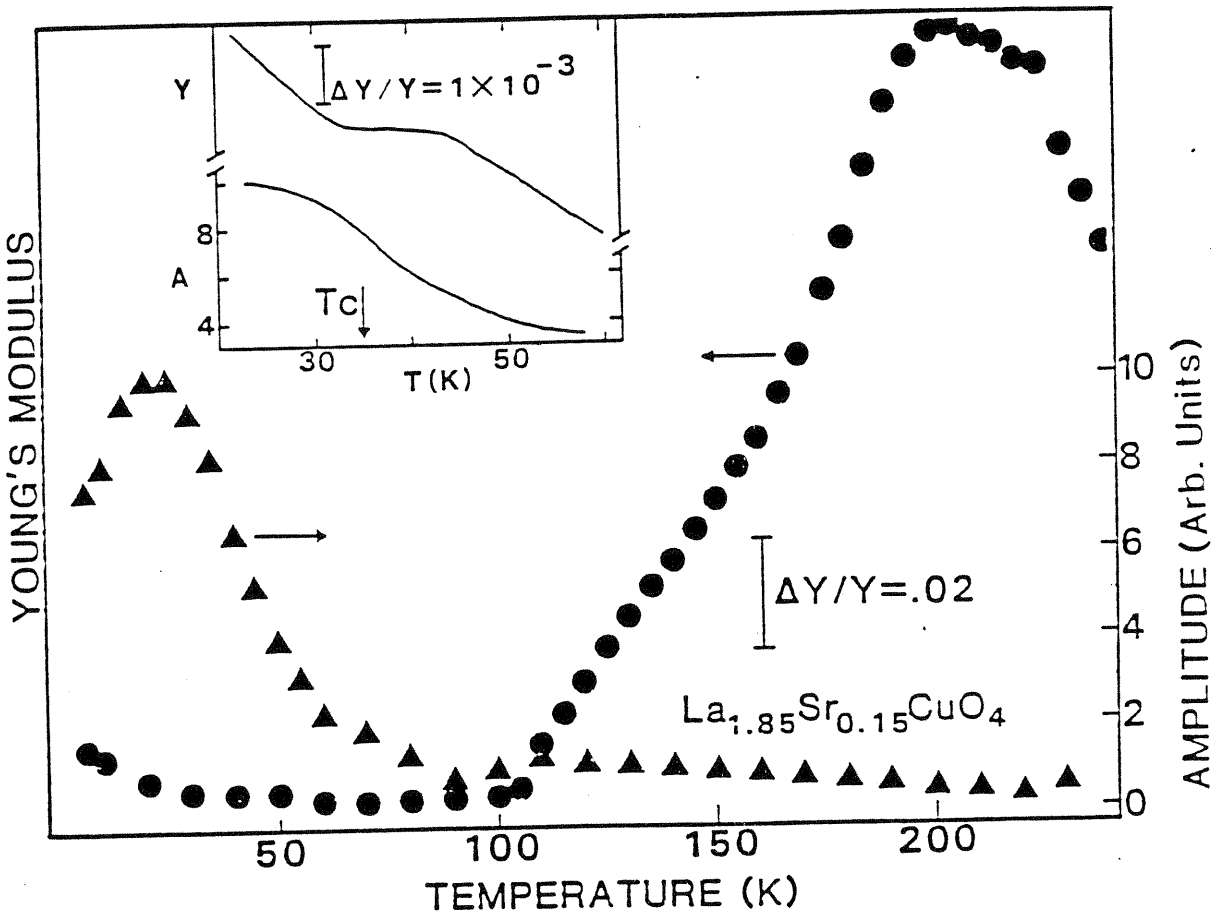

Fig. 1. Young's modulus Y and resonance amplitude A ($\propto 1/\delta$) in $La_{1.85}Sr_{0.15}CuO_4$. The inset shows the superconducting transition region in detail. T_c is indicated by an arrow.

behavior similar to that displayed in Fig. 1, but the drop in Y was increased to 20%, and the saturation point in Y was reduced to 70 K.

Changes in X were found to have a dramatic effect on Y and δ. Figure 2 shows Y for a $La_{2-X}Sr_XCuO_4$ sample with X=0.3 (T_c=20 K). Both cooling and heating curves are shown (vertically offset for clarity). It is apparent that a dramatic lattice softening is not observed for X=O.3. Instead, there are smaller anomalies in Y at 220 and 80 K; the anomaly at 220 K is hysteretic and is suggestive of a first-order phase transition. The internal friction for this sample was observed to decrease gradually with decreasing temperature, with no obvious structure.

The elastic behavior described above is remarkably similar to that observed in the A-15 compounds.[4] In these materials, decreases in Y with decreasing temperature have been interpreted as reflecting a soft phonon mode signaling a tendency toward structural phase transformation. The compounds are intrinsically unstable, and this structural instability is tied to both the elastic properties and to the superconductivity mechanism.

Recently, it was suggested[6-9] that the tetragonal K_2NiF_4-type phase in the $La_{2-X}A_XCuO_4$ compounds (A=Sr, Ba, Ca) also has soft phonon modes which can be responsible for the high superconducting temperature within the framework of conventional BCS superconductivity. This softening of the phonon modes is related to a two-dimensional Fermi surface nesting and a resulting Peierls-like instability. Although the undoped compound La_2CuO_4 crystallizes in an orthorhombic structure at temperatures below 530 K, alkaline-earth substitutes for the La^{3+} ions suppress the Peierls' distortions. In the doped samples, the superconducting tetragonal phase was found even at low temperatures around 10 K[10], and single crystal studies have shown a low-temperature tetragonal to orthorhombic transition (see below). The Sr^{2+} ion is the best substitute for the La^{3+} ion, resulting in a relatively strain-free lattice.

The softening of the Young's modulus observed here for $La_{2-X}Sr_XCuO_4$ samples with

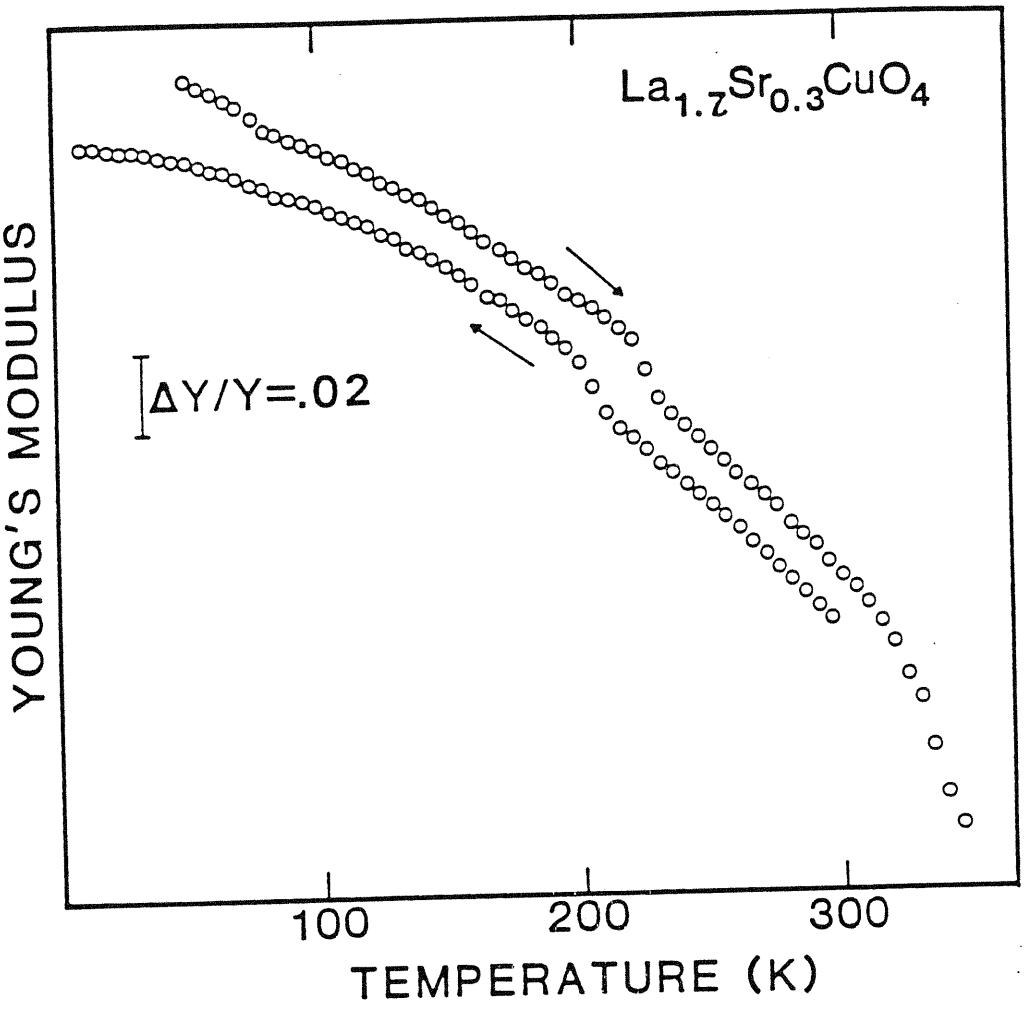

Fig. 2. Young's modulus Y for $La_{1.7}Sr_{0.3}CuO_4$. The cooling and warming curves have been vertically offset.

X=0.15 can be interpreted as a result of phonon mode softening. It is possible that that lattice is close to an instability and that an incipient structural transformation and its associated soft phonon mode enhance the superconducting temperature. As shown in Fig. 2, the softening of the modulus disappears when X=0.3, which suggests that most of the sample has the structural distortions which reduce the mode softening. Magnetic susceptibility measurements for samples of this composition show a diamagnetic effect of order 1%, indicating that the bulk of the sample does not become superconducting. Magnetic susceptibility measurements done elsewhere show that the fraction of the sample which is superconducting varies with composition, with a strong peak near X=0.15.[11]

A recent paper by Kataoka[20] considers the effect of a lattice instability on the superconducting transition temperature. His model contains two nearly degenerate, two dimensional electron bands that tend to drive a tetragonal to orthorhombic phase transition with a Jahn-Teller mechanism of band splitting. He shows that electron repulsion between bands produces an electron attraction within each band, with a maximum T_c achieved at the instability point. This model supports the qualitative arguments that associated lattice instabilities with high T_c's in the A-15 compounds.

The anomalous softening of the Young's modulus could also be due to a structural transition that occurs gradually in different parts of the sample as the temperature is changed. Recent single crystal X-ray studies[12] of $La_{2-X}Sr_XCuO_4$ for X=0.08 found that the crystal structure, which was tetragonal at room temperature, underwent a symmetry-lowering phase transition between 300 K and 180 K, with the macroscopic crystals breaking up into multiple domains of differing orientations. This transition could occur gradually in individual crystal grains for the X=0.15 samples; it is also possible that slight variations in Sr doping throughout the sample control the local transition temperature for the structural change. If the low-temperature structure is significantly softer than the room-temperature structure, either of these mechanisms

could produce the observed behavior of the Young's modulus.

The elastic anomaly near T_c can be used with equation 1-1 to estimate the corresponding heat capacity anomaly. From the inset in Fig. 1, there exists at T_c an anomaly in Y of magnitude $\Delta Y/Y=10^{-3}$. The porosity of the polycrystalline samples makes an absolute determination of Y difficult, and at the time of this work there were no published stress dependences of T_c in $La_{2-X}Sr_XCuO_4$ compounds. However, using the assumptions of $Y\equiv 10^{12}$ dyne/cm^2 and $\partial T_c/\partial P \equiv 1$ K/kbar (as found for the $La_{2-X}Ba_XCuO_4$ system[13]), the estimated specific heat anomaly is $\Delta C_p \equiv 4$ mJ/K cm^3, or $\Delta C_p/T_c \equiv 4$ mJ/K^2 mole Cu atoms. A specific heat anomaly of this magnitude should be measurable. (After this work was submitted for publication, we learned of a direct measurement[14] of ΔC_p of 20 mJ/K^2 mole, in reasonably good agreement with the value inferred from the elasticity measurements).

Finally, the effect of an external magnetic field H on the elastic properties of $La_{2-X}Sr_XCuO_4$ is considered. Figure 3 shows Y near the superconducting transition for a sample with X=0.15. In the absence of a magnetic field, the anomaly in Y is approximately 10 K wide. A major effect of H is to decrease the width of the Young's modulus anomaly; however, the magnitude of the anomaly $\Delta Y/Y$ at T_c is little affected up to H=40 kG. Figure 3 also shows that the position of the elastic anomaly (which we associate with T_c) is insensitive to H. Within the experimental resolution of 0.5 K, an increase in H from 30 to 40 kG does not affect the acoustic anomaly. This sets a lower bound to $\partial H_{c2}/\partial T$ of 20 kG/K, in agreement with the published value of 22 kG/K [15]. The initial narrowing of the transition with increasing H could be due to partial destruction of mixed-gap superconductivity, decoupling of superconducting grains, or to the suppression of superconducting fluctuations above T_c.

An ultrasonic study of $La_{1.85}Sr_{0.15}CuO_4$ performed by another group[16] was published simultaneously with this work; an anomalous lattice softening and a small anomaly in the ultrasonic sound velocity at T_c was observed, in agreement with our

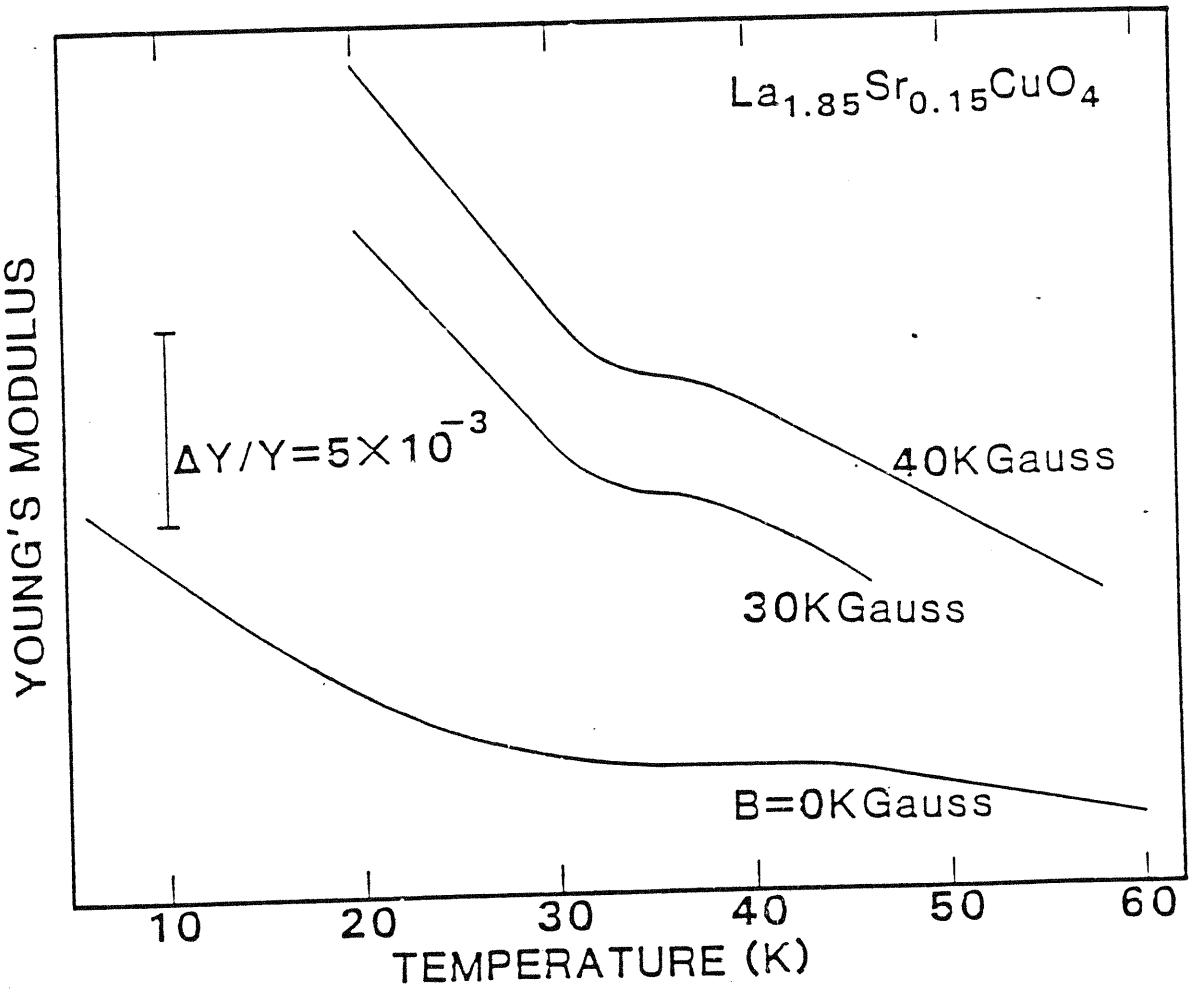

Fig. 3. Young's modulus Y for $La_{1.85}Sr_{0.15}CuO_4$ for selected values of magnetic field.

measurements. A later study of $La_{1.8}Sr_{0.2}CuO_4$ using the vibrating reed technique also found anomalous softening and a modulus anomaly at T_c.[17] Horie et al.[18] have made ultrasonic measurements in single crystals of $La_{2-X}Sr_XCuO_4$, and found anomalous softening in the range 150 - 240 K and peaks in the ultrasonic attenuation coefficient at 100 and 200 K for the X=0.14 composition, which they attributed to the presence of soft optical phonons. Finally, ultrasonic studies of $La_{1.85}Ba_{0.15}CuO_4$ have also found anomalous softening, beginning above room temperature and continuing down to about 150 K.[19] At this date, there is no accepted explanation for the anomalous softening.

In summary, the Young's modulus of $La_{2-X}Sr_XCuO_4$ shows an anomalous softening for the composition that gives the maximum superconducting transition temperature; the anomalous softening does not occur for a composition with an increased Sr concentration and a lower T_c. This softening could be related to a soft phonon mode that is responsible for high T_c's; however, the possibility that the softening is due to a structural transition that occurs gradually throughout the sample has not been ruled out. A small anomaly in the Young's modulus that occurs at T_c in $La_{1.85}Sr_{0.15}CuO_4$ has been used to predict the corresponding specific heat anomaly; the prediction is in reasonably good agreement with a direct measurement of the specific heat anomaly. Finally, a magnetic field sharpens the modulus anomaly at T_c in $La_{1.85}Sr_{0.15}CuO_4$, but the location of the anomaly does not change significantly in temperature as the field is increased, indicating a very high value for $\partial H_{c2}/\partial T$, in agreement with a direct measurement of this quantity.

CHAPTER 1 SECTION 3 REFERENCES

1. J.G. Bednorz and K.A. Muller, Z. Phys. B64,189 (1986).

2. L.C. Bourne, A. Zettl, K.J. Chang, Marvin L. Cohen, Angelica M. Stacy and W.K. Ham, Phys. Rev. B35, 8785 (1987).

3. P.B. Allen and B. Mitrovic, Solid state Phys. 37, 1 (1982).

4. L.R. Testardi, in Physical Acoustics, edited by W.P. Mason and R.N. Thurston (Academic, New York, 1973), Vol. 10, p. 193; L.R. Testardi, Rev. Mod. Phys. 47, 637 (1975).

5. R. J. Cava, R.B. van Dover, B. Batlogg and E.A. Rietman, Phys. Rev. Lett. 58, 408 (1987); S. Kanbe, K. Kishio, K. Kitazawa, K. Fueki, H. Takagi, and S. Tanaka, Chem. Lett. (to be published).

6. L.F. Mattheiss, Phys. Rev. Lett. 58, 1028 (1987).

7. J.J. Yu, A.J. Freeman, and J.H. Xu, Phys. Rev. Lett. 58, 1035 (1987).

8. H.B. Schuttler, J.D. Jorgensen, D.G. Hinks, D.W. Capone II and D.J. Scalapino (unpublished).

9. W. Weber, Phys. Rev. Lett. 58, 1371 (1987); 58, 2145(E) (1987).

10. J.D. Jorgensen, D.G. Hinks, D.W. Capone II, K. Zhang, H.B. Schuttler and M.B. Brodsky (unpublished).

11. R.B. van Dover, R.J. Cava, B. Batlogg and E.A. Rietman, Phys. Rev. B35, 5337 (1987).

12. Urs Geiser, Mark A. Beno, Arthur J. Schultz, Hau H. Wang, Thomas J. Allen, Marilyn R. Monaghan and Jack M. Williams, Phys. Rev. B35, 6721 (1987).

13. C.W. Chu, P.H. Hor, R.L. Meng, L. Gao, Z.J. Huang and Y.Q. Wang, Phys. Rev. Lett. 58, 405 (1987).

14. B.D. Dunlap, M.V. Nevitt, M. Slaski, T.E. Klippert, Z. Sungaila, A.G. McKale, D.W. Capone, R.B. Poeppel and B.K. Flandermeyer, Phys. Rev. B35, 6721 (1987).

15. T.P. Orlando, K.A. Delin, S. Foner, E.J. McNiff Jr., J.M. Tarascon, L.H. Greene, W.R. McKinnon and G.W. Hull, Phys. Rev. B35, 5347 (1987).

16. D.J. Bishop, P.L. Gammel, A.P. Ramirez, R.J. Cava, B. Batlogg and E.A. Rietman, Phys. Rev. B35, 8788 (1987).

17. P. Esquinazi, J. Luzuriaga, C. Duran, D.A. Esparza and C. D'Ovidio, Phys. Rev. B36, 2316 (1987).

18. Y. Horie, T. Fukami and S. Mase, Solid State Commun. 63, 653 (1987).

19. K. Fossheim, T. Laegreid, E. Sandvoid, F. Vassenden, K.A. Muller and J.G. Bednorz, Solid State Commun. 63, 531 (1987).

20. M. Kataoka, Phys. Rev. B 37, 143 (1988).

CHAPTER 2

ELASTIC PROPERTIES OF CHARGE-DENSITY-WAVE CONDUCTORS IN APPLIED ELECTRIC FIELDS

Section 1: Introduction

Since the first observation of nonlinear conduction in the CDW compound $NbSe_3$, much attention has been focused on the unusual transport properties of the CDW condensate[1]. Materials such as $NbSe_3$, TaS_3, $(TaSe_4)_2I$, and $K_{0.3}MoO_3$ display enhanced dc conductivity for dc electric fields E_{dc} exceeding a well-defined threshold field E_T (corresponding to a depinning and subsequent sliding of the CDW), frequency dependent ac conductivity in the MHz frequency range (corresponding to polarization of the CDW about pinning centers), and coherent current oscillations (narrow band noise) for $E_{dc}>E_T$. Mixing between the internally generated narrow band noise and an externally applied ac electric field can also lead to electronic interference structure in the current-voltage (I-V) characteristics of the crystal, and mode locked states.

The elasticity measurement methods developed for static CDW systems are well suited to the study of CDW dynamics. Brill and Roark[2,3] first showed that both the Young's modulus Y and the internal friction δ in TaS_3 are strongly affected by applied dc fields $E_{dc}>E_T$. In general, dc field-induced depinning of the CDW causes the crystal lattice to soften and the internal friction to increase. Similar field dependences were obtained by Mozurkewich et al.[4,5] for $NbSe_3$ and $(TaSe_4)_2I$. A detailed account of low frequency elastic properties of TaS_3 for applied dc electric fields is given in reference 6. CDW depinning in TaS_3 has also been studied by conventional ultrasonic techniques adapted to the long thin crystal geometry[7]. More recently, it has been shown that the shear modulus G and its corresponding dissipation in TaS_3 show behavior similar to that of Y and δ when the CDW is depinned[8].

This section will describe measurements of the elastic properties (Y and δ) of TaS_3 (orthorhombic phase) and $NbSe_3$, in the presence of externally applied ac, dc, and combined ac + dc electric fields. The elastic properties are found to be sensitive to CDW motion, even in the limit where the CDW is excited by a very low amplitude ac field $E_{ac}<E_T$. For applied dc fields E_{dc}, lattice softening is observed for $E_{dc}>E_T$, consistent with previous studies[2-5]. In the presence of combined ac+dc fields, a strong correspondence between the electronic response of the CDW (as determined by differential resistance measurements) and the elastic response is observed. These results suggest an important role played by internal degrees of freedom of the CDW condensate.

The section is organized as follows: The experimental results are described in section 2. Section 3 presents applicable theoretical models and a discussion of the experimental results in terms of these models. This is followed by a conclusion in section 4. Most of this material has been published in the regular literature[9,10].

Section 2. Experiments and Results

Materials used in this study consisted of single crystal samples of $NbSe_3$ and orthorhombic TaS_3, synthesized by conventional vapor transport methods. dc I-V characteristics yielded threshold fields E_T=30mV/cm for $NbSe_3$ (T=48K) and E_T=500mV/cm for TaS_3 (T=200K), suggesting moderately pure crystals. Both Young's modulus Y and internal friction δ were measured simultaneously using the vibrating reed technique as described in the appendix. The samples were clamped at both ends so that ac and dc currents could be passed through the sample; this led to Joule heating of the samples when the sample chamber was evacuated, a problem that was largely eliminated by pressurizing the chamber to 5 torr (nitrogen or helium), thus improving the thermal conductance between the sample and the chamber walls. An undesirable side effect of the pressurization was, however, a noticeable increase in the

measured internal friction. Because of this effect and the possibility of additional friction introduced at imperfectly rigid clamps, only absolute changes in δ are used in the analysis.

A simplified schematic of the electronics for the experiment is shown in Fig. 1. An adder circuit combined dc bias field E_{dc}, ac field $E_{ac}\cos(\omega_{ex}t)$, a low frequency modulation signal $E_{mod}\cos(\omega_{mod}t)$ suitable for derivative measurements, and a high frequency carrier signal $E_{car}\cos(\omega_{car}t)$. Typically, $\omega_{ex}/2\pi$ ranged from 0.5 to 10 MHz and $\omega_{mod}/2\pi$ was set at 200 Hz. $\omega_{car}/2\pi$ was tuned to 590 MHz to provide impedance matching between the pickup electrode and the detection circuitry. The modulation and carrier amplitudes were kept very small ($<0.01E_T$), and neither the carrier nor the modulation signals had any measurable effect on the electronic or elastic properties of the crystal. The low potential (inertially clamped) end of the sample was attached to a suitable rf choke, which allowed full carrier signal strength along the length of the sample, independent of the dynamic impedance of the sample.

For the most sensitive measurements, involving the detection of mode locking in the elastic properties, the experiment was repeated many times and the shifts were signal averaged for an improvement in signal to noise ratio. In single sweep data recordings, the experimental method was typically sensitive to relative changes in Y of order 10^{-4}, and absolute changes in δ also of order 10^{-4}; with signal averaging the sensitivity of both parameters could be improved by at least one order of magnitude.

a. TaS_3

Fig. 2 shows, for a TaS_3 crystal at T= 152K, Y, δ, and dV/dI as measured in the presence of an externally applied longitudinal ac field $E_{ac}\cos(\omega_{ex}t)$ with $\omega_{ex}/2\pi$=1MHz. No dc bias is present. The horizontal ac amplitude scale has been normalized to the dc conductivity threshold field E_T, measured in the absence of any ac excitation. From Fig. 2 it is clear that an ac field of moderate amplitude has a

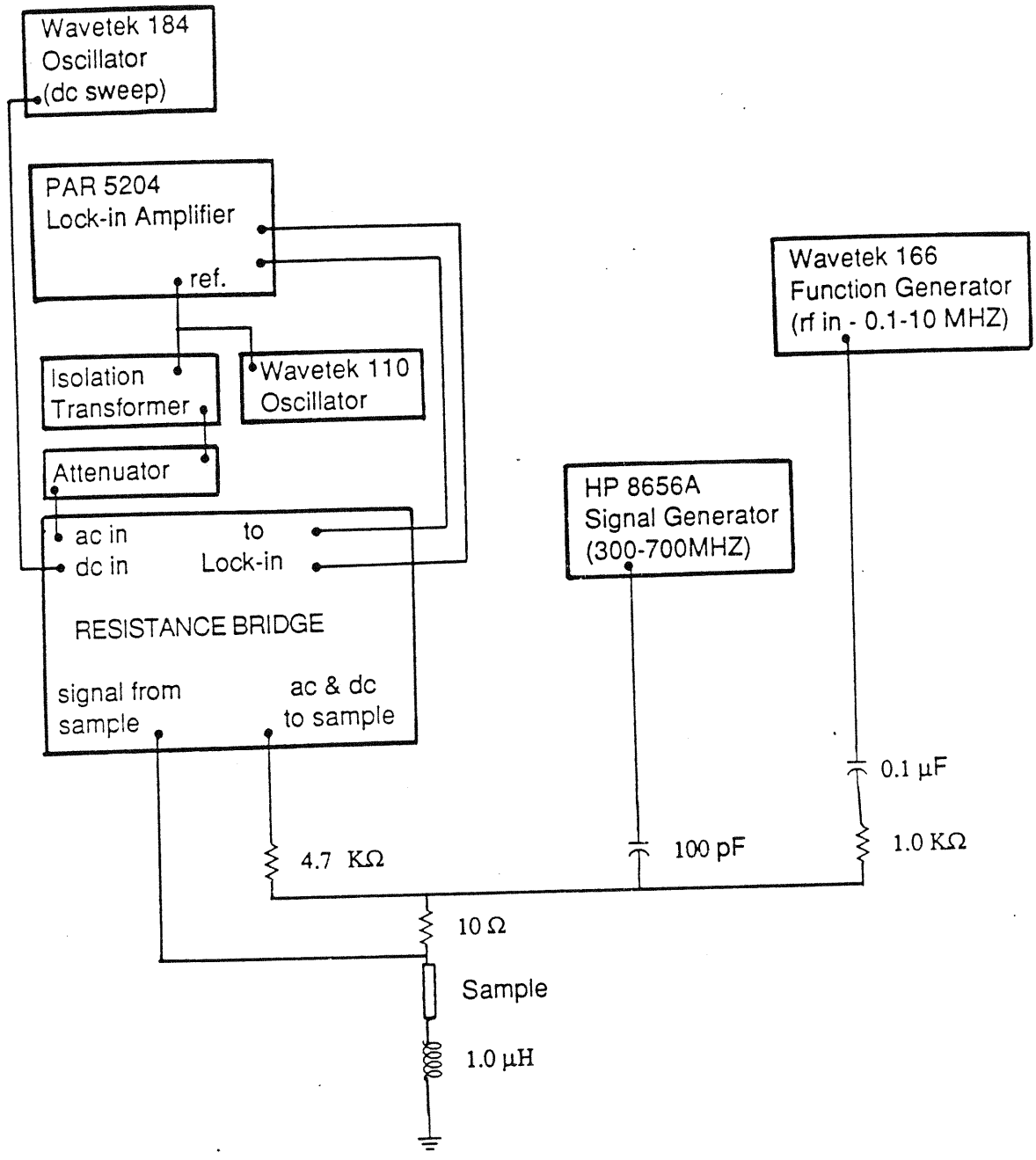

Fig. 1 Schematic showing electronics for Mode-Locking the sample.

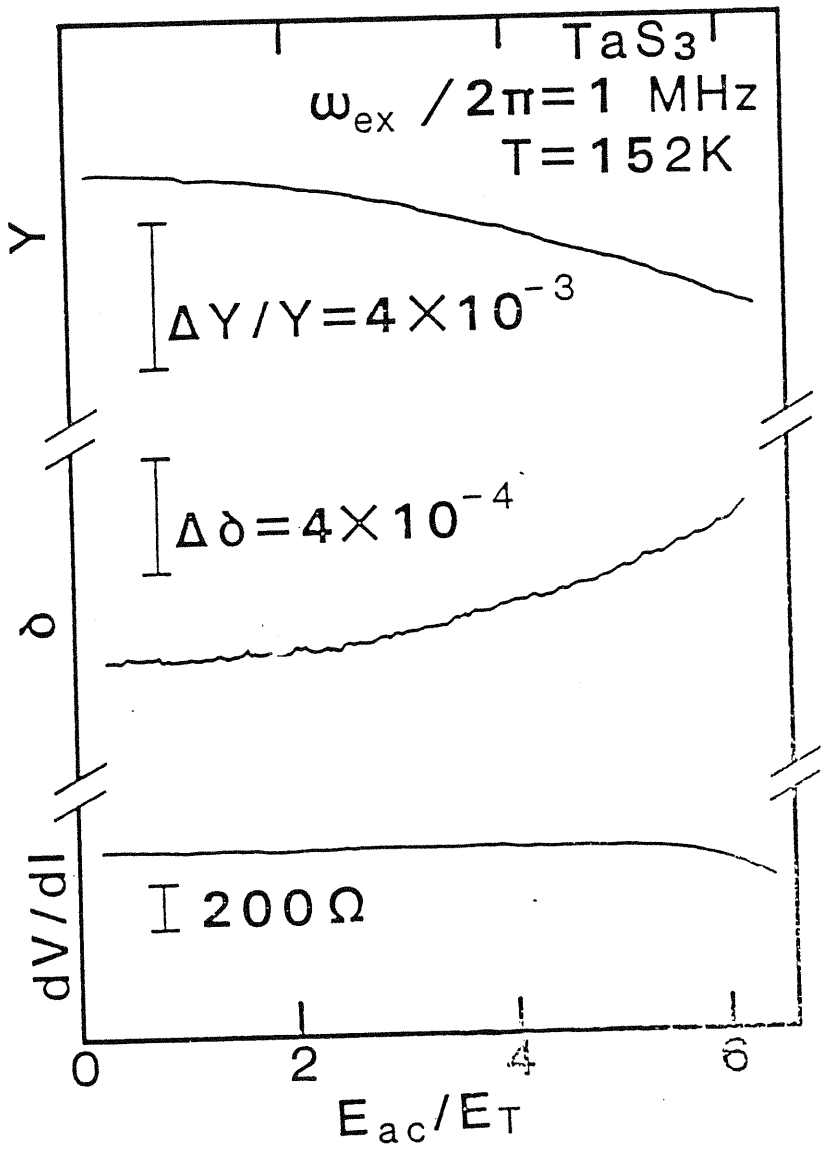

Fig. 2. Y, δ, and dV/dI in TaS_3 as functions of ac field amplitude E_{ac}. The crystal lattice softens and internal friction increases with increasing E_{ac}. No dc bias field is present. (Sample TaS_3 #32: R=2.9KΩ, I_T=63μA, Length=1.5mm).

significant effect on both Y and δ; dV/dI is far less sensitive, and begins to deviate from its E_{ac}=0 value only above approximately E_{ac}/E_T=5. The observed decrease in Y and increase in δ with increasing E_{ac} indicates that the external ac field tends to soften the crystal lattice while increasing the internal friction. Both parameters are here measured on timescales much longer than ω_{ex}^{-1}.

From Fig. 2 it is difficult to see clearly if Y and δ deviate from their zero field values for E_{ac} finite but less than E_T. Fig. 3 shows this parameter range in detail, again for TaS_3. Even for $E_{ac}/E_T<1$, Y is seen to decrease smoothly with increasing E_{ac}, with no evidence for any threshold behavior. Assuming simple classical dynamics for the CDW, the CDW is expected to remain always pinned for $E_{ac}/E_T<1$, independent of damping. The lattice softening of Fig. 3 is therefore identified with excitation of the pinned phason mode, not the sliding Fröhlich mode. Fig. 3 also shows the internal friction δ. The vertical scale has been greatly expanded, and the fine structure observed is entirely due to instrumental drifts. The dashed line represents the averaged E_{ac}=0 value. For $E_{ac}/E_T<1$, there is, within experimental resolution, no change in δ; for E_{ac}/E_T=2, however, δ has increased significantly, with $\Delta\delta=2\times10^{-5}$.

The lattice softening observed in Figs. 2 and 3 is strongly frequency (ω_{ex}) dependent. Fig. 4 shows, for a TaS_3 crystal at T=151K, the relative change in Y with increasing E_{ac} measured for three different values of ω_{ex}. As with the data of Figs. 2 and 3, Fig. 4 was obtained with E_{dc}=0. Fig. 4 shows that the ac field-induced lattice softening effect is only observed for relatively low values of ω_{ex}. Curve A, for example, which corresponds to $\omega_{ex}/2\pi$=0.5MHz, shows a relative change in Y of order 10^{-3} at E_{ac}/E_T=1, while curve C, corresponding to $\omega_{ex}/2\pi$=10MHz, shows no change in Y even for $E_{ac}/E_T>3$.

A vertical cut through data similar to that presented in Fig. 4 is shown in Fig. 5, where the relative change in Y is plotted as a function of ω_{ex}, for fixed E_{ac}/E_T=2.6. Over a limited range in frequency, ΔY/Y changes linearly with frequency, while as

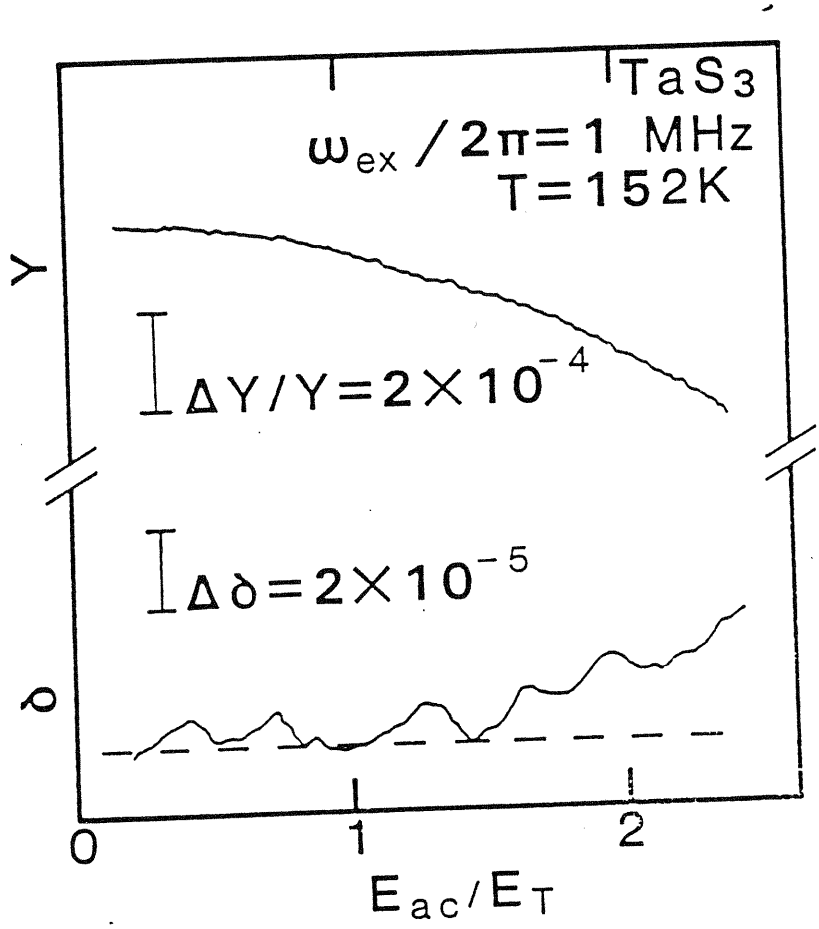

Fig. 3. Detailed behavior of Y and δ as functions of E_{ac} in TaS_3. Lattice softening occurs even for E_{ac} much smaller than the dc threshold field E_T. (Sample TaS_3 #32).

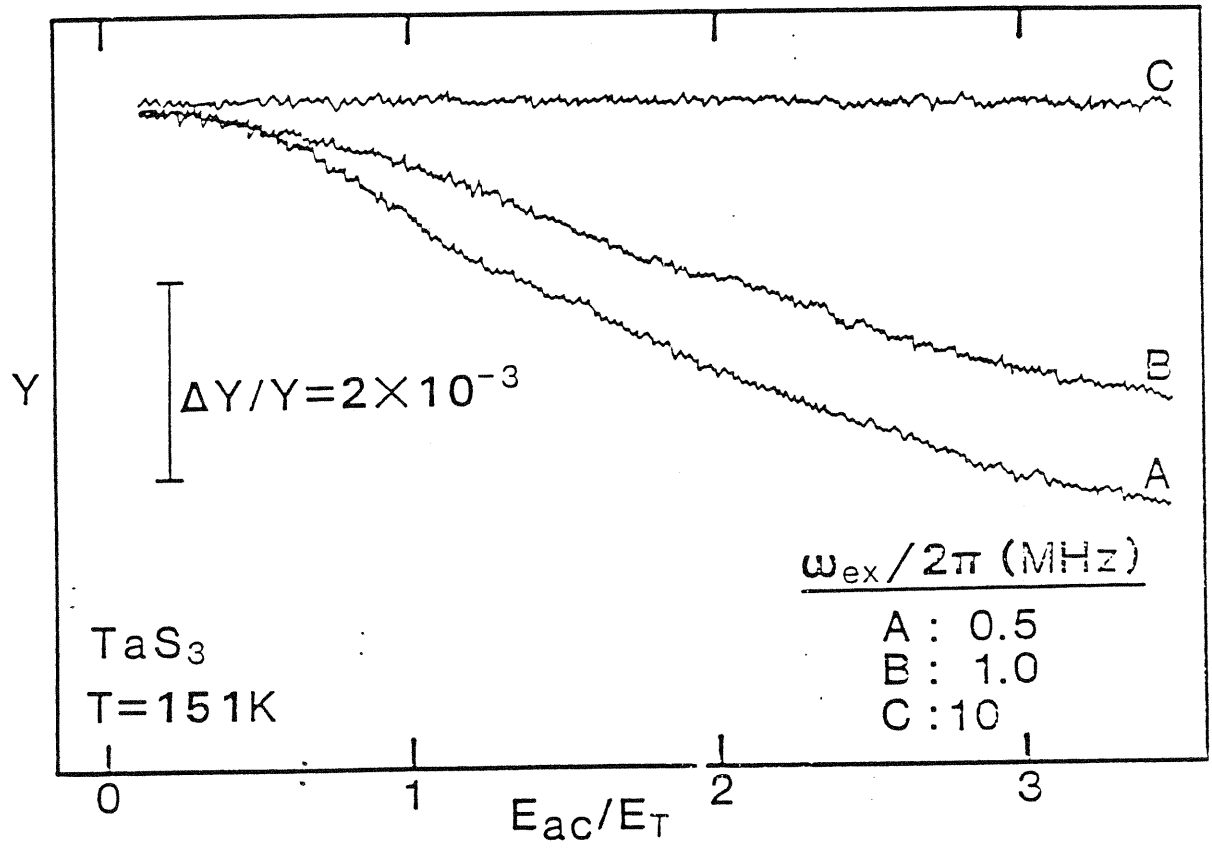

Fig. 4. Y as a function of E_{ac} in TaS_3, for three different values of ac frequency ω_{ex}. (Sample TaS_3#31: R=3.8KΩ, I_T=75μA, Length= 0.8mm).

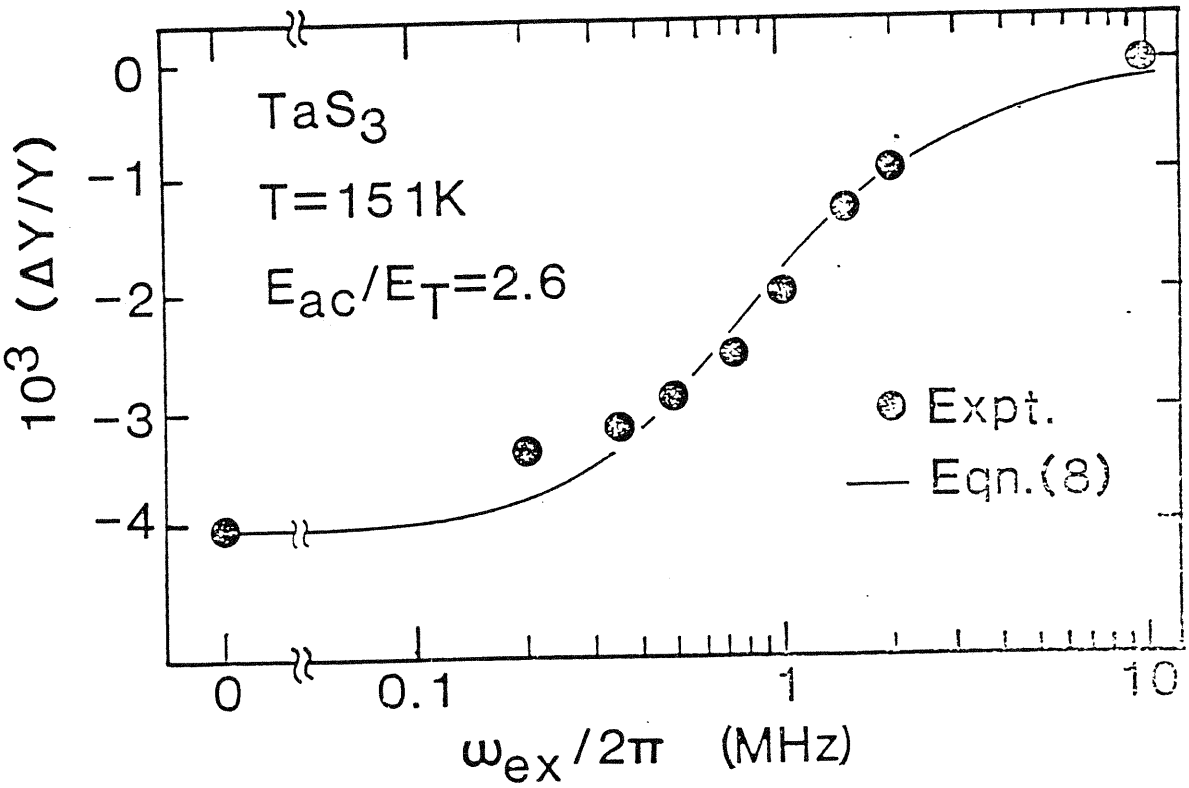

Fig. 5. $\Delta Y/Y$ as a function of ac frequency ω_{ex} in TaS_3, with E_{ac} exceeding E_T. The solid line is Eq. (8), with fitting parameters given in the text. (Sample TaS_3#31).

ω_{ex}-->0 $\Delta Y/Y$ asymptotically approaches the dc limit (measured independently with an applied dc field $E_{dc}/E_T=2.6$). At high values of ω_{ex}, Y approaches the zero bias limit.

Behavior similar to that shown in Fig. 5 was obtained in TaS_3 for other fixed values of $E_{ac}/E_T>>1$. For $E_{ac}/E_T=1$, however, the behavior of Y is strikingly different. Fig. 6 shows $\Delta Y/Y$ versus ω_{ex} for $E_{ac}/E_T=1$. The dashed line is a guide to the eye drawn through the few accurately determined data points. From Fig. 6 it appears that $\Delta Y/Y$ deviates dramatically and smoothly from zero as the frequency is lowered from 10MHz, yet the $\omega_{ex}=0$ (dc) point is clearly at $\Delta Y/Y=0$. As is discussed later, this behavior may suggest critical behavior in Y as ω_{ex} approaches a characteristic frequency ω_{cr}.

The effect of combined ac and dc electric fields on Y and δ is now considered. Fig. 7 shows Y, δ, and dV/dI for a TaS_3 crystal at T=152K, as functions of dc bias. The dc bias is represented as a ratio of applied dc bias current I_{dc} to the dc threshold current I_T (measured with no ac field applied). The dc bias field is related to I_{dc} by $E_{dc}=I_{dc}R/l$, where R is the (nonlinear) sample resistance and l is the sample length. For all data in Fig. 7, the frequency of the applied ac field is $\omega_{ex}/2\pi=1$MHz. Curves A in Fig. 7 are for $E_{ac}=0$; this limit corresponds to dc CDW depinning experiments performed previously on TaS_3 and other CDW conductors[2-7]. In the bottom group of traces in Fig. 7, curve A is a conventional dV/dI versus dc bias plot. The sharp break in the curve at $I_{dc}/I_T=1$ clearly identifies the dc threshold for CDW depinning. As seen in the upper sets of traces labeled "A" in Fig. 7, similar breaks in Y and δ are again observed in Y and δ at $I_{dc}/I_T=1$. For $I_{dc}>I_T$, Y decreases smoothly with increasing dc bias, and δ increases rapidly and apparently saturates near $I_{dc}/I_T=1.5$. The general features of these traces, corresponding to finite E_{dc} and zero E_{ac}, are in good agreement with previous studies[2-6]. Curves B, C, and D in Fig. 7 show the effects of ac field on Y, δ, and dV/dI. The dV/dI traces show clearly that the break in dV/dI, i.e. the threshold

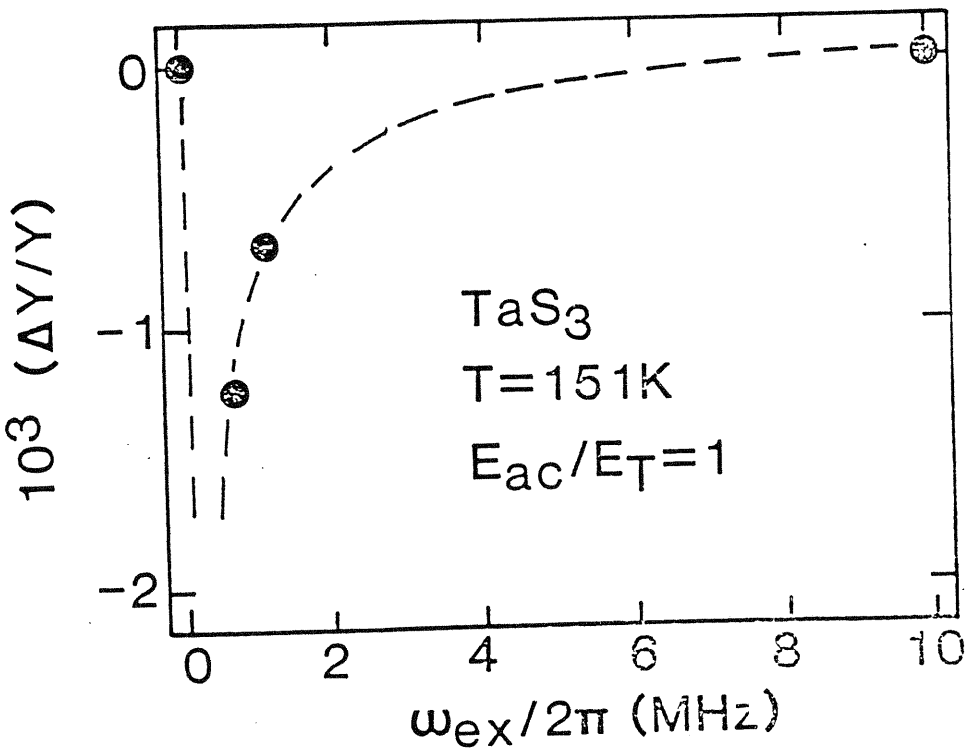

Fig. 6. $\Delta Y/Y$ as a function of ac frequency ω_{ex} in TaS_3, for $E_{ac}=E_T$. Note that $\Delta Y/Y=0$ at $\omega_{ex}=0$. The dashed line is a guide to the eye. (Sample TaS_3#31).

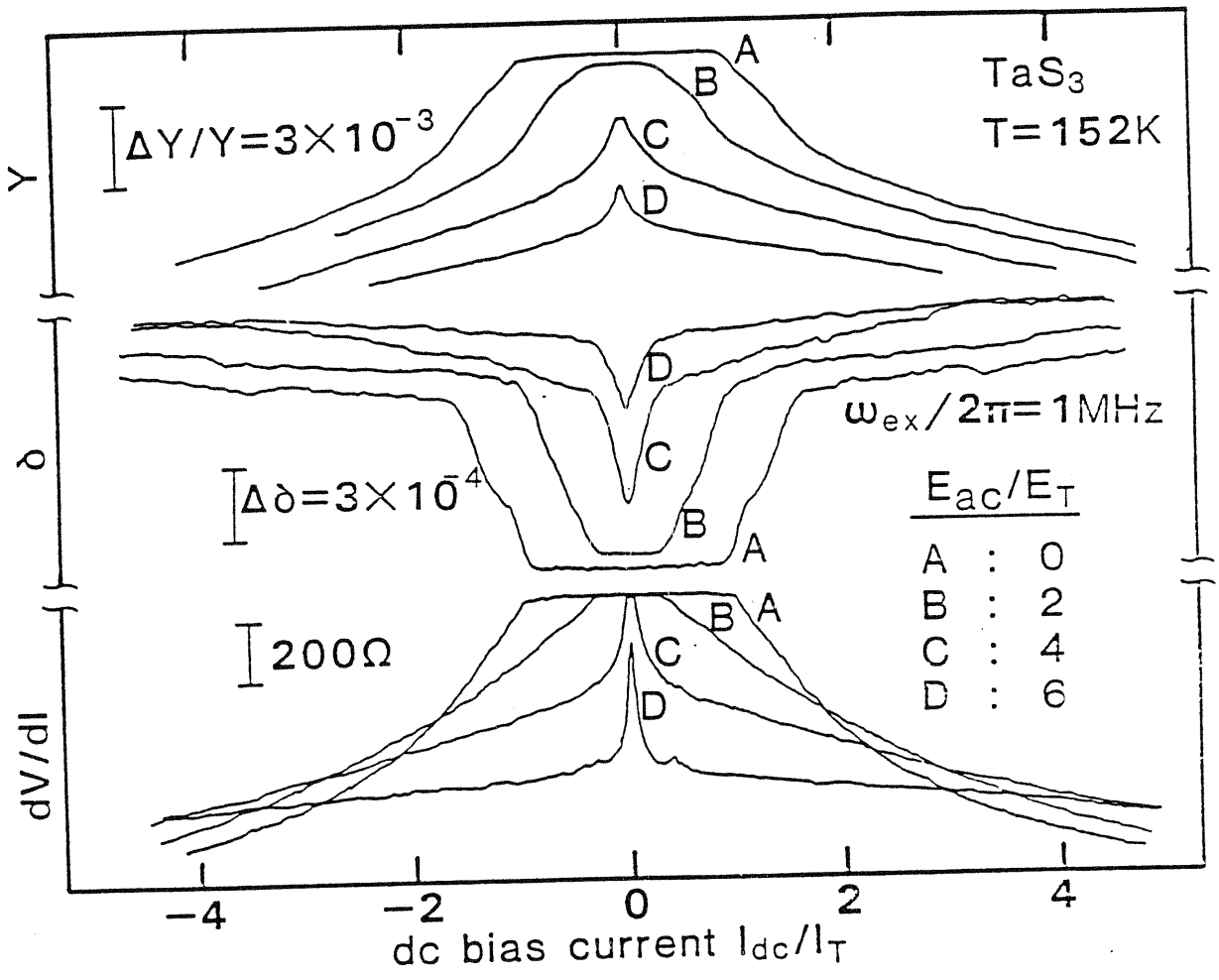

Fig. 7. Y, δ, and dV/dI as functions of dc bias in TaS_3 at T=152K, for four different values of E_{ac}. Curves within each group have not been vertically displaced. (Sample TaS_3#32).

for dc CDW conduction, is reduced to a lower value I_T' with the application of ac field. This electronic effect has been previously observed and studied quite extensively in TaS_3 and $NbSe_3$[11-14]. An important point to note is that for the dV/dI curves B and C in the lower part of Fig. 7, no change in dV/dI is observed at $I_{dc}=0$. Only when the effective depinning threshold has been reduced to zero does dV/dI at $I_{dc}=0$ become E_{ac} dependent, as is the case for curve D.

The Y and δ traces of Fig. 7 show that finite E_{ac} has a dramatic effect on the functional dependence of Y and δ on I_{dc}. It should be emphasized that in Fig. 7 the traces within a group have <u>not</u> been vertically offset. With $I_{dc}=0$, the E_{ac} dependence of Y and δ in Fig. 7 is consistent with the lattice softening and increasing internal friction with increasing E_{ac} previously demonstrated in Fig. 2. For increasing I_{dc}, E_{ac}-dependent breaks in Y and δ are observed; these appear to correspond to the dc depinning threshold I_T' (see below). General features of Young's modulus are a general depression in Y with increasing E_{ac}, and a weaker dependence of Y on dc bias with increasing E_{ac}. For $I_{dc}/I_T>2$, traces of Y corresponding to different E_{ac} values appear to converge. Extrapolating the Y data of Fig. 7 to higher I_{dc} values results in a convergence point at $I_{dc}/I_T=9$. This convergence cannot be extracted directly from the data, due to significant Joule heating of the sample at large values of I_T and E_{ac}.

The E_{ac}-dependence of internal friction δ parallels that of Y. With increasing E_{ac}, δ increases, and the value of I_{dc} at which δ "saturates" (i.e. assumes a relatively flat slope) decreases with increasing E_{ac}. The absolute saturation value of δ in the saturated region appears to increase with increasing E_{ac}, although this does not rule out the possibility that at large I_{dc} δ becomes roughly independent of E_{ac}. Indeed, curves C and D for $I_{dc}/I_T>4$ suggest this may be the case.

As mentioned above, the initial "breaks" in the dV/dI, Y and δ versus I_{dc} curves appear correlated. Fig. 8 shows this correlation in detail for another TaS_3 sample at 151K, with $\omega_{ex}/2\pi=1$MHz. The vertical axis represents that value of I_{dc}

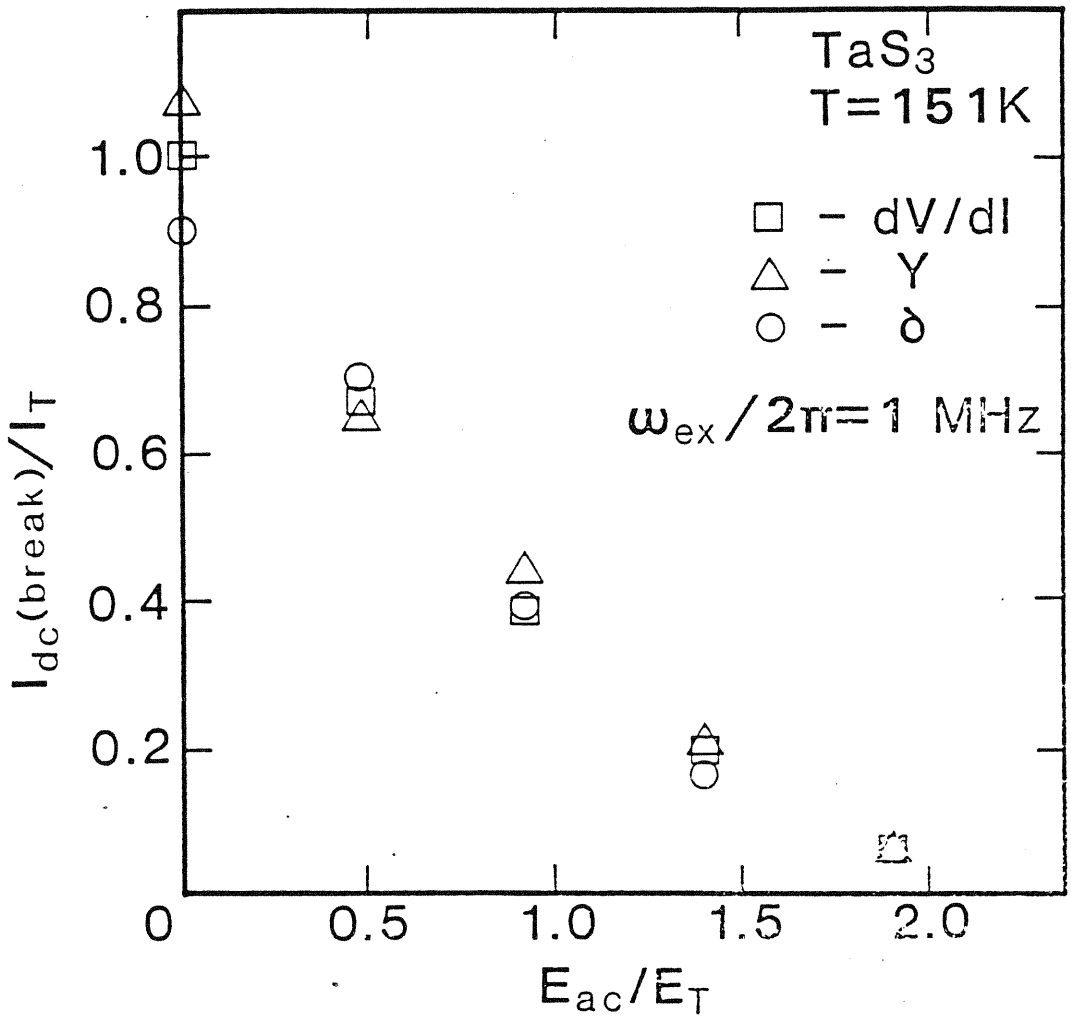

Fig. 8. Effect of an ac field on the critical dc bias for changes in dV/dI, Y, and δ. I_{dc}(break) is the dc current value at which the measured quantity begins to deviate from the $I_{dc}=0$ value. I_T is the depinning current for $E_{ac}=0$; E_T is the corresponding dc threshold field. (Sample TaS_3#31).

(normalized to I_T) at which a finite slope first appears in the dV/dI, Y, or δ versus I_{dc} curve. For $E_{ac}/E_T>2$, there is, for all three parameters, no region of finite slope and the breaks all occur at $I_{dc}=0$. The critical value of E_{ac}/E_T above which the breaks all occur at $I_{dc}=0$ (i.e. the critical value of E_{ac}/E_T for which I_T' is suppressed to zero) is sample dependent; for the TaS_3 sample of Fig. 7, for example, the critical value is $E_{ac}/E_T\approx4$. The strong correlations observed in Fig. 8 indicate that Y and δ are very sensitive to dc motion of the CDW, even in the case where the elastic constants have already been strongly perturbed by a large amplitude ac field. In the limit $E_{ac}\dashrightarrow\infty$, however, Fig. 7 would suggest no additional I_{dc} dependence for either Y or δ.

The general features of the Y and δ versus E_{ac} and E_{dc} behaviors shown in Fig. 7 are, for TaS_3, very temperature dependent, and to some extent sample dependent. Fig. 9 shows, for TaS_3 at T=115K, data in the same format as was used for Fig. 7. The same sample was used to generate the data for Figs. 7 and 9. While the dV/dI versus I_{dc} traces in Fig. 9 are qualitatively very similar to those of Fig. 7, there are important differences in dV/dI, and in particular in Y and δ. Note that a much larger ratio of E_{ac}/E_T is required at low temperature to reduce the dc threshold field to zero; at 115K the ratio is three times the ratio at 152K. However, the general form of dV/dI versus I_{dc} is relatively temperature independent in this temperature range. The low temperature behavior of Y and δ versus I_{dc} is unusual. In curve A of Fig. 9, which corresponds to $E_{ac}=0$, the initial break in Y is associated with an initial increase in Y with increasing I_{dc}; at higher values of I_{dc} Y again decreases strongly with increasing I_{dc}, consistent with the high temperature behavior. With increasing E_{ac}, this "bump" structure in Y remains, but moves to lower dc bias values and decreases in magnitude. For curve C, corresponding to $E_{ac}/E_T=12$, the bump structure has nearly coalesced near the $I_{dc}=0$ origin, and for curve D, corresponding to $E_{ac}/E_T=19.2$, the anomalous feature is no longer observable.

Fig. 9 shows that there are no corresponding "bump" anomalies in δ near the dc

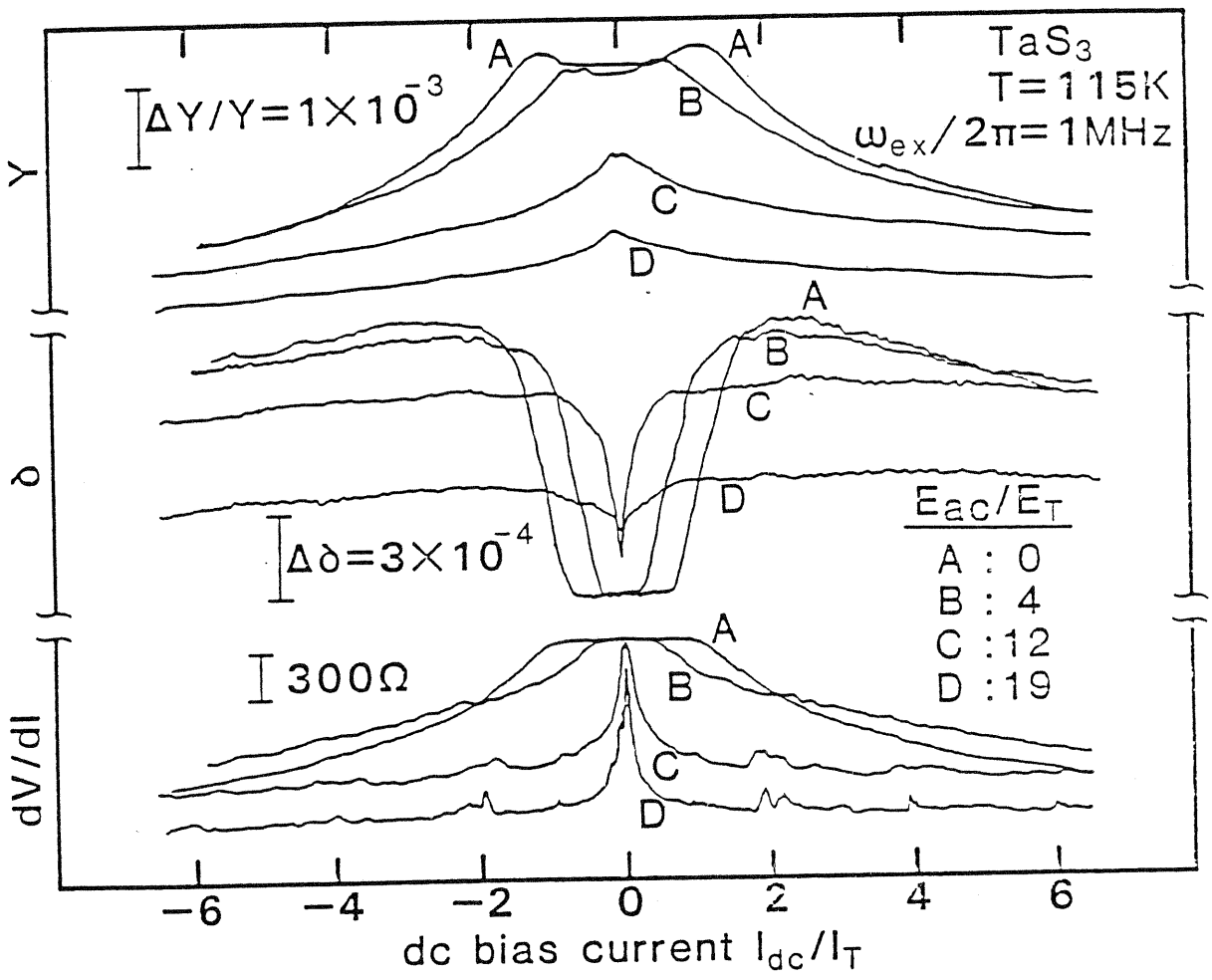

Fig. 9. Y, δ, and dV/dI as functions of dc bias in TaS_3 at T=115K, for four different values of E_{ac}. The curves within each group have not been vertically displaced. This data should be compared to analogous data in Fig. 7, which is for the same TaS_3 crystal but at a higher temperature. (Sample TaS_3#32).

threshold I_T'; the depinning behavior is similar to that observed at higher temperatures. At greater values of dc bias, however, Fig. 9 shows, for E_{ac}=0, no fast transition to a zero slope (saturated) state. Rather, curve A shows a broad maximum in δ near I_{dc}/I_T=2. At high values of E_{ac} the maximum is suppressed, and again "saturation" behavior, similar to that observed at high temperatures, results. It is important to note also that at low temperatures, the application of ac field E_{ac} causes a dramatic decrease in δ in the sliding CDW state; this tendency in δ is exactly opposite to that observed at high temperatures.

Although the anomalous bump structure in Y and "broad maximum" structure in δ in TaS_3 is routinely observed at low temperatures, the features are not apparent in all crystals. These features to not appear to be related to other crystal parameters, for example threshold field (corresponding to sample impurity concentration) or sample size. Similar anomalies have been previously observed in TaS_3 at 96K by Brill et al[6], in the finite E_{dc}, E_{ac}=0 limit.

The dV/dI traces of Fig. 9 corresponding to large E_{ac} show peak structure for applied I_{dc} well beyond I_T. These peaks identify Shapiro step interference between ω_{ex} and the internal narrow band noise frequency ω_{in}. In TaS_3 and $NbSe_3$, Shapiro step interference in general occurs whenever ω_{in}/ω_{ex}=p/q=n, with p and q integers[12, 15,16]. Peaks corresponding to integral values of n are denoted as harmonic interference steps, and those corresponding to non-integral values as subharmonic steps. For a fully volume coherent crystal, Shapiro step interference can result in complete mode locking[17], where the entire CDW condensate assumes a constant drift velocity whose magnitude is dictated by ω_{ex}. During such mode locking the dc differential resistance dV/dI assumes its pinned, E_{dc}-->0 value. The Shapiro step structure observed in Fig. 9 is clearly not in the fully mode locked regime, and the interference peaks (at I_{dc}/I_T=2, for example) correspond to only a small portion of the CDW mode locked. Similar low-fractional locking is present in the data of Fig. 7,

for example at $I_{dc}/I_T=0.3$ in dV/dI curve D. In neither Figs. 7 nor 9 is the experimental resolution of Y and δ sufficient to observe any corresponding structure in elastic parameters during electronic interference. Such structure does, however, exist.

Fig. 10a shows the results of a very careful measurement of Y, δ, and dV/dI in TaS_3 at 151K, in the presence of an ac field at $\omega_{ex}/2\pi=1$MHz with $E_{ac}/E_T=1.3$. In the bottom dV/dI trace, Shapiro step interference is observed at $I_{dc}=55\mu A$, as identified with the vertical arrow and dashed line. This peak corresponds to $n=p/q=1/1$. Fig. 10a shows that, corresponding to electronic Shapiro step interference in dV/dI, there occur small anomalies in Y and δ. Y shows a peak structure similar to that observed in dV/dI, while δ shows a dip during the interference. These features are seen more clearly in Fig. 10b, which shows the detailed behavior of Y and δ in the region of the dominant Shapiro step for the same TaS_3 crystal. It is apparent that, during the electronic interference, both Y and δ tend toward their respective values assumed in the pinned CDW state. Fig. 10b also shows that additional Shapiro step structure in dV/dI is observed at $I_{dc}=63\mu A$. This interference peak also corresponds to $n=p/q=1/1$, and is unrelated to the peak at $I_{dc}=55\mu A$. The peak at $I_{dc}=63\mu A$ apparently arises from a different portion of the sample mode locking to ω_{ex}, as can result from a non-uniform CDW current distribution in the crystal and a multi-valued narrow band noise spectrum. Fig. 10b shows that this second interference peak is again associated with well-defined anomalies in Y and δ.

b. $NbSe_3$

The experiments described above have in part been repeated for $NbSe_3$, with similar results. $NbSe_3$ has two CDW transitions, the first at $T_1=144$K and the second at $T_2=59$K. Both the upper ($T_2<T<T_1$) and lower ($T<T_2$) CDW states are associated

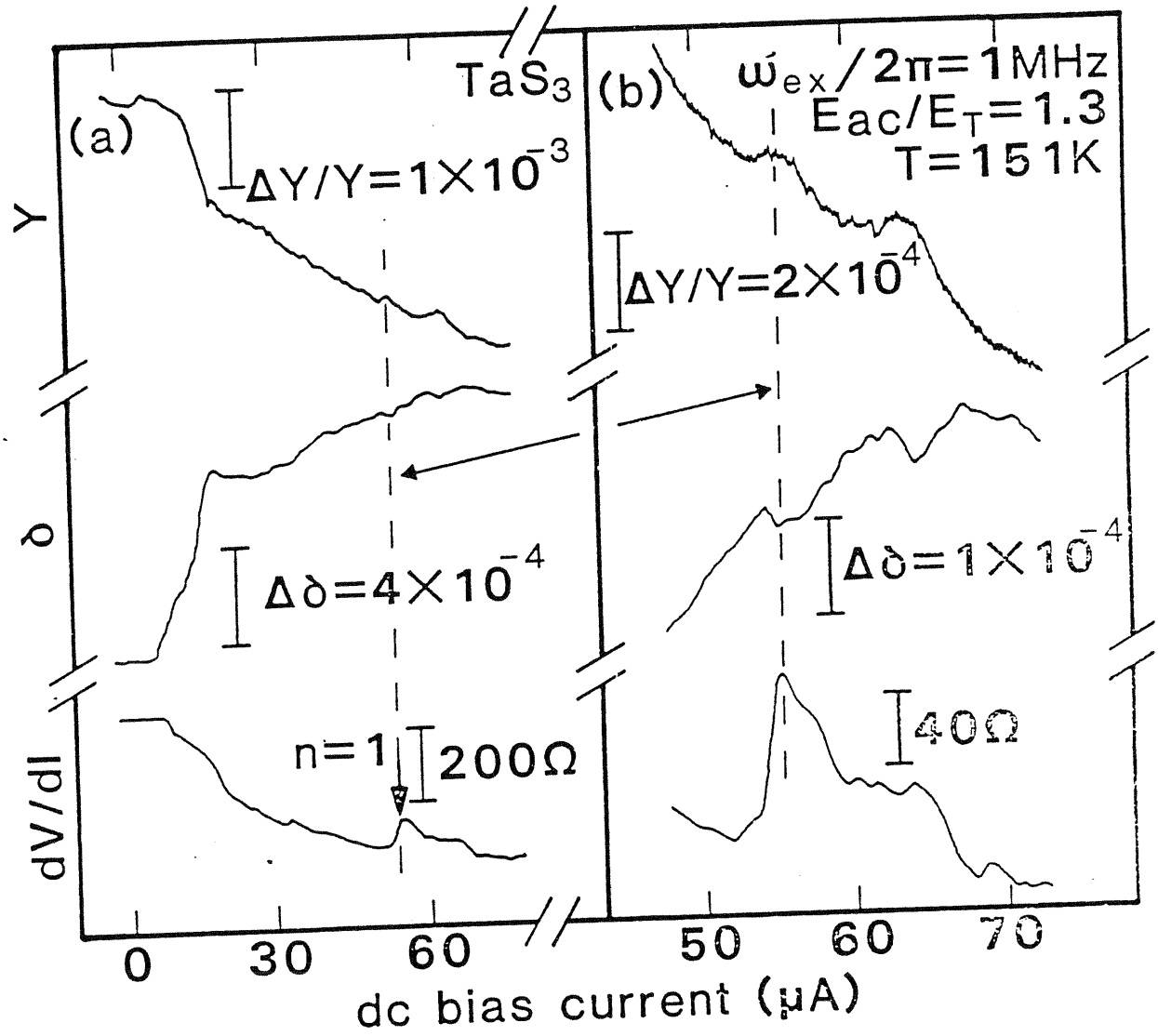

Fig. 10. Y, δ, and dV/dI in TaS_3 as functions of dc bias in the presence of an ac field. The position of the n=1 Shapiro step interference peak is identified with a vertical arrow. Corresponding structure is observed in Y and δ (dashed vertical line). (Sample TaS_3#31).

with pinned phason mode excitations, nonlinear Fröhlich mode conduction, narrow band noise, and Shapiro step interference[1]. Most electronic experiments on $NbSe_3$ have been performed in the lower CDW state, where the response properties are in general more dramatic. Interestingly, the elastic response parameters have exactly the opposite sensitivity, with changes in the elastic properties due to the depinning of the CDW reported as being substantial in the upper CDW state but immeasurably small in the lower CDW state[4].

Fig. 11 shows Y, δ, and dV/dI as functions of dc bias current I_{dc} in the lower CDW state of $NbSe_3$ at T=37.9K. No ac field is present. The very sensitive measurement of Y and δ is associated with a large amount of instrumental noise. Nevertheless, it is apparent that the strong nonlinearity in dV/dI for $I_{dc}>I_T$ is associated with a decrease in Y and an increase in δ, similar to the behavior observed in TaS_3. For $I_{dc}/I_T=2$, there are well defined changes in Y of order $\Delta Y/Y=5\times10^{-5}$ and in δ of order $\Delta\delta=5\times10^{-3}$. There is a broad maximum in δ near $I_{dc}/I_T=2$; for larger values of dc bias δ appears to decrease smoothly with increasing I_{dc}. No saturation in Y is observed for $I_{dc}/I_T<5$.

Because of the relatively small changes in the elastic parameters of $NbSe_3$ in the lower CDW state in the presence of bias fields, this study focuses more carefully on the elastic response in the upper CDW state. Fig. 12a shows Y, δ and dV/dI as functions of dc bias current I_{dc} for $NbSe_3$ at T=135K. Similar to the behavior observed in the lower CDW state, Y and δ show sharp breaks at I_T, with Y decreasing and δ increasing with increasing I_{dc} past threshold (the small increase in δ with increasing I_{dc} below I_T is due to instrumental drift). For $I_{dc}/I_T=1.5$, δ is seen to approach a maximum and saturate. At $I_{dc}/I_T=2$, Y shows a relative change of approximately $\Delta Y/Y=2\times10^{-4}$, and $\Delta\delta=5\times10^{-5}$. The change in Y is nearly an order of magnitude larger than that associated with the lower CDW state of $NbSe_3$. Fig. 12b shows the additional effect of an ac field on Y, δ, and dV/dI, with $\omega_{ex}/2\pi=2$MHz and $E_{ac}/E_T=3.8$. In the lower dV/dI

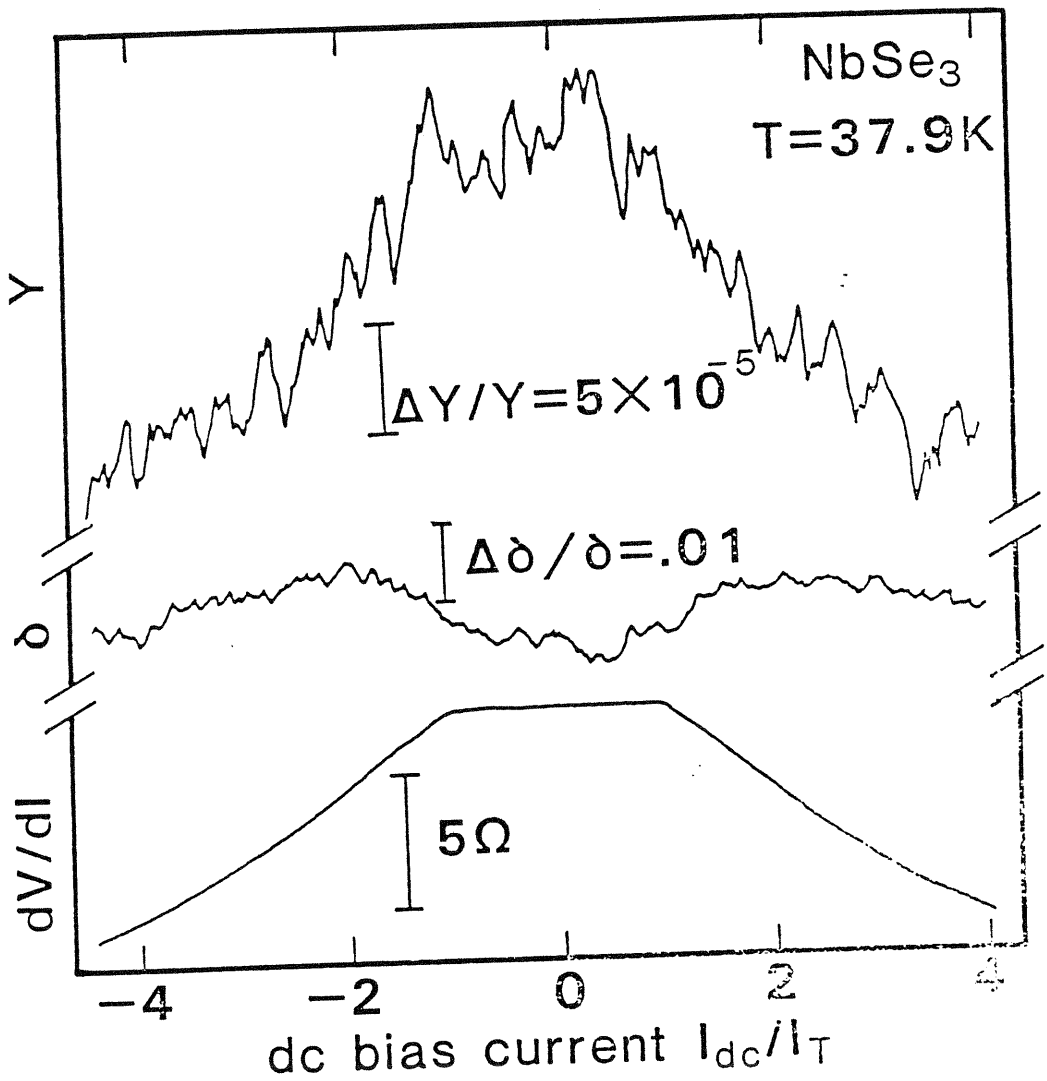

Fig. 11. Y, δ, and dV/dI as functions of dc bias in the lower CDW state of $NbSe_3$. (Sample $NbSe_3$#38: R=13Ω, I_T=68μA, Length≈1 mm).

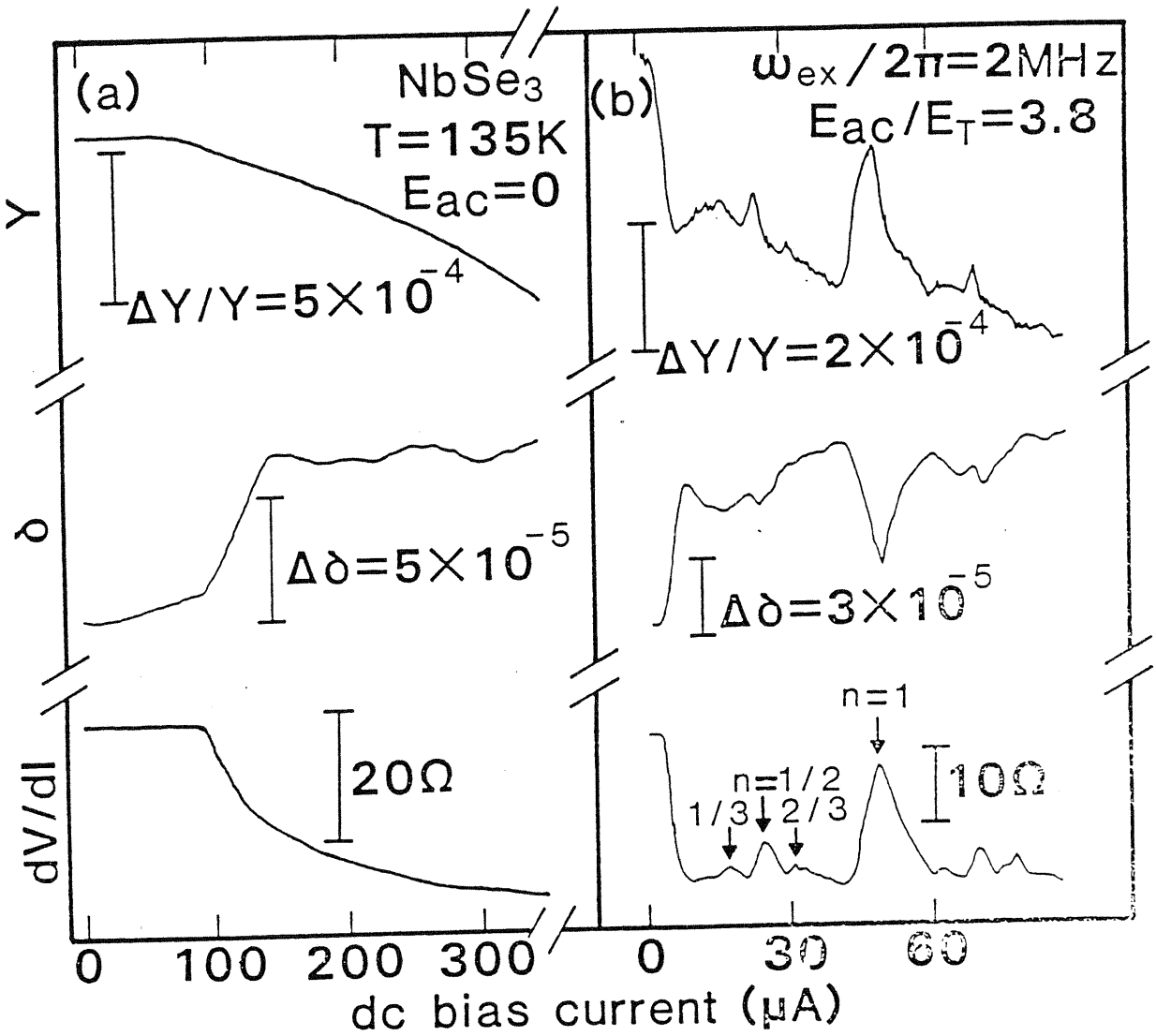

Fig. 12. Y, δ, and dV/dI as functions of dc bias in the upper CDW state of $NbSe_3$, (a) with $E_{ac}=0$, and (b) with $E_{ac}/E_T=3.8$. In (b), harmonic and subharmonic Shapiro step structure is observed in dV/dI (vertical arrows) with corresponding anomalies in Y and δ. During the electronic interference, dV/dI, Y, and δ tend toward their respective values assumed in the pinned CDW state. (a: Sample $NbSe_3$#35. R=220Ω, I_T=82μA, Length=1.1mm.

b: Sample $NbSe_3$#33. R=214Ω, I_T=100μA, Length=1.0mm).

trace, Shapiro step interference peaks are identified with corresponding values of n. Both harmonic and subharmonic steps are observed. The n=1/1 peak is dominant and displays nearly complete mode locking. The Y and δ traces in Fig. 12b show that the electronic mode locking is associated with striking anomalies in Y and δ, for harmonic as well as subharmonic interference. As previously demonstrated for TaS_3, in $NbSe_3$ Y and δ during mode lock approach the values appropriate to the pinned CDW state. In $NbSe_3$ there is an approximate scaling between the degree of mode lock and the magnitude of the elastic anomalies (peak in Y and dip in δ). For example, the dominant electronic interference peak at n=1/1 is associated with the largest anomalies in Y and δ.

3. Models and Discussion

CDW dynamics have been of considerable theoretical interest since the revival of Fröhlich's theory of superconductivity[1]. Models have been advanced which treat the CDW as a quantum system in which the CDW electrons coherently tunnel across an impurity pinning gap[18], or as a classical medium with[19-21] or without[22] internal degrees of freedom. Such models have been surprisingly successful in accounting for the electronic CDW response to applied electric fields, but in general the elastic response is not addressed.

In the absence of pinning and neglecting amplitude fluctuations, the phase φ of the CDW may be treated as a classical field and related to a (one dimensional) Lagrangian[23]

$$\mathcal{L} = n_1[(m^*/2)(1/2K_F)^2(d\phi/dt)^2 - (\kappa/2)(d\phi/dx)^2] \qquad (2-1)$$

where n_1 is the one-dimensional CDW carrier concentration, m^* is the effective mass of CDW carriers, k_F is the Fermi wavevector, and κ is a phenomenological elastic

constant of the CDW given by $\kappa=hv_F/2\pi$. Including the effects of impurities and dissipation leads to an equation of motion[24]

$$d^2\phi/dt^2 + (1/\tau)d\phi/dt + \omega_o{}^2\sin(\phi) + (m/m^*)hv_F{}^2d^2\phi/dx^2 = 2k_FeE/m^* \quad (2-2)$$

where τ is the CDW damping time, m is the electron (band) mass, ω_o is the CDW pinning frequency, and E is the applied electric field. Assuming that the CDW phase varies only slowly in space, Eq. (2-2) leads to a simplified equation of motion for the collective CDW phase

$$d^2\phi/dt^2 + (1/\tau)d\phi/dt + \omega_o{}^2\sin(\phi) = 2k_FeE/m^* \quad (2-3)$$

as first derived by Grüner, Zawadowski, and Chaikin[22]. Eq. (2-3) has been used extensively as a first order model to describe dc, ac, and coupled ac+dc electronic dynamics of the CDW condensate[12]. However, since the CDW is here described as a rigid particle in a rigid periodic pinning potential, all elastic effects are absent, and Eq. (2-3) can at best only describe the behavior of dV/dI in the presence of applied electric field; Y and δ are absent from the model.

A number of models have been advanced which specifically address elastic properties of CDW conductors. Coppersmith and Varma[25] have calculated the shift in longitudinal sound velocity (phonon frequency) for the underlying deformable lattice due to a sliding CDW. The predicted softening of the lattice due to CDW depinning is, however, found to be orders of magnitude smaller than that observed experimentally. Mozurkewich et al.[4,5] have suggested that the total stiffness of a CDW crystal can be separated into contributions from the CDW condensate (Y_C) and the underlying lattice (Y_L). For a pinned CDW, the stiffnesses are additive, $Y=Y_C+Y_L$, while for a fully depinned CDW, Y_C is decoupled from the lattice, hence $Y=Y_L$. Estimated changes in

Y_C/Y_L, based on the Lee-Rice[26] and Fukuyama-Lee[27] models, yield[4,5] values of order 1%. The coupled phason-phonon approach thus yields elasticity anomalies within the range of experimentally observed shifts, and provides good evidence that the lattice softening upon CDW depinning is indeed due to decoupling of the CDW from the underlying lattice. Littlewood[28] has further suggested second order contributions to Y arising from screening effects, where strain gradient terms are coupled to CDW phase gradients. In the limit of large dc bias fields, Littlewood finds a slow saturation of Y, with $\Delta Y/Y \sim (E_{dc})^{-1/2}$.

Brill et al[6] have applied standard anelastic relaxation theory to describe the detailed behaviors of Y and δ. Assuming a single relaxation time τ_o, the frequency dependent elastic constants become

$$Y(\omega) = Y(0) + F\omega^2\tau_o^2/(1 + \omega^2\tau_o^2) = Y(\infty) - F/(1 + \omega^2\tau_o^2) \qquad (2-4)$$

$$\delta = F\omega\tau/(1 + \omega^2\tau_o^2) \qquad (2-5)$$

where F is an (unspecified) internal variable of the system, perhaps related to temperature. By assuming constant F and a relaxation time $\tau_o=(1.5/\omega)[E_T/(E_{dc}-E_T)]^{0.75}$, Eqns. 2-4 and 2-5 produce Y and δ versus E_{dc} curves with functional forms similar to Y and δ experimentally observed in TaS_3, but with incorrect magnitudes (experimentally, changes in Y dominate those in δ, while Eqns. 2-4 and 2-5 predict comparable shifts[6]). Brill et al[6] find that, within the anelastic relaxation model, the experiments suggest a field dependent relaxation strength, such as $F(E_{dc},\tau_o)$ increasing with E_{dc} for $\tau_o<<\omega^{-1}$. Jericho and Simson[7] have proposed a related model, with a temperature and field dependent relaxation strength and relaxation time, to account for high frequency ultrasonic pulse

propagation in TaS_3.

The CDW condensate and underlying lattice can be treated as coupled deformable media obeying classical mechanics[8,29,30]. Sneddon[30] has considered the case of an incommensurately pinned CDW in the presence of applied dc fields E_{dc}. For $E_{dc}>E_T$, Y and δ assume forms similar to those predicted by Eqns. 2-4 and 2-5, with δ displaying a broad maximum near $E_{dc}/E_T=2$. A sharp anomaly (peak) in Y is also found for E_{dc} near E_T. Sneddon's model suggests an important role played by internal CDW degrees of freedom in determining the behavior of δ. A related model suggested by Sherwin et al.[9,29] treats the deformable CDW interacting (via an impurity pinning potential and CDW damping) with a deformable underlying lattice. In its simplest form, the equations of motion for the CDW and lattice are[9]

$$m^*d^2r/dt^2 + \gamma_c d(r-x)/dt + k_c r + eE_T\sin[2k_F(r-x)]=e[E_{dc}+E_{ac}\cos(\omega_{ex}t)] \quad (2-6)$$

$$Md^2x/dt^2 + \Gamma_L dx/dt + \gamma_c d(x-r)/dt + K_L x + eE_T\sin[2k_F(x-r)] = F\cos(\omega_r t) \quad (2-7)$$

where r and x are respectively the positions of the CDW center of mass and lattice, m^* is the total CDW effective mass, M_L the lattice mass, γ_c and Γ_L respectively the total CDW damping and internal lattice friction. k_c and K_L parameterize respectively the total elasticity of the CDW and underlying lattice, and $F\cos(\omega_r t)$ is the mechanical force applied to the lattice. Eqns. 2-6 and 2-7 have been solved in the limit of clamped-clamped boundary conditions for applied dc fields E_{dc}, ac fields $E_{ac}\cos(\omega_{ex}t)$, and combined ac+dc fields[29]. In the limit of finite E_{dc}, $E_{ac}=0$, Eqns. (2-6) and (2-7) predict shifts in Y due to CDW depinning consistent with experiment and in accord with the stiffness of the CDW condensate; the predicted increases in δ are also consistent with experiment[29]. The model fails in the critical region $E_{dc}=E_T^+$ where, as expected, square root singularities dominate. In the limit of finite E_{dc} and E_{ac}, the

predictions of Eqns. (2-6) and (2-7) are in agreement with lattice softening by an ac field and a recovery of lattice stiffness on mode locked steps[29]. The following discussion considers the importance of incorporating internal degrees of freedom of the CDW condensate in the interpretation of electro-elastic CDW phenomena.

a. Finite E_{ac}; $E_{dc}=0$

Figs. 2-6 clearly demonstrate that the stiffness of a TaS_3 crystal is decreased by application of an external ac electric field. The decrease is a sensitive function of the ac amplitude and frequency, with stronger effects occurring for larger ac amplitude and smaller ac frequency. For $E_{ac}>E_T$, Fig. 5 shows that ac electric fields with frequency in excess of approximately 10MHz have no effect on Y, while at very low frequencies the dc limit of $\Delta Y/Y$ is recovered. This suggests that the lattice softening is a direct result of CDW motion (i.e. displacement). Because of the finite damping of the CDW, ac-induced displacement of the CDW from equilibrium becomes more limited at higher frequencies. Hence, at high frequencies the CDW remains strongly tied to the lattice, and Y remains large at $Y=Y_C+Y_L$. At low frequencies, the CDW displacement from the equilibrium becomes large; at low enough ω_{ex} the CDW is for much of the cycle essentially depinned. In the limit $\omega_{ex}\text{-->}0$, the dc value for $\Delta Y/Y$ of a depinned CDW is then naturally obtained, and in the limit $E_{ac}\text{--> }\infty$, saturation at $Y=Y_L$ is expected.

For $E_{ac}<E_T$ the situation is similar, with $\Delta Y/Y$ becoming larger in magnitude with decreasing ω_{ex}, as observed in Fig. 6. The distinction here, when compared to the results of Fig. 5, is that as ω_{ex} tends to zero the dc limit is <u>not</u> approached smoothly, since $\Delta Y/Y=0$ at $\omega_{ex}=0$. This feature reflects the fact that, for $E_{ac}<E_T$, the CDW motion or displacement is zero at zero frequency[31].

An important question is whether there exists a simple relation between $\Delta Y/Y$ and the maximum CDW displacement X_o for a given frequency ω_{ex}. As a first

approximation to the CDW displacement in the presence of E_{ac}, the CDW and lattice elasticity are neglected altogether and the "rigid particle" motion of Eq. (2-3) is assumed. The maximum displacement is then[11]

$$X_o = (eE_{ac}\omega_o^{-2}/m^*)[1 + (\omega_{ex}/\omega_o^2\tau)^2]^{1/2}. \qquad (2-8)$$

Eq. (2-8) has been used to describe ac-induced enhancement of the low-field dc conductivity in $NbSe_3$ and TaS_3, and there provides excellent quantitative fits[11,13]. The form

$$\Delta Y/Y = c_2 X_o \qquad (2-9)$$

is assumed, with c_2 a normalization constant. Eq. (2-9) provides a good fit to the data of Fig. 5. The solid line in Fig. 5 is Eq. (2-9), with fitting parameters $\omega_o^2\tau$=0.4MHz and $c_2eE_{ac}/m^*\omega_o^2 = -4x10^{-3}$. On the other hand, the value used for the "crossover" frequency $\omega_o^2\tau$ is unrealistically small in light of ac conductivity experiments[32] on TaS_3 which show $\omega_o^2\tau \approx 900$MHz. This rules out simple rigid particle displacement as being the sole origin of the the ac-induced lattice softening.

Ac conductivity provides an independent probe of averaged CDW displacement. Even for $E_{ac} << E_T$, the CDW electronic response in TaS_3 and $NbSe_3$ is highly nonlinear. Stokes et al[33] have demonstrated a highly E_{ac}- and ω_{ex}-dependent complex dielectric function ε in TaS_3 in the frequency range $\omega_{ex}/2\pi$=3KHz to 1MHz. They find a dielectric constant which, with increasing E_{ac}, deviates markedly from its E_{ac}-->0 value, the deviation being more severe at lower frequency. This behavior is analogous to the elastic data of Fig. 5. Stokes et al. conclude that the E_{ac} dependence of ε is inconsistent with rigid motion of the CDW condensate, and suggest a distribution of pinning fields; such a distribution introduces new degrees of freedom. A direct

comparison between $Y(E_{ac})$ and $\varepsilon(E_{ac})$ is complicated by the fact that the electronic response is highly nonlinear for E_{ac}-->E_T. For a sinusoidal electric field excitation, a non-sinusoidal response follows, and only the Fourier component of the response at ω_{ex} contributes to ε. In the elastic measurements, on the other hand, all Fourier components of the electronic response may couple into ΔY, which is measured mechanically in the limit of linear mechanical response.

The coupled Eqns. (2-6) and (2-7), which take both CDW and lattice elasticity into account, predict[29] a decrease in Y with increasing E_{ac}, even with $E_{ac}<<E_T$. This is a direct result of the multiple degrees of freedom of the CDW condensate (parameterized by k_c) in the model, which again suggests an important role played by CDW incoherence in the elastic properties of a CDW crystal.

Independent of any particular model, the sharp anomaly in the $\Delta Y/Y$ behavior of Fig. 6 as ω_{ex}-->0 is suggestive of critical behavior. If $\Delta Y/Y$ is assumed to have the form

$$\Delta Y/Y = C[\omega_{ex}/2\pi - \omega_{cr}/2\pi]^{-\alpha}, \qquad (2-10)$$

with C a constant, then the dashed line of Fig. 6 may again be fit with α=0.867 and C=108 (assuming $\omega_c<<\omega_{ex}$). From the limited data points of Fig. 6 the value of ω_{cr} cannot be determined.

b. Finite E_{ac}, Finite E_{dc}

In the presence of dc electric fields E_{dc} alone, Y and δ in TaS_3 and $NbSe_3$ are unaffected by the dc field until E_{dc} exceeds E_T. Fig. 7 demonstrates that the same holds true also in the presence of an additionally applied ac field E_{ac}. In effect, the lattice softening and increase in internal friction generated by E_{ac} (with E_{dc}=0) define new effective "pinned" values for Y and δ. Deviations in Y and δ from the "pinned" values

are apparently first observed at $E_{dc}=E_T'$, the dc threshold field measured in the presence of the ac field.

The reduction of E_T with increasing E_{ac} has been previously discussed for $NbSe_3$ and TaS_3 from an electronic transport point of view. The conductivity observations are consistent with Eq. (2-3), the simple rigid particle description, or a quantum tunneling mechanism[11-14]. In the analysis of the electronic behavior, it is generally assumed that the magnitude of the periodic pinning potential is unaffected by E_{ac}; the ac field simply helps the CDW overcome the fixed pinning potential barrier, leading to enhanced dc conductivity. Since pinning of the CDW involves CDW phase fluctuations and the underlying lattice structure (containing the impurity atoms), the question naturally arises if the reduction in E_T due to E_{ac} may in fact be due solely to the softening of the lattice elasticity. A careful comparison between Fig. 8 (which shows I_T' versus E_{ac}) and Fig. 3 (which shows Y versus E_{ac}) indicates that there exists no simple relationship between I_T' and Y: for small E_{ac}, $\Delta Y/Y$ vanishes asymptotically as E_{ac}-->0, while I_T' decreases linearly with increasing E_{ac} for small ac excitations. A similar lack of direct correspondence between Y and E_T is found in the temperature dependences of those parameters in $NbSe_3$ and TaS_3 (measured with $E_{ac}=0$).

A constant local pinning potential barrier is assumed also in Eqns. (2-6) and (2-7). The predicted reduction in E_T with increasing E_{ac} in that model is very similar to that associated with rigid particle behavior[11]. The corresponding elastic properties predicted[29] by Eqns. (2-6) and (2-7) demonstrate breaks in Y and δ as functions of E_{dc} which correspond precisely to E_T', the threshold field for CDW depinning. This is consistent with experiment and is a consequence of the assumption $Y = Y_L + Y_C$.

In the discussion of original elasticity experiments on TaS_3 in the presence of dc electric fields, it was suggested[2] that the functional forms of Y and δ may be directly related to the CDW drift velocity v_d. The data of Figs. 10 and 12, which shows the

elastic properties during Shapiro step electronic interference, demonstrates that this is clearly not the case for TaS_3 or $NbSe_3$. During Shapiro step interference, a portion (macroscopic domain) of the CDW condensate becomes mode locked to the external ac drive, effectively fixing the CDW drift velocity of that domain at $v_d = J_{CDW}/n_c e = \lambda(p/q)\omega_{ex}/2\pi$, with λ the CDW wavelength. J_{CDW} is the excess current carried by the CDW through the macroscopic domain. If Y and δ were strictly functions of v_d, then mode locking would result in regions of constancy in the Y and δ versus I_{dc} curves, in sharp contrast to the strong peak anomalies observed in Fig. 10 for TaS_3 and in Fig. 12 for $NbSe_3$.

As mentioned previously, during mode locking the behavior of Y and δ is to tend toward the value characteristic of the "pinned", $I_{dc}=0$ state; the same holds true for dV/dI. In general, in a dV/dI interference experiment the interference peaks do not attain the ohmic value. Consequently the height h of the dV/dI peak (measured from the effective baseline, neglecting the peak structure) is only a fraction of the maximum possible peak height[34] $h_{max} = [(dV/dI)_{Idc=0}] - [(dV/dI)_{unlocked}]$. This is clearly observed in Fig. 12b for $NbSe_3$, where the n=1/1 interference peak in dV/dI has $h/h_{max}=0.75$, suggesting that the locked domain comprises 75% of the sample volume, while for the n=1/2 peak $h/h_{max}=0.25$, suggesting that the locked domain comprises 25% of the sample volume for this interference. As seen in the Y and δ traces in the same figure, the corresponding peak anomalies in Y and δ show nearly identical scaling. For example, the n=1/1 interference peak corresponds to an anomaly in Y which reaches (correcting for the sloping baseline) approximately 75% of the $I_{dc}=0$ value; the same holds true for the n=1/1 anomaly in δ. Similar 25% peak heights are observed in Y and δ during the n=1/2 interference. This suggests that a fully mode locked CDW, with $h/h_{max}=1$, would display elastic constants indistinguishable from the "pinned", $I_{dc}=0$ state.

On the other hand, the data of Fig. 10b, appropriate to TaS_3, shows a rough but

inexact scaling between the anomalies in dV/dI, Y, and δ. In particular, the smaller dV/dI peak at I_{dc}=64μA is associated with the larger peak anomalies in Y and δ. This suggests that the mode locked region associated with this interference peak might be physically located near the clamped region of the crystal, where small changes in local elastic constants have a strong influence on the elastic properties determined for the overall crystal.

The behavior of Y and δ during electronic mode locking suggests that Y_L and Y_C again couple strongly during mode lock and $Y = Y_L + Y_C$. This is not an obvious result, since during mode lock the CDW dynamics are determined primarily by the external ac field. Hence one might expect that Y_L and Y_C fully decouple during mode lock, yielding $Y=Y_L$. The experimental results show this to not be the case, and argue strongly that internal degrees of freedom of the CDW condensate are central to the elastic anomalies. Although the behavior of Y and δ during mode locking has not been investigated in the framework of anelastic relaxation models, it is apparent that if the functional forms of Y and δ versus E_{dc} are the direct result of CDW incoherence, then an increase in CDW coherence, such as that resulting from electronic mode locking, will lead to peak structure in Y and δ during mode lock.

CDW incoherence arising from CDW internal modes is central to Eqns. (2-6) and (2-7), which predict electronic mode locking in the presence of combined dc and ac electric fields. The model also predicts corresponding sharp peak anomalies in Y and δ in excellent agreement with experiment. Fig. 13 shows an analog computer solution[29] of Eqns. (2-6) and (2-7) for dV/dI, Y , and δ, for an ac drive field E_{ac}/E_T=5 and with $\omega_{ex}/\omega_o{}^2\tau = 0.05$. It is apparent that, during electronic mode locking, Y and δ tend toward their "pinned", I_{dc}=0 values, consistent with the experimental results of Figs. 10b and 12b. In the model, the behaviors of Y and δ during mode lock reflects a reduction in effective internal degrees of freedom; the CDW phason couples strongly to the underlying phonon structure, and $Y = Y_L + Y_C$.

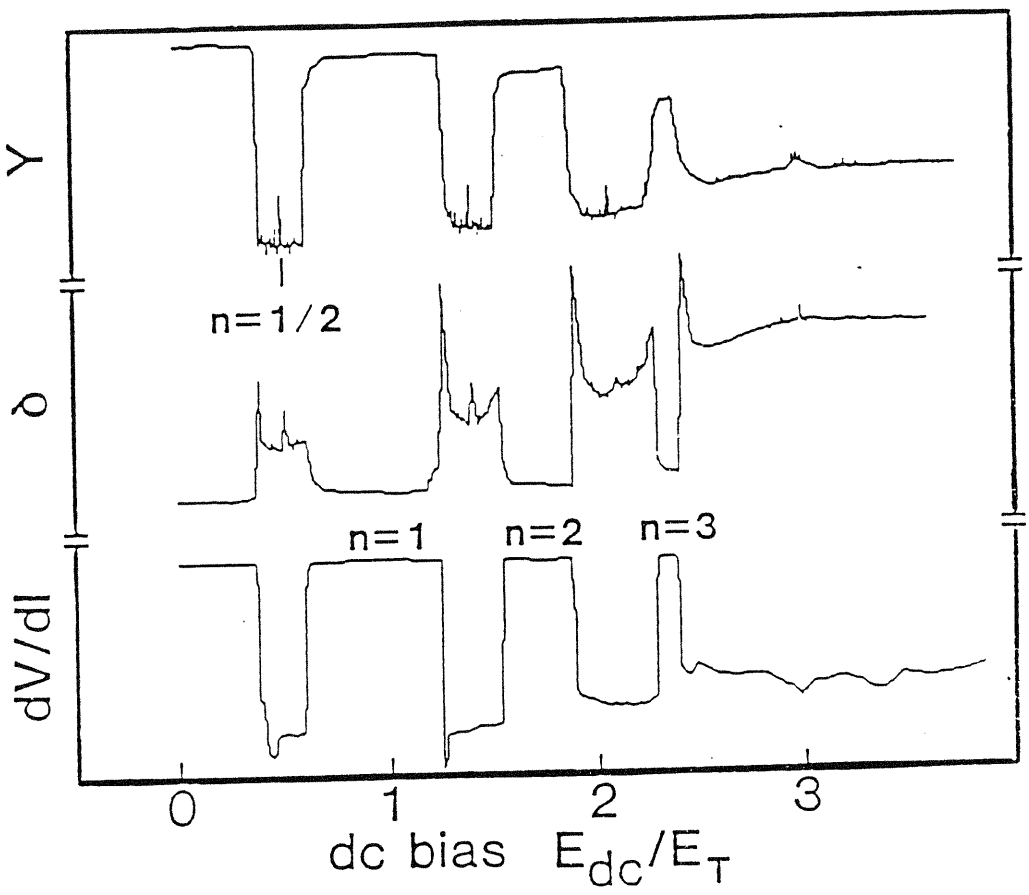

Fig. 13. Y, δ, and dV/dI as calculated from a many-degree-of-freedom model (Eqs. (6a) and (6b)). Interference structure is observed analogous to that found experimentally in TaS_3 and $NbSe_3$ (Figs. 10 and 12). The calculated curves are from ref. 29.

A reduction in internal degrees of freedom during electronic mode locking has been observed in other CDW transport measurements, in particular the broad band noise. During complete ($h/h_{max}=1$) mode locking, broad band noise generated by a moving CDW is fully eliminated[17]. Since the source of the broad band noise may be interpreted as arising from CDW incoherence, the vanishing of the noise is evidence for a "freeze out" of effective internal degrees of freedom during mode locking. Hence there may exist a fundamental correspondence between the broad band noise and the elastic properties of CDW conductors. Note also that the decrease in δ caused by an ac field in the sliding CDW state of TaS_3 at 115K (Fig. 9) could be the result of ac-induced coherence between CDW domains. Strong ac fields applied to CDW conductors result in enhanced CDW electronic phase homogenization, as evidenced by the suppression of broad band noise by large amplitude ac fields[17], the independence of Shapiro step quality on the narrow band noise spectrum[16], and an increased resistance to splitting of mode-locked regions in the presence temperature gradients[35]. An analogous elastic process in a conventional metal is the substantially greater (at certain frequencies and temperatures) internal friction δ for a polycrystalline specimen than for a single crystal specimen; this results from relaxation of domain boundaries under stress[36]. In TaS_3, the narrow band noise spectrum becomes extremely complex as the temperature is lowered[37], signifying increased disorder and generation of multiple current domains at lower temperatures. This may explain why δ decreases dramatically with increasing ac field amplitude in TaS_3 at low temperatures, as demonstrated for the region $I_{dc}/I_T>2$ in Fig. 9.

Section 4. Conclusion

Measurement of the elastic properties of TaS_3 and $NbSe_3$ in the presence of ac and combined ac and dc electric fields has revealed important results complementary to those previously obtained in the limit of dc fields alone. Lattice softening in the

presence of ac fields with $E_{ac}<E_T$ demonstrates that the CDW need not be depinned in the Fröhlich sliding mode sense to achieve a decrease in Y, but need only be in motion on a local scale. The behavior of Y and δ on electronically mode-locked steps demonstrates that the CDW drift velocity alone does not dictate elastic properties in the sliding state, and that an absolutely essential role is played by the internal degrees of freedom of the CDW condensate. The assumption that $Y = Y_L + Y_C$ in the pinned and mode locked states, and $Y = Y_L$ in the sliding state, appears valid.

The strong correspondence between the elastic and electronic properties of CDW conductors has important implications for the interpretation of previously obtained electronic response parameters[1]. It is also apparent that any complete model of CDW electronic response must incorporate in a fundamental way coupling of the deformable CDW (obeying classical or quantum dynamics) to the deformable lattice.

CHAPTER 2 REFERENCES

1. For recent reviews, see G. Grüner and A. Zettl, Phys. Rep. 119, 117 (1985); Electronic Properties of Inorganic Quasi-One-Dimensional Materials, vols. 1&2, P. Monceau, ed. (Reidel, Dordecht, 1985); Charge Density Waves in Solids, Gy. Hutiray and J. Solyom, eds. (Springer, New York, 1985).

2. J.W. Brill and W. Roark, Phys. Rev. Lett. 53, 846 (1984).

3. J.W. Brill, in Charge Density Waves in Solids, Gy. Hutiray and J. Solyom, eds. (Springer, New York, 1985) p. 347.

4. G. Mozurkewich, P.M. Chaikin, W.G. Clark, and G. Grüner, in Charge Density Waves in Solids, Gy. Hutiray and J. Solyom, eds. (Springer, New York, 1985) p. 353.

5. G. Mozurkewich, P.M. Chaikin, W.G. Clark, and G. Grüner, Solid State Commun. 56, 421 (1985).

6. J.W. Brill, W. Roark, and G. Minton, Phys. Rev. B33, 6831 (1986).

7. M.H. Jericho and A.M. Simpson, Phys. Rev. B34, 1116 (1986).

8. X. D. Xiang and J.W. Brill, Phys. Rev. B36, 2969 (1987).

9. L.C. Bourne, M.S. Sherwin, and A. Zettl, Phys. Rev. Lett. 56, 1952 (1986).

10. L.C. Bourne and A. Zettl, Phys. Rev. B36, 2626 (1987).

11. G. Grüner, W.G. Clark, and A.M. Portis, Phys. Rev. B24, 3641 (1981).

12. A. Zettl and G. Grüner, Phys. Rev. B29, 755 (1984).

13. G. Grüner and A. Zettl, Phys. Rep. 119, 117 (1985).

14. J.R. Tucker, J.H. Miller, Jr., K. Seeger, and J. Bardeen, Phys. Rev. B25, 2979 (1982); R.E. Thorne, W.G. Lyons, J.W. Lyding, J.R. Tucker, and John Bardeen, (unpublished).

15. A. Zettl and G. Grüner, Solid. State Commun. 46, 501 (1983).

16. R.P. Hall and A. Zettl, Phys. Rev. B30, 2279 (1984).

17. M.S. Sherwin and A. Zettl, Phys. Rev. B32, 5536 (1985).

18. J. Bardeen, Phys. Rev. Lett. 45 1978 (1980).

19. L. Sneddon, M.C. Cross, and D.S. Fisher, Phys. Rev. Lett. 49, 292 (1982).

20. L. Sneddon Phys. Rev. B29, 719 and 725 (1984); Phys. Rev. Lett. 52, 65 (1984).

21. P.B. Littlewood 33, 6694 (1986).

22. G. Grüner, A. Zawadowski, and P.M. Chaikin, Phys. Rev. Lett. 46, 511 (1981).

23. A.J. Berlinsky, Rep. Prog. Pnys. 42, 1243 (1979).

24. See, for example, H. Fukuyama and H. Takayama, in Electronic Properties of Inorganic Quasi-One-Dimensional Materials, vol. 1, P. Monceau, ed. (Reidel, Dordecht, 1985)p. 41.

25. S.N. Coppersmith and C.M. Varma, Phys. Rev. B30, 3566 (1984).

26. P.A. Lee and T.M. Rice, Phys. Rev. B19, 3970 (1979).

27. H. Fukuyama and P.A. Lee, Phys. Rev. B17, 535 (1978).

28. P.B. Littlewood, (unpublished).

29. M.S. Sherwin and A. Zettl, Physica D 23, 62 (1986)

30. L. Sneddon, Phys. Rev. Lett. 56, 1194 (1986).

31. Of course, with finite $E_{dc}<E_T$ the CDW becomes polarized, and hence there is a finite static displacement from true "equilibrium". However, curve A in Fig. 2 (see also refs. 4-6) shows that both Y and δ are insensitive to dc CDW polarization as long as $E_{dc}<E_T$. In other words, the elastic properties of a static CDW are insensitive to local metastable state configurations.

32. S. Shridar, D. Reagor, and G. Grüner, Phys. Rev. Lett. 55, 1196 (1985).

33. J.P. Stokes, M.O. Robbins, and S. Bhattacharya, Phys. Rev. B32, 6939 (1985).

34. A. Zettl, Physica D (in press).

35. M.F. Hundley and A. Zettl, Phys. Rev. B33, 2883 (1986).

36. A.S. Nowick and B.S. Berry, Anelastic Relaxation in Crystalline Solids, (Academic Press, New York, 1972) p. 439.

37. A. Zettl and G. Grüner, Phys. Rev. B28, 2091 (1983).

CHAPTER 3

ISOTOPE SUBSTITUTIONS IN HIGH-TEMPERATURE SUPERCONDUCTORS

Section 1: Introduction

The discovery that the superconducting transition temperature T_c in mercury was dependent on the isotopic mass M of the mercury atoms[1] was the first experimental evidence that superconductivity was related to lattice vibrations, and provided one of the important clues leading to the Bardeen-Cooper-Schrieffer (BCS) theory[2] of superconductivity, in which electron pairing occurs through the electron-phonon interaction. According to the simple BCS model, T_c is directly proportional to the Debye frequency ω_D, which in turn goes as $M^{-0.5}$ in an ideal harmonic solid. In real materials, T_c is proportional to $M^{-\alpha}$, with α usually ranging between 0 and 0.5 (see table I). When the electron-phonon interaction and the coulomb repulsion are treated separately in a two-square-well model[4] within BCS theory, α is reduced from the 0.5 value of the BCS model:

$$\alpha = \frac{1}{2}\left[1 - \left(\frac{\mu^*}{\lambda - \mu^*}\right)^2\right] \qquad (3\text{-}1)$$

where λ and μ^* are the phonon and effective coulomb interaction parameters. Most of the experimental values of α can be explained[3] within this model.

We have made isotope substitutions of O, Ba and Cu in the 90 K superconductor $YBa_2Cu_3O_7$, and O isotope substitutions in the 40 K superconductor $La_{1.85}Sr_{0.15}CuO_4$, to test for isotope effects in the high-T_c oxides. The experimental techniques and results are presented in this chapter, followed by discussions of other experimental work and of recent theoretical approaches to the isotope work. Most of this work has been reported in the scientific literature[5-7]; a number of other groups have also published results on this topic[8-15].

"Best" Experimental Values for β Obtained in Fitting the Relation $T_c \propto M^{-\beta}$ Compared with the Theoretical Value of BCS (*1*), Swihart (*22,23*), Morel and Anderson (*9*), and Garland (*26*)

Element	β_{expt}	β_{BCS}	β_{SWI}	β_{MA}	β_{GAR}	$\beta_{GAR(latest)}$
Zn	0.45 ± 0.01 / 0.30 (*27*)	0.5	0.2	0.35	0.40	0.415 ± 0.015
Cd	0.50 ± 0.10	0.5	0.2	0.34	0.37	0.385 ± 0.025
Hg	0.50 ± 0.03	0.5	0.4	0.46	0.465	0.48 ± 0.005
Al		0.5	0.3	0.34	0.35	0.37 ± 0.025
Tl	0.50 ± 0.10	0.5	0.3	0.43	0.45	0.48 ± 0.02
Sn	0.47 ± 0.02	0.5	0.3	0.42	0.44	0.455 ± 0.01
Pb	0.48 ± 0.01	0.5	0.3	0.47	0.47	0.485 ± 0.005
Ti		0.5		0.25	0.2	0.145 ± 0.17
Zr	0.0	0.5		0.30	0.35	0.15 ± 0.17
V		0.5		0.41	0.15	0.25 ± 0.125
Ta		0.5		0.42	0.35	0.35 ± 0.075
Mo	0.33 ± 0.05	0.5	0.15	0.3	0.35	0.35 ± 0.075
Ru	0.0 ± 0.10	0.5	0.0	0.35	0.0	0.065 ± 0.15
Os	0.20 ± 0.05	0.5	0.1	0.25	0.1	0.225 ± 0.10
Ir		0.5		0.3	-0.2	-0.015 ± 0.17
Hf		0.5		0.5	0.3	0.1 ± 0.2
Re	0.39 ± 0.01	0.5		0.41	0.3	0.355 ± 0.05
U(α)	-2.2 ± 0.2	0.5	[(*32a*); see also (*198a*)].			

Table I. Experimental and theoretical values of the isotope shift in the elements, from reference 3. The parameter β is identical to the parameter α in the text. References in this table are found in ref. 3.

Section 2: Experimental

Since T_c is proportional to ω_D in the simple BCS model, one would expect that in the high-T_c oxide systems the high-frequency oxygen atomic vibrations would play a key role in the superconducting mechanism. At temperatures above about 500 C, oxygen can be reversibly removed from the $YBa_2Cu_3O_{7-\delta}$ system[8,15], making this an ideal system for studies of the oxygen isotope effect. Our samples were placed in platinum boats in quartz tubes that were sealed at one end, and then placed in an oven with the open ends of the tubes protruding from the oven. The tubes were connected to reservoirs of the desired oxygen isotopes, with the expectation that at sufficiently high temperatures the different isotopes would diffuse through the samples, eventually establishing the same isotope ratios for a given sample and its reservoir. Since the samples are formed by solid state reaction of micron-sized powders of the constituent oxides, it is reasonable to expect high oxygen mobilities at the reaction temperature. Control samples were placed in identical quartz tubes next to the test samples, with identical oxygen reservoir systems.

Three techniques were used to determine oxygen isotope ratios in the samples. The simplest of these is the sample weight change: a substitution of ^{18}O for ^{16}O increases the sample weight by 2.1% in $YBa_2Cu_3O_7$ and by 2.0% in $La_{1.85}Sr_{0.15}CuO_4$. This technique is susceptible to errors from mechanical fracture, platinum contamination, changes in sample oxygen content and desorption of gases other than oxygen, but when performed carefully with a control sample, the error is usually less than 5%.

Thermally Programmed Desorption (TPD) was used to determine oxygen isotope ratios in $YBa_2Cu_3O_7$. The samples were heated in a vacuum, reducing oxygen stoichiometries to approximately $YBa_2Cu_3O_6$, with the desorbed oxygen sampled by a mass spectrometer. The samples were then heated in flowing hydrogen, with the

resulting water vapor again sampled by a mass spectrometer. A total of 50% of the oxygen was removed in this way, reducing the samples to Y_2O_3, BaO and Cu metal. The isotope ratios did not vary between runs in vacuum and in hydrogen gas, showing no site selectivity for the oxygen isotopes.

Probably the most accurate technique of isotope determination available to us is Laser-assisted Ion Mass Analysis (LIMA), which is run by Luis Bernardez and John Kinney at the Lawrence Livermore National Laboratory. A laser with a 4 eV beam pulse and power densities of up to 10^{11} W/cm^2 vaporizes and ionizes a small portion of the sample and passes the products through a series of ion optics and finally a time-of-flight mass spectrometer. The sensitivity level for the technique is quoted at about 1% for differentiation of isotopes of a given element. To test for spatial variation of isotopic ratios within the sample, tests were performed on the original sample surface, on freshly cleaved sample surfaces, and as a function of depth by drilling holes up to several microns deep with the laser. The laser power was varied from levels barely high enough to produce ions up to levels that produced ionization values of five or more, and both negative and positive ions were tested, to search for any possible chemical effects related to the ionization process. There was essentially no variation of isotopic ratios for any of these tests; our samples had a uniform isotope distribution, with ratios that were in good agreement with the other tests of isotope substitution.

a. $La_{1.85}Sr_{0.15}CuO_4$

$La_{1.85}Sr_{0.15}CuO_4$ samples were prepared by mixing La_2O_3, $SrCO_3$ and CuO in a ball mill with acetone, then drying and calcining on a platinum sheet at 900 C for 6 hours. The material was then ground in an agate mortar, pressed into pellets, heated to 1050 C for 20 hours and then slowly cooled. All heat treatments were done in flowing oxygen. The resulting dense sintered pellets were ground again in an agate mortar and re-pressed, thus increasing the porosity and the oxygen diffusivity. Isotope exchanges

were performed as described above, using 92% enriched $^{18}O_2$. One set of samples ("C" and "D") was heated at a series of increasing temperatures to maximize the oxygen diffusion through the pellet before densification occurred, followed by a slow cool to maximize oxygen content; the heat cycle was 940 C for 10 hours, 1000 C for 3 hours, 1080 C for 2 hours, and 870 C for 5 hours followed by an oven cool. The oxygen pressures at room temperature were 728 torr in the ^{16}O reservoir and 745 torr in the ^{18}O reservoir, with both pressures increasing by about 4 torr at the highest temperatures. Another set of samples ("E") were prepared with identical pressures in the two reservoirs (755 torr at 20 C, increasing to 760 torr at 1050 C), with a heat cycle of 1050 C for 32 hours, 900 C for 3 hours, 760 C for 1 hour, and 540 C for 2 hours followed by an oven cool. Changes in sample weights indicated ^{18}O enrichments of 81% in sample "C" and 71% in sample "E", in reasonable agreement with LIMA measurements of 75%±2% in sample "C" and 78%±3% in sample "E". The two inequivalent O sites in $La_{1.85}Sr_{0.15}CuO_4$ each contain half of the oxygen, so these measurements show that both sites are accessible to oxygen isotope diffusion. Values of α were calculated assuming 76% enrichment in the ^{18}O samples, giving an average atomic mass of 17.52.

Magnetization measurements were performed on a SHE model VTS-805 SQUID magnetometer. Saturation magnetization values in polycrystalline $YBa_2Cu_3O_7$ were found to vary by up to 20% for repeated measurements of a given sample, presumably due to variations in flux trapping, but magnetization values of less than 50% of the saturation value were very reproducible; we therefore measured shifts in T_c only within this region. Below 50 K, the temperature calibration of the instrument was stable to within .01 K. A field of 33 Oe was used for samples "C" and "D", and a field of 23 Oe was used for samples "E". Resistance measurements were performed with four-point silver paint contacts, with the samples placed side by side on a copper bar next to a calibrated diode, surrounded by a copper heat shield. The samples were cooled

with a helium gas flow system. The T_c's were observed to vary by no more than 0.05 K when the sample positions were exchanged.

Figure 1 shows the magnetization data for samples "C" and "D". The shift in T_c is equal to 0.41±.03 K and does not vary with temperature for at least 6K below the superconducting onset, giving α=0.14±.01. For samples "E", in figure 2, the shift is again constant in temperature with a value 0.42±.04 K, giving α=0.15±.01. The resistive measurements give an isotope shift that varies with temperature. In figure 3, samples "C" and "D" show a shift of 0.31±.00 K (α=0.10±.00) in the onset region near 37 K, but the shift decreases to zero at 33 K and then increases again in the resistive tail at around 29 K, reaching values of up to 0.78 K (α=0.29). Samples "E" in figure 4 show a shift of 0.19±.03 K (α=.06±.01) in the onset region near 35 K, with the shift again decreasing to zero near 33 K. The resistive tail was absent in the "E" samples.

Magnetic susceptibility measurements are more representative of bulk superconducting properties than are resistive measurements. The observation of an isotope shift in the susceptibility that did not vary across the transition and was essentially the same for both sets of samples leads us to conclude that the value α=0.145±0.01 is the correct result in this compound. Resistance measurements select the lowest resistance current paths in the sample, and are thus easily affected by trace inhomogeneities in the samples. Phillips has suggested[32] (see discussion) that the isotope shift may depend on the Sr concentration; it is possible that material inhomogeneities are affecting the current paths in such a way as to cause the resistivity to sample different stoichiometries as the temperature is varied.

b. $YBa_2Cu_3O_7$

LIMA measurements have shown that when polycrystalline $YBa_2Cu_3O_7$ containing essentially pure ^{16}O is placed in an atmosphere of 95% $^{18}O_2$ at 950 C for

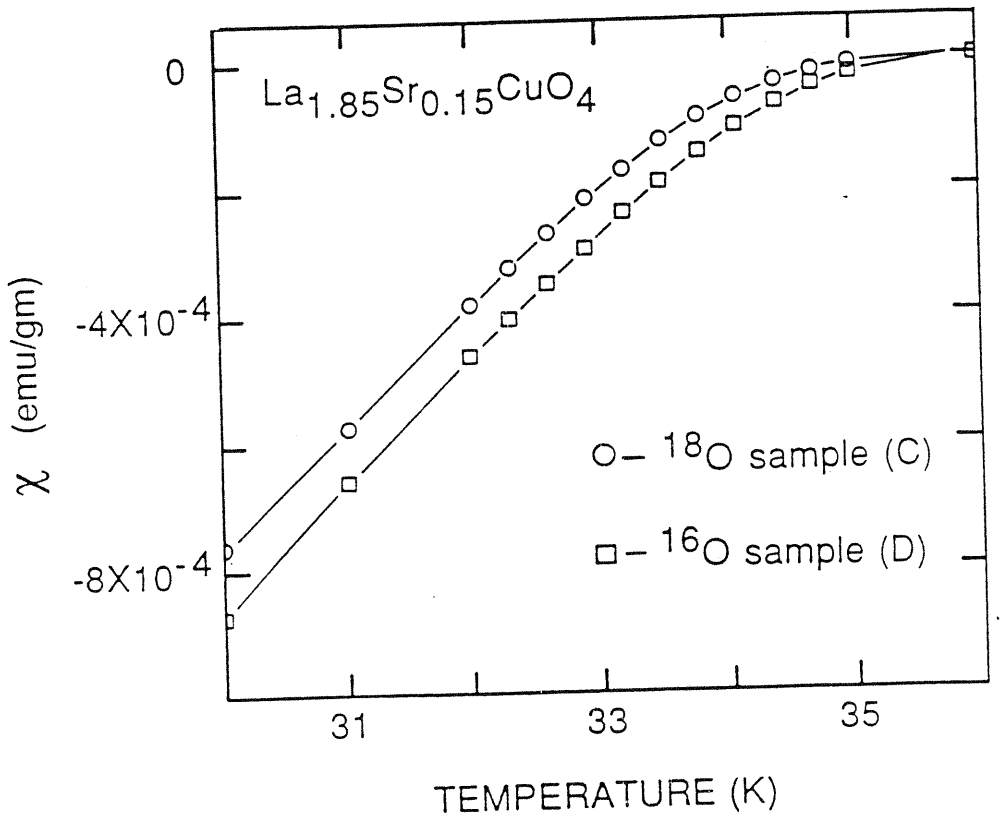

Fig. 1. Magnetic susceptibility vs. temperature for $La_{1.85}Sr_{0.15}CuO_4$ samples "C" and "D". (Measurement by S. Hoen and W.M. Creager).

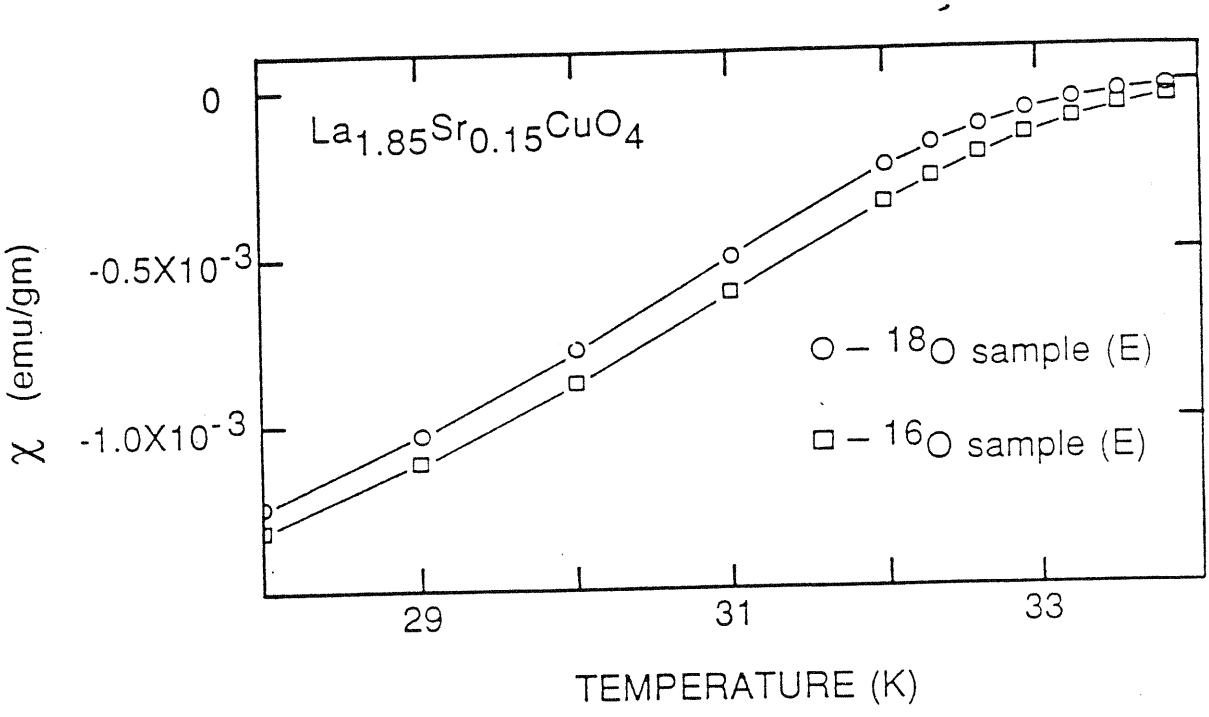

Fig. 2. Magnetic susceptibility vs. temperature for $La_{1.85}Sr_{0.15}CuO_4$ samples "E". (Measurement by S. Hoen and W.M. Creager).

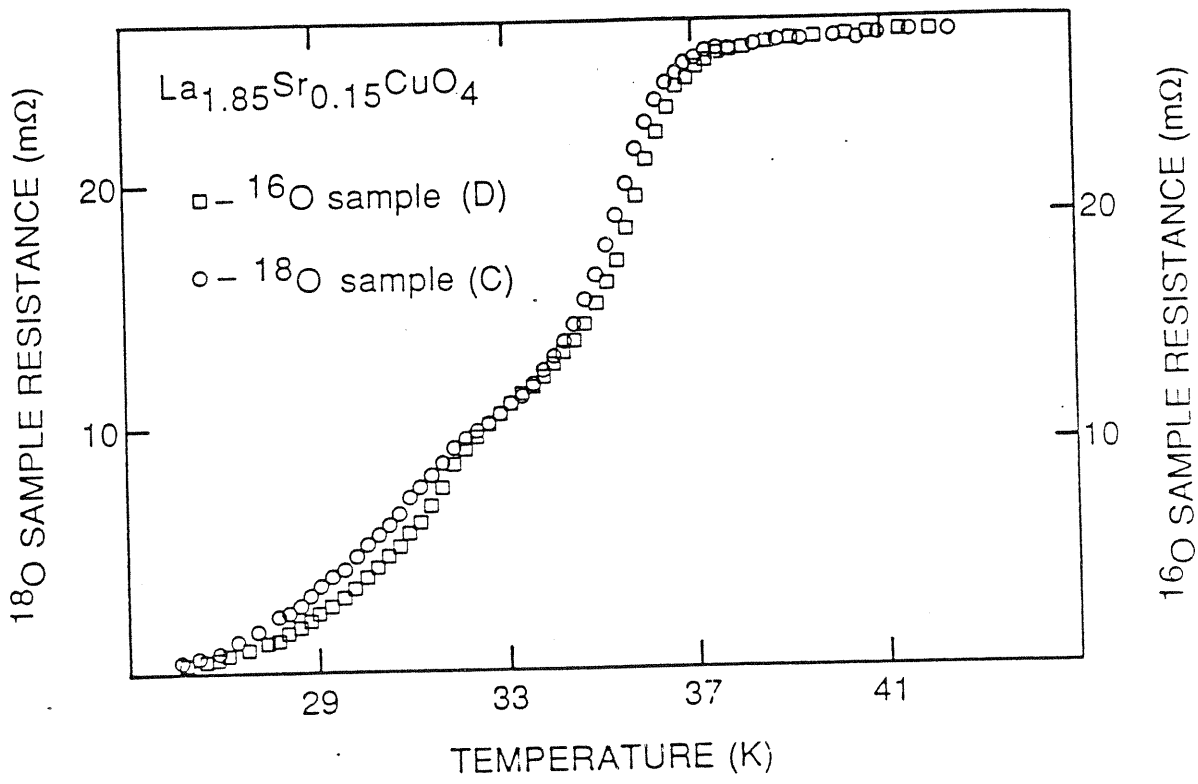

Fig. 3. Resistance vs. temperature for $La_{1.85}Sr_{0.15}CuO_4$ samples "C" and "D". (Measurement by S. Hoen and M.F. Crommie).

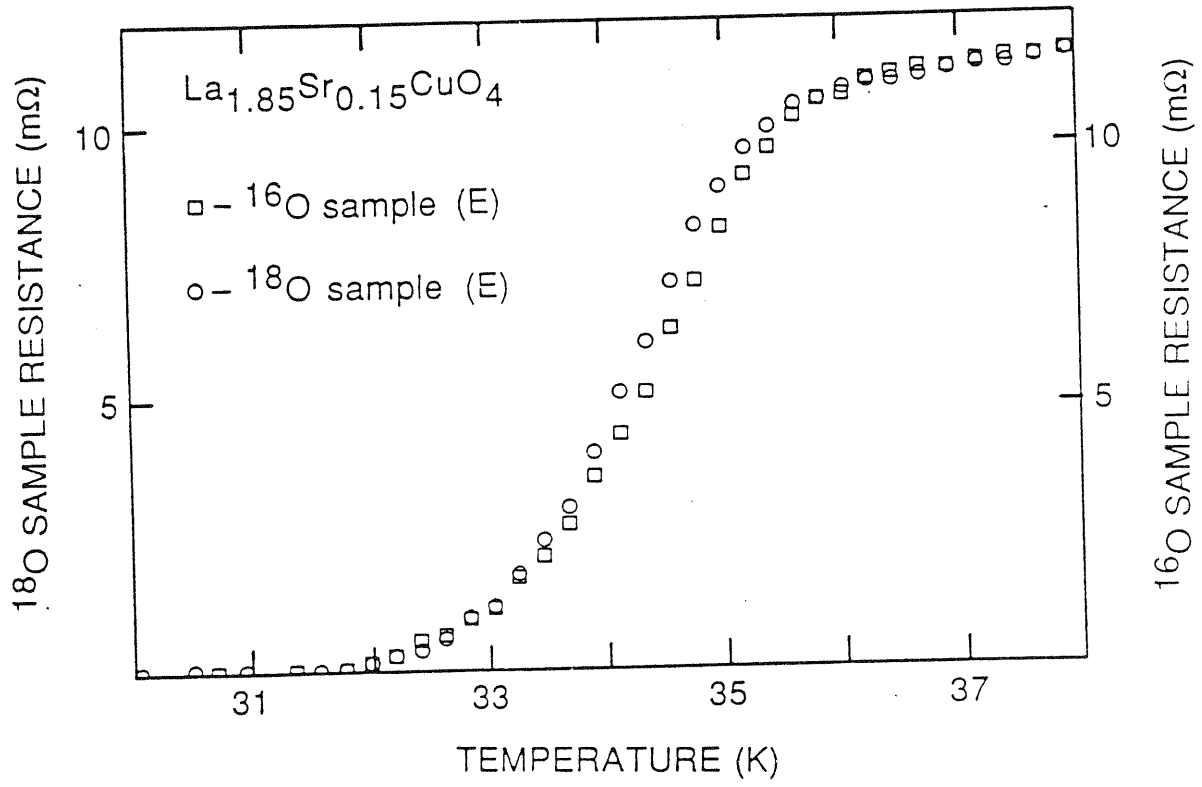

Fig. 4. Resistance vs. temperature for $La_{1.85}Sr_{0.15}CuO_4$ samples "E". (Measurement by S. Hoen and M.F. Crommie).

12 hours, the isotopic ratio in the sample reaches equilibrium with the isotopic ratio in the surrounding atmosphere. The highest isotopic enrichments we achieved were around 90%, due to the presence of the additional ^{16}O in the sample.

The unit cell of $YBa_2Cu_3O_7$ has four inequivalent oxygen sites[16-18]. The site that forms the linear Cu-O chains along the b axis contains one out of the seven oxygen atoms in the unit cell. The oxygen atoms at this site are easily removed at high temperatures[19-21], allowing for easy isotope substitution of the site. Each of the other three oxygen sites contain two of the seven oxygen atoms in the unit cell; if one of these sites was inaccessible to high-temperature oxygen diffusion, then the maximum isotope substitution for the sample would be only 71%. Our ability to achieve isotope substitutions of 90% shows that all of the oxygen sites are accessible in this way.

$YBa_2Cu_3O_7$ samples were prepared by a solid state reaction of Y_2O_3, $BaCO_3$ and CuO. The materials were dissolved in nitric acid, evaporated to dryness, and decomposed on a platinum sheet at 800 C. The powder was then reground, pressed into a pellet, sintered in an ^{16}O atmosphere at 950 C and cooled slowly in flowing oxygen. Powder x-ray diffraction showed that the sample consisted of a single phase, and resistance measurements showed a sharp transition to the superconducting state at T_c=90 K. Oxygen isotope exchanges were performed as described above, using two chips broken from the same parent sample, with a heat cycle of 12 hours at 950 C followed by a slow cool to 200 C over 6 hours. TPD measurements showed an ^{18}O enrichment of 90% in the ^{18}O sample.

Figure 5 shows resistance measurements for both samples. To within our experimental uncertainty of 0.3 K, the midpoint of the transition is at 90.0 K for both samples. A similar result is found for the magnetic susceptibility measurements (Fig. 6), giving an isotope shift of α=0.0±0.027. We are currently performing a series of isotope exchanges and re-exchanges, and have found[43] a small isotope shift with a

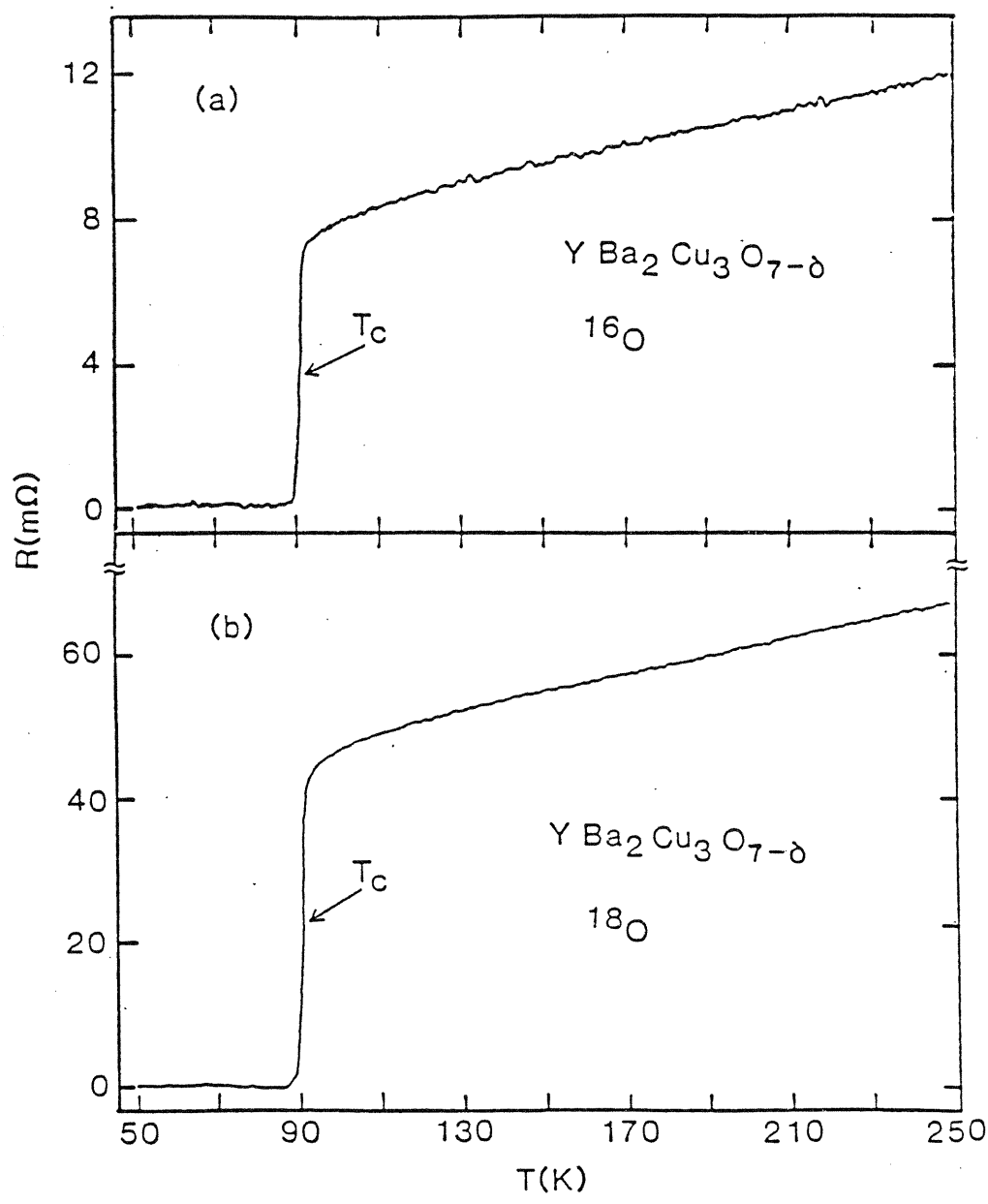

Fig. 5. (a) Resistance vs. temperature for $YBa_2Cu_3O_7$ with ^{16}O. (b) Same as (a) but for 90% ^{18}O enrichment. (Measurement by M.F Crommie).

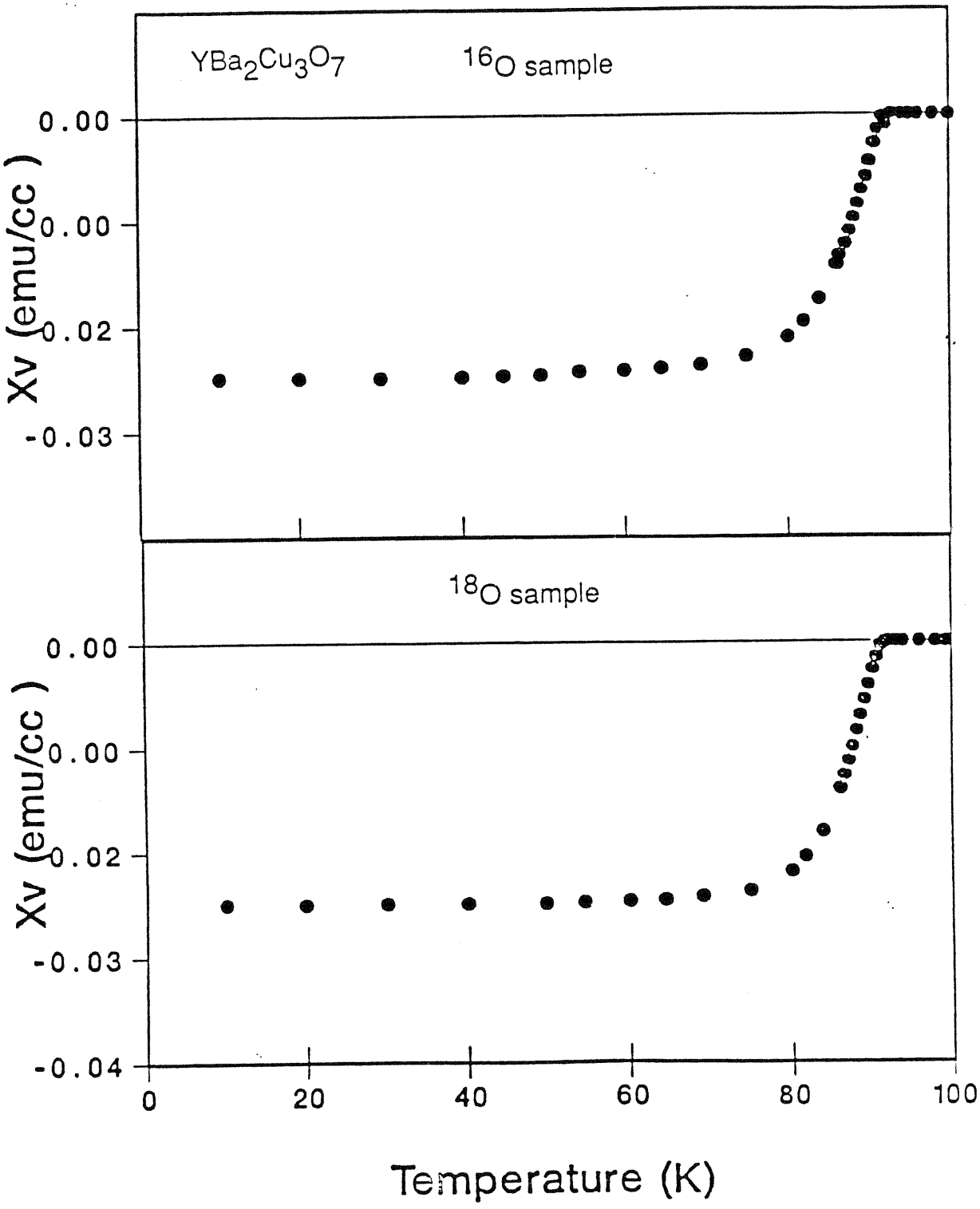

Fig. 6. Magnetic Susceptibility χ vs. T for a $YBa_2Cu_3O_7$ sample with ^{16}O and for a $YBa_2Cu_3O_7$ sample with 90% ^{18}O enrichment. (Measurement by H.-C. zur Loye).

preliminary result of $\alpha=0.02\pm0.006$

The absence of a significant isotope effect for oxygen in $YBa_2Cu_3O_7$ does not rule out the possibility that superconductivity may be related to phonon modes other than those due to the oxygen atoms. Substitutions of other rare-earth elements with significant mass differences on the Y site do not show a consistent dependence of T_c on the rare-earth mass[22,23]; this leaves the Ba and Cu atoms as possible contributors to phonon superconductivity.

We prepared samples of $YBa_2Cu_3O_7$ from starting materials of Y_2O_3, $BaCO_3$ and CuO. CuO with 99.6% ^{65}Cu enrichment and CuO with 99.7% ^{63}Cu enrichment were used to prepare two pairs of samples. One pair of samples was prepared from 78.8% ^{135}Ba enriched $BaCO_3$ and from 99.7% ^{138}Ba enriched $BaCO_3$.

We have observed that minor differences in preparation conditions can shift T_c by several degrees. In order to eliminate these differences, the samples used in this study were prepared simultaneously in pairs under identical conditions for each pair. Fine powders of the starting materials were thoroughly mixed and reacted at 850 C for several hours under flowing oxygen. The reacted powder was then dissolved in HNO_3, evaporated to dryness, and decomposed at 500 C. The resulting compounds were reground and heated at temperatures of up to 850 C under flowing oxygen, with several intermediate cooling and regrinding steps. The final powders were pressed into pellets and heated at 950 C in oxygen for 12 h, followed by slow cooling to room temperature. Test samples prepared in this manner had T_c's of approximately 90 K with full resistive transition widths of less than 2 K. Different samples produced side by side in the heating and cooling steps had T_c's differing by no more than approximately 0.2 K. T_c's were determined by standard four-probe resistivity measurements using silver-paint contacts.

Figure 7 shows sample resistance as a function of temperature for one of the sample pairs prepared with different copper isotopes. The ^{63}Cu sample has a midpoint

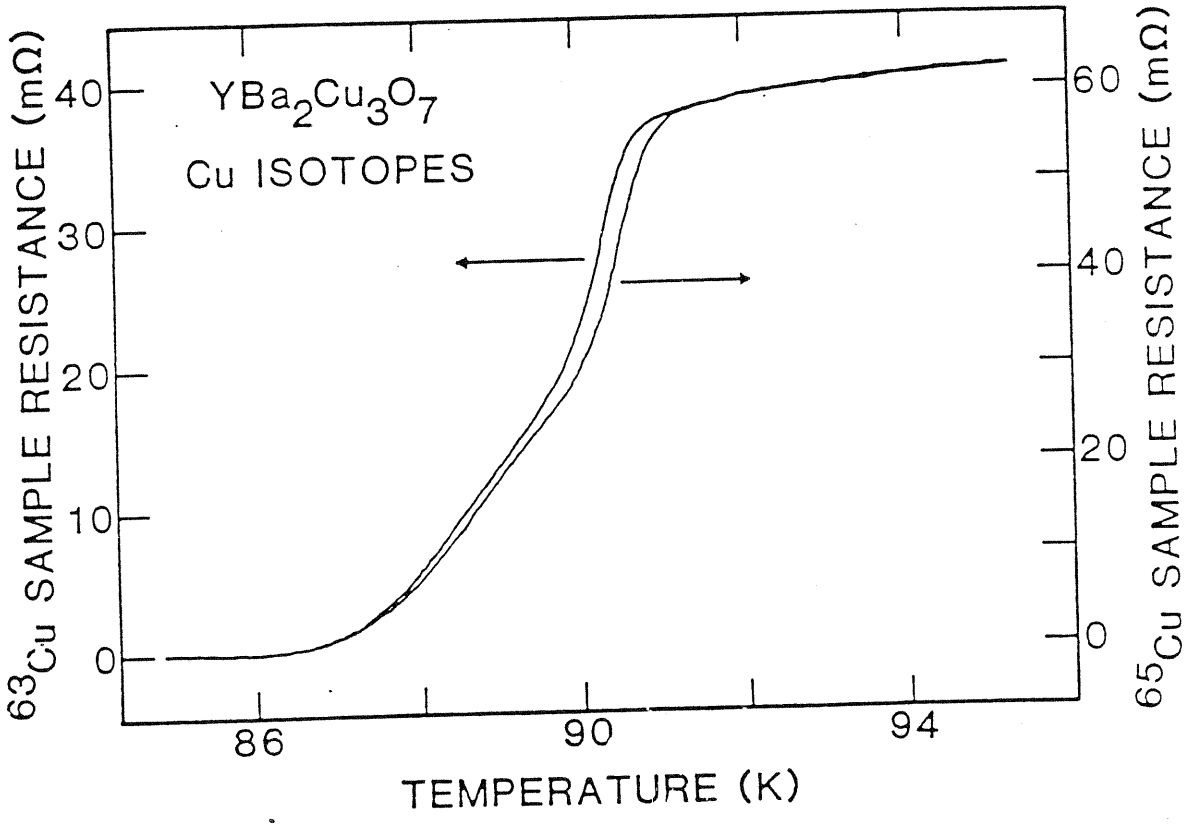

Fig. 7. R vs. T for $YBa_2Cu_3O_7$ prepared with ^{63}Cu and ^{65}Cu. To within experimental error, no isotope effect is observed.

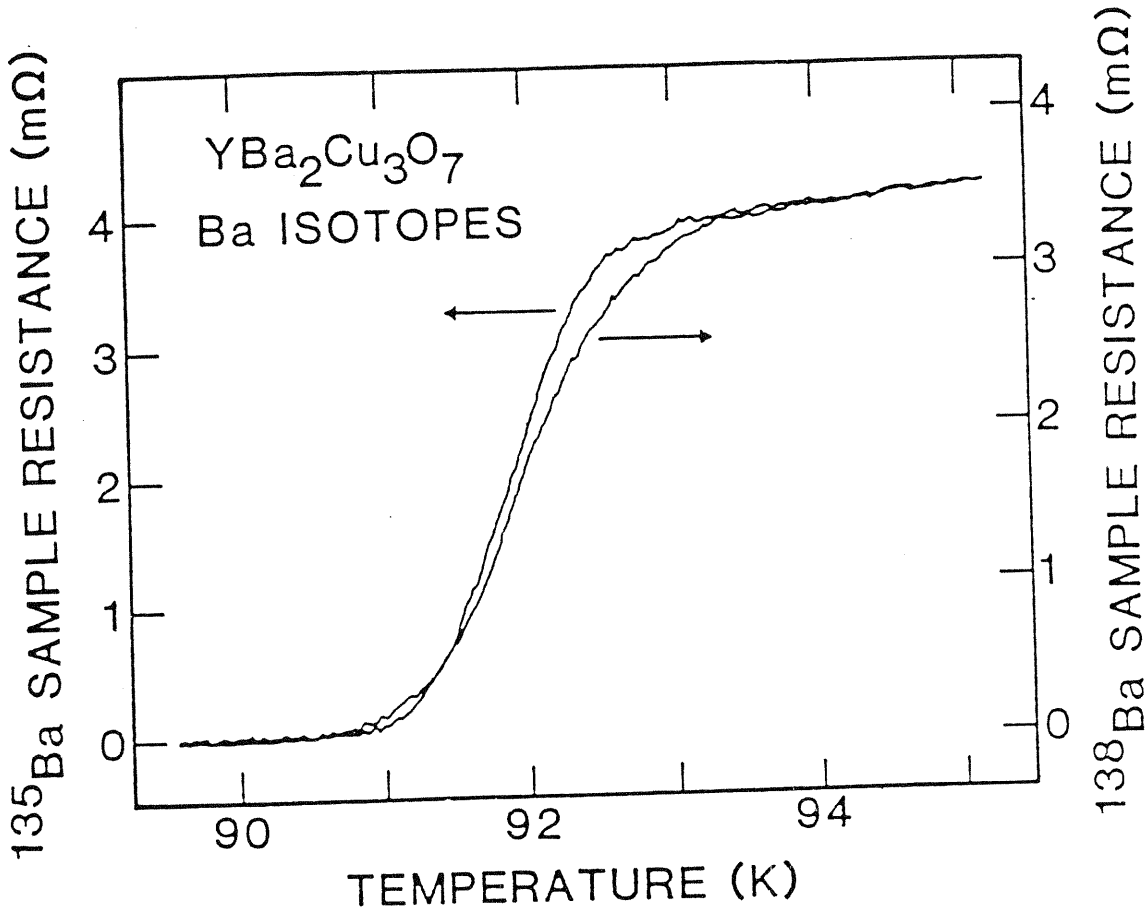

Fig. 8. R vs. T for $YBa_2Cu_3O_7$ prepared with ^{135}Ba and ^{138}Ba. To within experimental error, no isotope effect is observed.

transition temperature T_c=89.70 K, while the ^{65}Cu sample has T_c=89.90 K. This shift of 0.2 K is also found for the onset T_c's. The second pair of copper isotope samples had a similarly small shift, but of opposite sign.

Figure 8 shows resistance data for samples prepared from the two different Ba isotopes. The midpoint transition temperatures are 91.85 K for the ^{135}Ba sample and 91.95 K for the ^{138}Ba sample, a shift of 0.1 K. Note that the T_c's in figure 5 are approximately 2 K higher than the T_c's in figure 4; this difference is due to the slightly different annealing conditions for the two sets of samples. ^{135}Ba and ^{138}Ba isotope samples prepared using exactly the same conditions as were used for the Cu samples of Fig. 4 were found to have T_c's near 90.0 K, again with no significant shift between the Ba samples.

For α=0.5, T_c is expected to shift by 1.0 K for the Ba substitutions and 1.4 K for the Cu substitutions. We find no isotope shift for either Ba or Cu to within our experimental error of 0.2 K, giving limits of $\alpha_{Cu}=0\pm0.07$ and $\alpha_{Ba}=0\pm0.11$. Together with the oxygen isotope and rare-earth substitutions, this work shows that there are no large isotope shifts for any of the phonon modes in $YBa_2Cu_3O_7$.

Section 3. Other Experimental Work

Batlogg et al.[8] substituted ^{18}O isotopes in $YBa_2Cu_3O_7$ and in $EuBa_2Cu_3O_7$ by heating samples to 550 C in vacuum, thus removing approximately 10% of the oxygen, an heating again in an $^{18}O_2$ atmosphere. After 3 cycles, 74%±7% of the ^{16}O had been substituted with ^{18}O, as determined by Rutherford backscattering spectroscopy. They observed resistive shifts of 0.3K to 0.4K in T_c, but observed no shifts in the magnetization data and therefore set a limit on the isotope shift of $\alpha=0\pm.02$. A Raman line at 500 cm^{-1} that was assigned[12] to the O(1) site (the site that bridges the inequivalent Cu atoms) showed isotope shifts of about 4%, demonstrating that at least some of the phonon modes were isotope shifted.

Batlogg et al.[9] also substituted oxygen isotopes in $La_{1.85}Sr_{0.15}CuO_4$ by heating samples in $^{16}O_2$ or $^{18}O_2$ atmospheres at temperatures of up to 700 C for several weeks. Rutherford backscattering spectroscopy was used to determine the ^{18}O isotope enrichments, which were found to be 52%±5% and 73%±5% in two different samples. A Raman line at 428 cm^{-1}, which was assigned to the out-of-plane oxygen atoms, was shifted by 3.4% for the 52% ^{18}O sample and by 4.2% for the 73% ^{18}O sample, in agreement with calculated shifts that assumed no site-selective exchange for the two inequivalent O sites in the material. Magnetization measurements showed T_c shifts of 0.39±.03 K for the 53% ^{18}O sample and 0.46±.04 K for the 73% ^{18}O sample, resulting in a calculated α of 0.16±.02 for each of the samples. Batlogg et al.[9] also extended the work of Weber[42] in $La_{1.85}Sr_{0.15}CuO_4$ to show that for a T_c of 36 K due to an electron-phonon interaction, the α values should be 0.03 for the out-of-plane O site and 0.275 for the in-plane site, resulting in a net α of 0.305 for oxygen. They suggested that the discrepancy between the theoretical and experimental values of α could be due to anharmonic effects or to additional unconventional coupling mechanisms, and concluded that phonons play an important role in the superconductivity of $La_{1.85}Sr_{0.15}CuO_4$.

Leary et al.[10] reported a finite oxygen isotope shift in $YBa_2Cu_3O_7$. Using the gas exchange technique described previously in this chapter, they obtained ^{18}O enrichments of 73% to 90% (determined by TPD), and claimed shifts in T_c of 0.3K to 0.5K from magnetization data. The shifts in T_c were reversed in one sample and partially reversed in a second sample by re-substituting ^{16}O for the ^{18}O. The same group later reported[11] ^{18}O isotope shifts of 0.5K to 0.6K in $BaPb_{0.75}Bi_{0.25}O_3$ (T_c=11.0K, 60% ^{18}O enrichment, α=0.64 to 0.78), 1.3K to 1.6K in $La_{1.85}Ca_{0.15}CuO_4$ (T_c=20.6K, 75% ^{18}O enrichment, α=0.73 to 0.90), 0.5K to 1.0K in $La_{1.85}Sr_{0.15}CuO_4$ (T_c=37.0K, 75% ^{18}O enrichment, α=0.15 to 0.31) and 0.5K to 0.9K in $YBa_2Cu_3O_7$ (T_c=91.1K, 67% ^{18}O enrichment, α=0.07 to 0.12). α

values greater than 0.5 are inexplicable within conventional BCS theory; no mechanisms have been proposed to explain the above data in $BaPb_{0.75}Bi_{0.25}O_3$ and $La_{1.85}Ca_{0.15}CuO_4$. A recent experiment by Batlogg et al.[8] found a much smaller value of α=0.22±0.03 for oxygen isotopes in $Ba(Pb,Bi)O_3$.

A careful study of the isotope shift in $YBa_2Cu_3O_7$ has been reported by Morris et al[13], using magnetization measurements of gas phase isotope exchanged samples. Two samples from the same $YBa_2Cu_3O_7$ pellet were prepared with identical high-temperature annealing treatments in either $^{16}O_2$ or 92% enriched $^{18}O_2$ atmospheres. After measuring T_c's, the isotope species of the two samples were reversed with another annealing treatment and the T_c's were measured again. The temperature calibration of the SHE model VTS-805 SQUID magnetometer that was used for the study was found to drift by up to 0.3 K, and magnetic field values of only 10 Oe were found to substantially increase the measured widths of the T_c's. These problems were minimized by using field values of 3 Oe and by repeating T_c measurements, alternating ^{16}O and ^{18}O samples, to determine the drift rate of the temperature calibration. With ^{18}O isotope enrichments of approximately 88% in the ^{18}O samples (estimated from sample weight changes), the value of α was determined to be 0.019±.005. The error value was estimated from variations in ΔT_c at different points in the susceptibility vs. temperature curves and from variations between the two annealing runs.

Lopdrup et al.[40] have also performed gas phase oxygen isotope exchange studies. Samples containing up to 95% ^{18}O enrichment (determined from TPD measurements) were initially reported[40] to have T_c's as much as 1 K lower than the corresponding ^{16}O samples, but subsequent work[41] has found shifts in T_c of only about 0.2 K, again giving α=0.02. One sample prepared with 98% enriched $^{18}O_2$ gas was found to have 97% ^{18}O enrichment[41].

Ott et al.[14] prepared isotope enriched $YBa_2Cu_3O_7$ samples by dissolving Y, Cu

and $BaC^{16}O$ in ^{18}O and ^{17}O enriched HNO_3, and preparing final superconducting samples in independent batches. The resistive midpoint transition temperatures were 93 K for the ^{16}O samples, 77 K for samples with 39% ^{17}O and 35% ^{18}O, and 59 K for samples with 95% ^{18}O. The sample quality decreased dramatically with decreasing T_c's, with magnetic susceptibility measurements showing transition widths of 40 K or more for the lower T_c's. A brief heat treatment in ^{16}O increased T_c from 59 to 77 K for an ^{18}O sample and from 77 to 90 K for an ^{17}O sample. Subsequent work[39] has shown that the copper content in the superconducting grains of the $YBa_2Cu_xO_7$ samples varies depending on the isotopic enrichment of the HNO_3 used in the preparation process: x=3.0 for ^{16}O, but is approximately 2.9 and 2.8 respectively for the ^{17}O and ^{18}O samples. The excess copper is apparently in the form of unreacted CuO at the grain boundaries. This work shows that the sample quality can apparently depend on the isotopes used in this particular preparation route, but it does <u>not</u> demonstrate a direct isotope shift. Isotope enriched samples prepared by burning Y, Ba and Cu metals in isotope-enriched O_2 gases with subsequent mixing and annealing of the oxides result in samples with T_c's that vary by less than 1K between ^{16}O and ^{18}O samples[39], in agreement with the gas phase isotope exchange experiments.

Section 4. Discussion

Barbee and Cohen[6,7,24] attempted to fit the measured isotope shifts and transition temperatures in $YBa_2Cu_3O_7$ and in $La_{1.85}Sr_{0.15}CuO_4$ within the two-square-well model, but found unphysical values for λ and μ^*. They therefore performed an extensive series of calculations using the Eliashberg equations and a variety of electron-phonon interaction spectra $\alpha^2F(\omega)$ which included realistic phonon spectra derived from neutron and Raman scattering as well as an Einstein and a "square-well" spectrum (here $\alpha^2(\omega)$ represents the electron-phonon matrix element, not the isotope exponent). They found that when the entire $\alpha^2F(\omega)$ spectrum

was shifted, calculated values of the isotope shift were independent of the shape of $\alpha^2F(\omega)$ at small values of μ^*, and were only weakly dependent at very large values (>0.2) of μ^*. Since the oxide superconductors contain several different atomic species, and isotope substitution of one species affects only part of the phonon spectra, they shifted various portions of the spectrum and found that the calculated isotope shifts were reduced, particularly for large values of μ^*, and that the high-frequency modes gave larger isotope shifts than did the low-frequency modes. They found that values of α(oxygen)=0.14 and T_c=37 K in $La_{1.85}Sr_{0.15}CuO_4$ could be explained within their model, but only by using values of λ and μ^* larger than originally estimated by Weber[42]. They were unable to obtain reasonable values of λ and μ^* in $YBa_2Cu_3O_7$, even for α(oxygen) as large as 0.05, and concluded that the model could not account for experimental measurements in this compound.

The existence of Cu-O planes and chains suggests that a reduced dimensionality of the Fermi surface may play a role in the superconducting mechanism. Several recent papers have considered the effects of reduced dimensionality on the isotope effect. Labbe and Bok[25] have studied a model in which the Fermi surface is pinned at a van Hove singularity in one or two dimensions. In two dimensions, the electron density of states diverges logarithmically at a van Hove singularity. If the Fermi surface is pinned at the singularity, then the transition temperature should go as

$$K_B T_C = 1.13 D \exp(-1/\lambda^{\frac{1}{2}}) \quad ; \quad \lambda = \frac{4\pi^2 D}{v} + \log^2\left[\frac{h\omega_D}{2\pi D}\right] - 1.22 \qquad (3\text{-}2)$$

where D is the width of the singularity and v is the electron-electron coupling constant. This theory predicts that variations in the Debye frequency caused by isotope substitutions should affect the transition temperature:

$$\frac{\delta T_C}{T_C} = \frac{1}{3}\frac{\delta \omega_D}{\omega_D} \qquad (3\text{-}3)$$

in agreement with Raman measurements of oxygen isotope substitutions in

$La_{1.85}Sr_{0.15}CuO_4$[9], which contains Cu-O planes that are presumably responsible for superconductivity. In one dimension, the electron density of states diverges at a van Hove singularity; the theory predicts that there is no isotope shift in the transition temperature when the Fermi surface is pinned at the singularity. If the Cu-O chains in $YBa_2Cu_3O_7$ are responsible for superconductivity at 90 K, this theory may explain the much smaller isotope shifts seen in this compound. One criticism of the theory is that only the first-order Feynman diagrams are used to calculate the electron-phonon interaction; this is a good approximation in three dimensions, as the higher-order diagrams are negligible, but in one or two dimensions the higher-order diagrams do not fall off as rapidly, giving important corrections to the above calculations.

Mattis and Mattis[26] proposed a two dimensional electronic structure with a bond asymmetry term that introduces a gap in the oxygen band, giving logarithmic singularities at the band edges that enhance T_c when the Fermi surface is pinned at a singularity. Their theory is independent of the electron-electron attraction mechanism, but they perform a model calculation with Cu vibrations providing the phonons for electron-electron attraction and find a Cu isotope shift of $\alpha=0.13$ for a T_c of 100 K. This shift is significantly larger than the experimental result $\alpha<0.07$[6], but they caution that the value for α is strongly dependent on other parameters in the model.

Okabe et al.[27] have suggested that T_c may be enhanced by a Charge-Density-Wave (CDW) mechanism. They propose that an intrinsic superconducting mechanism present in Cu-O planes in compounds like $La_{1.85}Sr_{0.15}CuO_4$ produces T_c's of roughly 40 K, and show that the formation of a CDW in Cu-O chains adjacent to the Cu-O planes enhances the electron density of states at the Fermi surface in the planes, thus enhancing T_c, and suppressing the isotope effect. Thus the presence of Cu-O chains in $YBa_2Cu_3O_7$ could explain both the higher T_c and the smaller isotope effect as compared to $La_{1.85}Sr_{0.15}CuO_4$. Experimental

support for the theory comes from the discovery of one-dimensional diffuse scattering in convergent-beam electron diffraction measurements in $YBa_2Cu_3O_7$[28], indicating that CDW fluctuations may be present. However, the recent discovery of superconductivity near 120K in the Bi-Sr-Ca-Cu-O system[29,30], which apparently contains Cu-O planes but not chains[31], shows that high-T_c superconductivity is not dependent on the chains.

Phillips[32] has given a qualitative argument that shows how the structural chemistry of oxygen vacancies could reduce the isotope effect from the value seen in $La_{1.85}Sr_{0.15}CuO_4$ to the much smaller value found in $YBa_2Cu_3O_7$. He assumes that superconductivity is due to the conventional electron-phonon mechanism, but that the number and positions of the oxygen vacancies adjust to maximize T_c in the presence of parameter changes in quantities such as pressure or isotope species. The Cu-O superconductors contain mixed copper valences, Cu^{2+} and Cu^{3+}; assuming that the Cu^{2+} is the energetically favorable valence, the system can minimize the number of Cu^{3+} vacancies by creating oxygen vacancies. The removal of each O^{2-} ion will leave 2 electrons behind, lowering 2 Cu ions from a 3+ to a 2+ valence state, and increase the density of states at the Fermi level, thus raising T_c. $YBa_2Cu_3O_7$ has roughly 20% formal O vacancies (the ideal structure is $YBa_2Cu_3O_9$) while $La_{1.85}Sr_{0.15}CuO_4$ has essentially no O vacancies; $YBa_2Cu_3O_7$ is therefore more able to maximize T_c by creating or displacing O vacancies. This could explain why T_c is much less sensitive to pressure or isotope substitutions in $YBa_2Cu_3O_7$ than in $La_{1.85}Sr_{0.15}CuO_4$. Since T_c in $La_{2-x}Sr_xCuO_4$ can be varied with strontium doping, an interesting experiment would be to compare the isotope shift with the pressure dependence of T_c as a function of strontium concentration in this compound.

The change of the electron-electron attraction caused by changes in phonon frequencies from isotope substitutions is only one of the mechanisms that gives an isotope shift in T_c. A recent paper by Fisher et al.[33] examines the effects of isotope

substitutions on lattice constants and hopping parameters, which can produce indirect isotope shifts in T_c. The change in the zero point atomic vibrational modes with isotope substitutions will change the lattice constants, producing in effect pressure changes on the lattice. Since T_c is much more sensitive to pressure in $La_{1.85}Sr_{0.15}CuO_4$ than in $YBa_2Cu_3O_7$ ($\partial T_c/\partial P \approx 1$ K/kbar in $La_{1.85}Ba_{0.15}CuO_4$[34], which is isoelectronic to $La_{1.85}Sr_{0.15}CuO_4$, and $\partial T_c/\partial P = 0.07$ K/kbar in $YBa_2Cu_3O_7$[35]), this effect should give a much larger isotope shift in $La_{1.85}Sr_{0.15}CuO_4$ than in $YBa_2Cu_3O_7$, as is experimentally observed. One would naively expect the lattice constant to decrease as ^{18}O is exchanged for ^{16}O, increasing T_c, but it is possible for the crystal anisotropy to give the correct shift if the contraction occurs along an axis that shows a negative pressure dependence of T_c. In any case, it should be possible to directly measure the change in lattice constant using X-ray diffraction; a relative change of order 10^{-3} would account for the oxygen isotope effect in $La_{1.85}Sr_{0.15}CuO_4$.

Fisher et al.[33] also consider the isotope shifts in T_c caused by changes in the Cu-O hopping parameters due to changes in the bond stretching and bending modes. For the bond stretching modes, assuming isotropic elastic constants, tetragonal crystal structure and a Cu-O interaction that goes as e^{-kr} with bond separation r, they find

$$\Delta T_c = \frac{-3}{8}\frac{B}{T_c}\frac{\partial \ln T_c}{\partial P}\frac{h}{2\pi m \omega_0 a_0}\frac{\Delta m}{m} \qquad (3\text{-}4)$$

where B is the bulk modulus, ω_0 the bond vibration frequency, a_0 the lattice constant and m the isotope mass. This gives a shift of roughly -0.2 K for the substitution of ^{18}O for ^{16}O in $La_{1.85}Sr_{0.15}CuO_4$, which compares to the experimental value of -0.6 K; the shift is expected to be much smaller in $YBa_2Cu_3O_7$ because of the reduced sensitivity of T_c to pressure in this compound. The calculation of the effect of the changes in the bond bending modes is more difficult, but they expect the shift to be similar or greater in magnitude than that found for the stretching modes, with the opposite sign. They warn that the readiness with which these compounds undergo a

tetragonal-orthorhomic phase transition could significantly enhance the zero point motion effects; it would be interesting to analyze the Debye-Waller factors for the oxygen atoms, and perhaps even to look for a dependence of the structural phase transition on isotope species. One final possibility is that superconductivity in these compounds might be based on one of the Hubbard models, which depend on the hopping parameters; they do not however expect an isotope shift from this mechanism unless the large $\partial T_c/\partial P$ is due to an instability caused by the proximity of the tetragonal-orthorhombic phase transition. Again, this is appealing because the structural phase transition is much closer to T_c in $La_{1.85}Sr_{0.15}CuO_4$ than in $YBa_2Cu_3O_7$, thus perhaps causing a smaller isotope shift in the latter compound.

The possibility of anharmonic atomic potentials is considered by Zacher[36], who argues that the structural positions of the Cu sites may give strongly non-harmonic behavior. The usual BCS calculations are based on the harmonic approximation, so he suggests that the breakdown of this approximation could give unusual results for isotope substitutions.

A combined phonon-exciton mechanism has been proposed by Marsiglio et al.[37] for the $La_{1.85}Sr_{0.15}CuO_4$ system. They propose a frequency spectrum which consists of a phonon spectrum with an additional delta function at 500 meV representing an exciton or other electronic excitation. They use the Eliashberg equations, ignoring the corrections expected from higher-order Fermi diagrams and the energy dependence of the self-energy that should become important at the high- energy peak. They vary the relative weights of the phonon and exciton mechanisms and calculate the values of various superconducting properties, such as the gap, the specific heat anomaly, and the isotope α factor, in four different regimes ranging from pure exciton to pure phonon coupling. The model shows α increasing from 0 to 0.5 as the coupling goes from pure exciton to pure phonon coupling; unfortunately, the ranges found for the other parameters are generally small compared to the experimental variation for the same

quantities, so a careful comparison between theory and experiment is not possible at this point.

Finally, Cohen et al.[38] have fit T_c's and α's in $YBa_2Cu_3O_7$ and $La_{1.85}Sr_{0.15}CuO_4$ using a three-square-well model that includes coulomb and phonon interactions along with an unspecified higher-energy interaction. They have predicted an isotope shift of α=0.26-0.30 for the 13 K superconducting Ba-Pb-Bi-O system, and negative isotope shifts for systems with T_c's above about 125 K.

Section 5. Conclusion

Oxygen isotope substitutions in $YBa_2Cu_3O_7$ have demonstrated a very small isotope effect; Cu and Ba isotope substitutions and rare earth substitutions have not shown isotope shifts for any of the other phonon modes. Oxygen isotope shifts in $La_{1.85}Sr_{0.15}CuO_4$ have also shown a small isotope effect. The measured shifts in $YBa_2Cu_3O_7$ are too small to be explained within conventional BCS theory, and the shift in $La_{1.85}Sr_{0.15}CuO_4$ can be explained only with strongly constrained values of λ and μ^*. Other theoretical explanations of the observed isotope effects have been proposed based on low dimensional effects, anharmonic properties or non-phonon pairing mechanisms, but none of these theories has yet demonstrated a clear experimental superiority.

CHAPTER 3 REFERENCES

1. E. Maxwell, Phys. Rev. 78, 477 (1950); C.A. Reynolds, B. Serin, W.H. Wright and L.B. Nesbitt, Phys. Rev. 78, 487 (1950).

2. J. Bardeen, L.N. Cooper and J.R. Schrieffer, Phys. Rev. 106, 162 (1957), and 108, 1175 (1957).

3. R. Meservey and B.B. Schwartz, in "Superconductivity", ed. R.D. Parks (Marcel Dekker, New York 1969).

4. J.C. Swihart, Phys. Rev. 116, 45 (1959); IBM J. Res. Develop. 6, 14 (1962).

5. L.C. Bourne, M.F. Crommie, A. Zettl, Hans-Conrad zur Loye, S.W. Keller, K.L. Leary, Angelica M. Stacy, K.J. Chang, Marvin L. Cohen and Donald E. Morris, Phys. Rev. Lett. 58, 2337 (1987); Phys. Rev. Lett. 60, 753 (1988).

6. L.C. Bourne, A. Zettl, T.W. Barbee III and Marvin L. Cohen, Phys. Rev. B 36, 3990 (1987).

7. Tanya A. Faltens, William K. Ham, Steven W. Keller, Kevin J. Leary, James N. Michaels, Angelica M. Stacy, Hans-Conrad zur Loye, Donald E. Morris, T.W. Barbee III, L.C. Bourne, Marvin L. Cohen, S. Hoen and A. Zettl, Phys. Rev. Lett. 59, 915 (1987).

8. B. Batlogg, R.J. Cava, A. Jayaraman, R.B. van Dover, G.A. Kourouklis, S. Sunshine, D.W. Murphy, L.W. Rupp, H.S. Chen, A. White, K.T. Short, A.M. Mujsce and E.A. Rietman, Phys. Rev. Lett. 58, 2333 (1987); Phys. Rev. Lett. 60, 754 (1988).

9. B. Batlogg, G. Kourouklis, W. Weber, R.J. Cava, A. Jayaraman, A.E. White, K.T. Short, L.W. Rupp and E.A. Rietman, Phys. Rev. Lett. 59, 912 (1987).

10. Kevin J. Leary, Hans-Conrad zur Loye, Steven W. Keller, Tanya A. Faltens, William K. Ham, James N. Michaels and Angelica M. Stacy, Phys. Rev. Lett. 59, 1236 (1987).

11. Hans-Conrad zur Loye, Kevin J. Leary, Steven W. Keller, William K. Ham, Tanya A. Faltens, James N. Michaels and Angelica M. Stacy, Science 238, 1558 (1987).

12. G.A. Kourouklis, A. Jayaraman, B. Batlogg, R.J. Cava, M. Stavola, D.M. Krol, E.A. Rietman and L.F. Schneemeyer, Phys. Rev. B 36, 8320 (1987).

13. Donald E. Morris, Randy M. Kuroda, Andrea G. Markelz, Janice H. Nickel and John Y.T. Wei, to be published in Phys. Rev. B.

14. K.C. Ott, J.L. Smith, J.O. Willis, R.M. Aikin, E. Garcia, M. Goldblatt, W.B. Hutchinson, G.H. Kwei, C.B. Pierce, J.F. Smith, J.D. Thompson and T.E. Walker, preprint.

15. Donald E. Morris, U.M. Sheven, L.C. Bourne, Marvin L. Cohen, M.F. Crommie and A. Zettl, in "Proceedings of Symposium S of the 1987 Spring Meeting of the Materials Research Society", Anaheim, California, 21-25 April 1987, eds. D.U. Gubser and M. Schluter (Materials Research Society, Pittsburgh, PA, 1987), Vol. EA-11.

16. T. Siegrist, S. Sunshine, D.W. Murphy, R.J. Cava and S.M. Zahurak, Phys. Rev. B 35, 7137 (1987).

17. P.M. Grant, R.B. Beyers, E.M. Engler, G. Lim, S.S.P. Parkin, M.L. Ramirez, V.Y. Lee, A. Nazzal, J.E. Vazquez and R.J. Savoy, Phys. Rev. B 35, 7242 (1987).

18. Y. LePage, W.R. McKinnon, J.M. Tarascon, L.H. Greene, G.W. Hull and D.M. Huang, Phys. Rev. B 35, 7245 (1987).

19. A. Santoro, S. Miraglia, F. Beech, S.A. Sunshine, D.W. Murphy, L.F. Schneemeyer and J.V. Waszcak, Mater. Res. Bull. 22, 1007 (1987).

20. R. Beyers, G. Lim, E.M. Engler, R.J. Savoy, T.M. Shaw, T.R. Dinger, W.J. Gallagher and R.L. Sandstrom, Appl. Phys. Lett. 50, 1918 (1987).

21. F. Beech, S. Miraglia, A. Santoro and R.S. Roth, Phys. Rev. B 35, 8778 (1987).

22. D.W. Murphy, S. Sunshine, R.B. van Dover, R.J. Cava, B. Batlogg, S.M. Zahurak and L.F. Schneemeyer, Phys. Rev. Lett. 58, 1888 (1987).

23. P.H. Hor, R.L. Meng, Y.Q. Wang, L. Gao, Z.J. Huang, J. Bechtold, K. Forster and C.W. Chu, Phys. Rev. Lett. 58, 1891 (1987).

24. T.W. Barbee III, Marvin L. Cohen, L.C. Bourne and A. Zettl, preprint.

25. J. Labbe and J. Bok, Europhys. Lett. 3, 1225 (1987); J. Labbe and J. Friedel, J. Phys. (Paris), 27, 303 (1966).

26. D.C. Mattis and M.P. Mattis, Phys. Rev. Lett. 59, 2780 (1987).

27. Y. Okabe, Y. Suzumura, T. Sasaki and H. Katayama-Yoshida, Solid State Commun. 64, 483 (1987).

28. M. Tanaka, M. Terauchi, K. Tsuda and A. Ono, preprint.

29. H. Maeda, Y. Tanaka, M. Fukutomi and T. Asano, preprint.

30. C.W. Chu, J. Bechtold, L. Gao, P.H. Hor, Z.J. Huang, R.L. Meng, Y.Y. Sun, Y.Q. Wang and Y.Y. Xue, Phys. Rev. Lett. 60, 941 (1988).

31. M.A. Subramanian, C.C. Torardi, J.C. Calabrese, J. Gopalakrishnan, K.J. Morrissey, T.R. Askew, R.B. Flippen, U. Chowdhry and A.W. Sleight, Science 239, 1015 (1988).

32. J.C. Phillips, Phys. Rev. B36, 861 (1987).

33. D.S. Fisher, A.J. Millis, B. Shraiman and R.N. Bhatt, preprint.

34. C.W. Chu, P.H. Hor, R.L. Meng, L. Gao, Z.J. Huang and Y.Q. Wang, Phys. Rev. Lett. 58, 405 (1987).

35. J.E. Schirber, D.S. Ginley, E.L. Venturini and B. Morosin, Phys. Rev. B 35, 8709 (1987).

36. R.A. Zacher, Phys. Rev. B 36, 7115 (1987).

37. F. Marsiglio, R. Akis and J.P. Carbotte, Solid State Commun. 64, 905 (1987).

38. R.W. Cohen, M.H. Cohen and M.L. Cohen, preprint.

39. K.C. Ott, private communication.

40. E. Lopdrup, M. Crawford, W.E. Farneth, R.K. Bordia, E.M. McCarron and S.J. Poon, Bull. Am. Phys. Soc. 33 No. 3, 558 (1988).

41. E. Lopdrup, private communication.

42. W. Weber, Phys. Rev. Lett. 58, 1371 (1987).

43. S. Hoen, L.C. Bourne, M.F. Crommie, W.M. Creager and A. Zettl, unpublished.

APPENDIX

THE VIBRATING REED TECHNIQUE

Our elasticity measurements were performed with an adaptation of the vibrating reed technique, first used by Barmatz et al.[1] and modified by Tiedje et al.[2,3] and Lacoe[4]. The technique is generally used to obtain information about the Young's modulus and the internal friction of a material by forcing a sample of the material to vibrate at a resonant frequency. The absolute accuracy of the technique is limited to only a few percent, but we have beer able to measure relative changes in the Young's modulus (as a function of temperature or other parameters) as small as one part in 10^5. We have used these measurements to study collective electron phenomena that influence the mechanical properties of the crystal lattice. This section explains the behavior of a "vibrating reed" and describes in detail our experimental setup.

The vibrational properties of objects with varying geometries have been studied extensively[5]. The resonant frequencies ω_n of the bending modes of a relatively long, thin sample are given by

$$\omega_n = \left(\frac{YI}{\rho A}\right)^{\frac{1}{2}} \left(\frac{M_n}{L}\right)^2 \qquad (A\text{-}1)$$

where Y is the Young's modulus along the long axis of the sample, ρ the sample density, L the sample length, A the cross-sectional area, and I the area moment of inertia of A about a line perpendicular to both the long axis of the sample and to the direction of vibrational displacement. The m_n are the solutions of a transcendental equation that is dependent on the boundary conditions of the sample (e.g., both ends fixed, one end free, etc.). It is difficult to obtain an absolute value of Y, because of sample inhomogeneities and imprecision in sample dimensions and boundary conditions, but it is important to note that Y is generally proportional to the square of the resonant frequency.

The derivation of equation (A-1) neglects the shear modulus and the effects of finite sample thickness. The first-order correction to (A-1) is

$$Y = Y_0 + K\left(\frac{t}{L}\right)^2 M_n \frac{Y_0}{G} \qquad (A\text{-}2)$$

where Y_0 is calculated from (A-1), $K \equiv 1$, G is the shear modulus, and t is the sample thickness in the direction of the vibrational displacement.

In some cases the sample is too short and thick to produce a resonance with an amplitude large enough for detection or with a frequency in the desired range. However, it is almost always possible to produce a mechanical resonance by clamping the sample at one end and placing an inertial mass on the free end. In most cases our inertial mass was a roughly spherical blob of silver paint built up by successive applications of paint. For a point mass M much larger than the sample mass, located a distance L from the clamped end of the sample, the Young's modulus is given to first order by the expression

$$Y = \frac{4L^3M}{t^3s}\omega_r^2 \qquad (A\text{-}3)$$

where s is the sample width, and ω_r is the resonant frequency.

The Q-value of a resonance is defined as

$$Q = \frac{\omega_r}{\Delta\omega} \qquad (A\text{-}4)$$

where $\Delta\omega$ is the frequency shift between the half-amplitude values of the resonance. The most convenient way to continuously measure changes in Q is to measure the resonant amplitude A, where

$$Q = \frac{Q_0}{A_0}A \qquad (A\text{-}5)$$

and Q_0 and A_0 are the initial values of Q and A. The internal friction δ is defined to be the reciprocal of Q. Friction from imperfectly rigid clamps (usually silver paint) and residual gas pressure in the sample chamber will add to the internal friction of the

sample, so we report only net changes in δ.

A simple schematic of our technique is shown in Figure 1. Flexural vibrations in the KHz range are induced in the sample by capacitively coupling the sample to a drive electrode. The electrode is dc biased to increase the driving force and to ensure that the frequency of the driving force is equal to the frequency of the drive oscillator (the frequency of the driving force is twice the frequency of the drive oscillator when the electrode is unbiased and the sample is referenced to a floating ground.). The sample is connected to an rf oscillator, and a pickup electrode placed near the sample detects the carrier rf signal, which is amplitude modulated by the mechanical motion of the sample. The carrier signal is typically 200-700 MHZ, and is tuned to provide impedance matching between the pickup electrode and the detection circuitry, thereby maximizing the signal strength.

The signal from the pickup electrode is amplified by a broad-band rf amplifier (Avantek GPM 1052) and demodulated by a diode detector (HP 11096B), then detected with a lock-in amplifier that is referenced to the drive signal. One of the sample resonances is selected and the system is then placed in a phase-lock-loop configuration that continuously monitors the resonance frequency and amplitude.

A driven simple harmonic oscillator with friction has a frequency-dependent phase shift ϕ between drive and response of[6]

$$\phi(\omega) = -\mathrm{Tan}^{-1} Q\left(\frac{\omega}{\omega_r} - \frac{\omega_r}{\omega}\right) \qquad (A\text{-}6)$$

The rapid change of the phase at the resonance peak provides the error signal that controls the phase-lock-loop. The phase of the lock-in amplifier is adjusted so that the quadrature output has odd parity as a function of frequency about the resonance peak. The frequency of the drive oscillator is then controlled by the quadrature signal, forcing the system to stay tuned to the resonant frequency of the sample. In this configuration the in-phase output of the lock-in amplifier is proportional to the

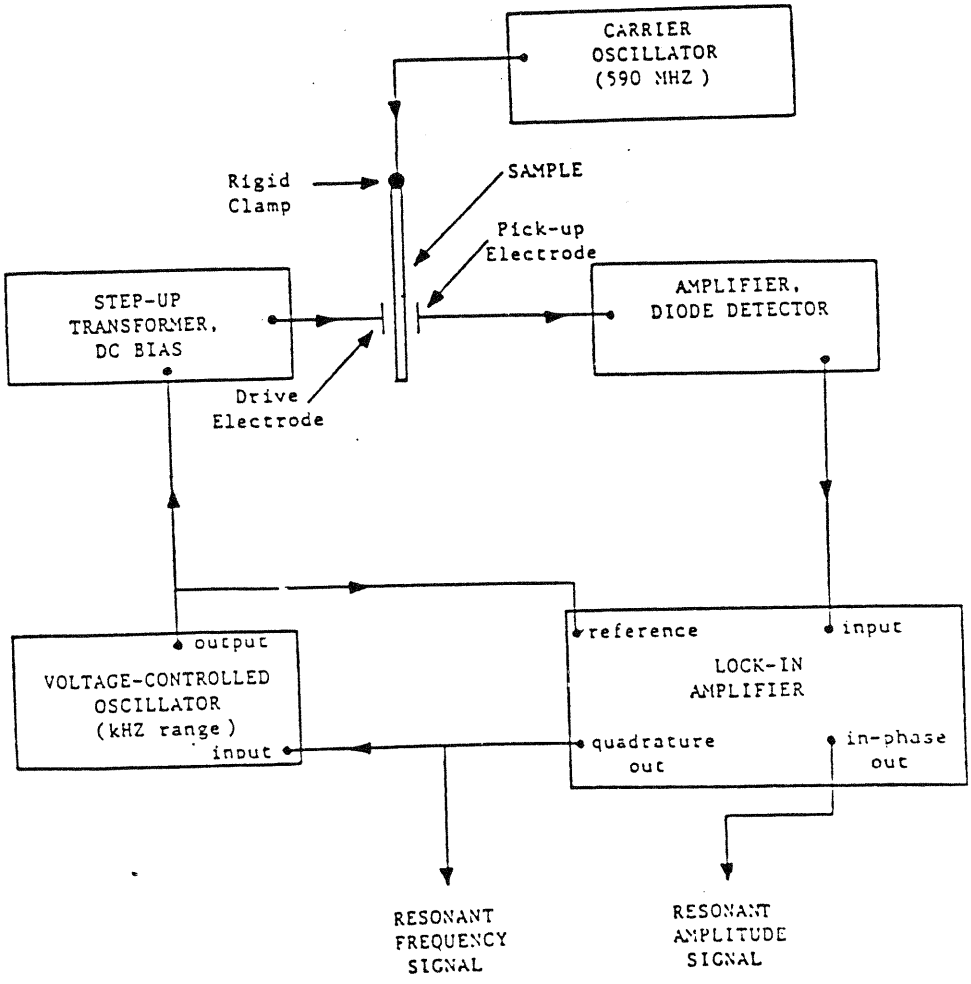

Figure 1. A schematic diagram of the apparatus used in the vibrating reed experiment, shown in a phase-locked-loop configuration.

vibrational amplitude of the sample, and the quadrature signal is proportional to the frequency shift of the resonance. These signals can be recorded and signal-averaged to improve the signal-to-noise ratio.

Several probes were constructed for the vibrating reed experiment. A detailed drawing of the sample chamber of one of the probes is shown in Figure 2. The body of the probe is a circular block of copper with a tapered edge that provides a vacuum seal. Three stainless steel microwave coaxial cables are soldered into the sample chamber, providing electrical connections for the drive and pickup electrodes and the carrier signal. In this drawing, the sample is mounted directly on the center wire of the center coaxial cable. The sample is usually mounted with silver paint (Dupont conductor composition 4929), which fixes the end of the sample and provides an electrical contact between the sample and the coaxial cable. To eliminate any thermal gradients between the sample and the surrounding chamber, a small copper cylinder is placed about the coaxial center wire near the sample. There is a narrow gap between the wire and the copper cylinder that is filled with a thermally conducting epoxy (Stycast 2850 ft black), and the cylinder itself is attached to the sample chamber with Stycast. A stainless steel tube (not shown) is also connected to the sample chamber, providing a vacuum port and access line for electrical wires running into the sample chamber. Temperature sensors consist of a calibrated diode (IN4447) and a carbon-glass resistor (Lakeshore CGR-1-1000) for use in magnetic fields. The sample chamber is placed in a cryogenic environment, and the temperature is controlled with a manganin heater wire that is attached with Stycast to the cover of the sample chamber.

The positions of the drive and pickup electrodes are controlled by two short pieces of coaxial cable held by set screws. The drive electrode is positioned roughly 0.25 mm from the sample. The resonances of the sample are identified by applying a large ac signal (100 volts or more, with up to 600 volts dc bias) to the drive electrode and observing the sample with a microscope while the drive frequency is varied.

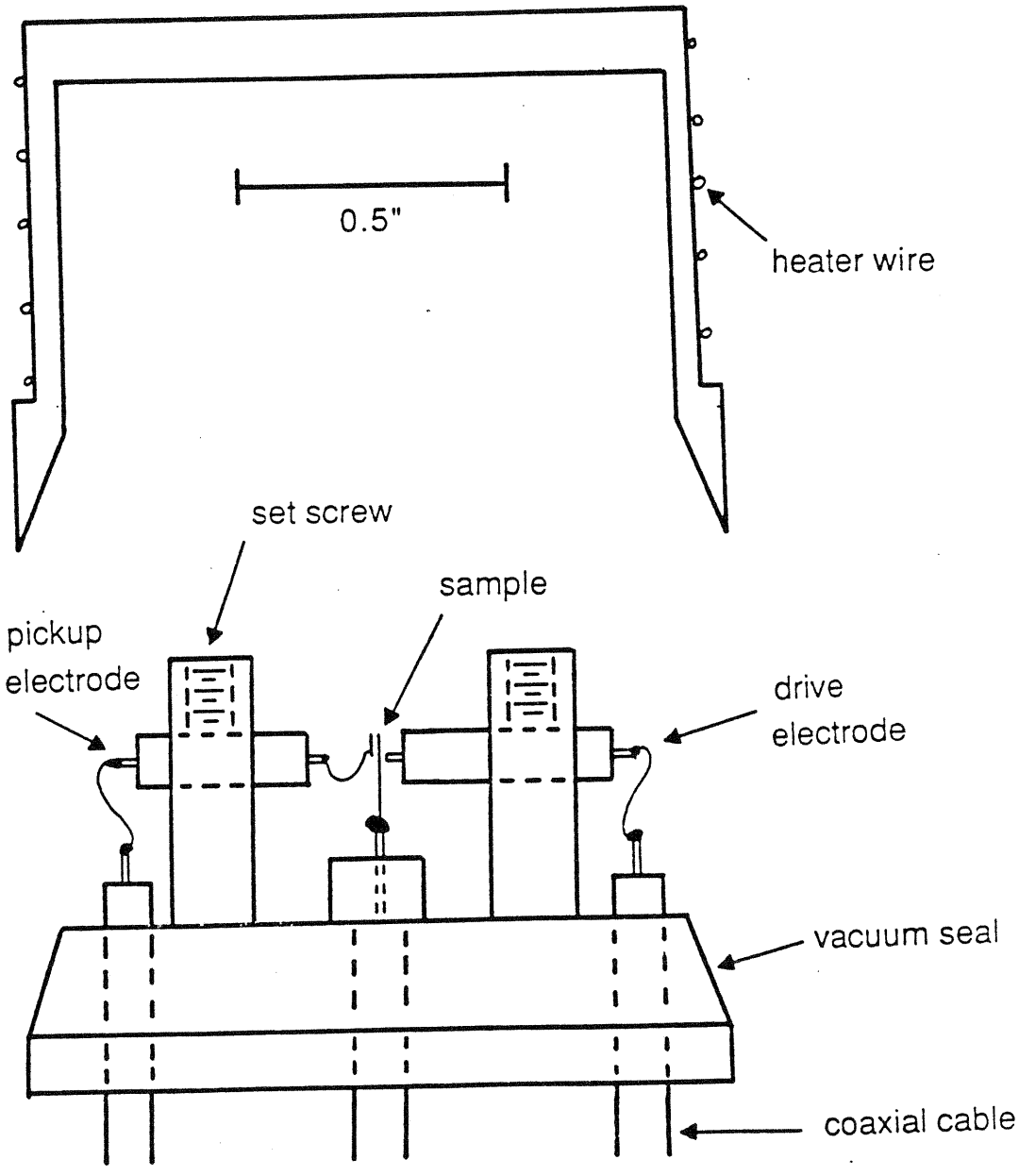

Figure 2. A side view of the sample chamber.

Resonances typically range from a few hundred hertz to a few tens of kilohertz. The resonances below a kilohertz are not usuaily chosen for study because they tend to be noisy due to interference from outside vibrations. When the experiment is running, the amplitude of the sample vibration is kept as small as possible to avoid nonlinear effects. A typical drive signal is 20 volts ac with a 10 volt dc bias. The onset of nonlinearity can be determined by increasing the drive voltage or dc bias until the resonant frequency begins to decrease.

Once a resonance is selected for study, the pickup electrode is placed near the sample. A small pad formed of silver paint is attached by a conducting wire to the moveable coax; this pad is positioned so that it is orthogonal to the vibration of the sample, with a gap of about 0.1 mm. The strength of the detected signal increases dramatically as the gap becomes very small, but allowance must be made for thermal contraction during the course of the experiment.

Electrical currents can be passed through the sample by mounting it in a clamped-clamped configuration that allows the sample to vibrate like a bowstring. One end of the sample is firmly clamped, and a relatively large blob of silver paint is placed on the other end, with a fine gold wire attached to the paint blob at right angles to the sample. The paint blob acts as an inertial clamp, but keeps the sample free of strain induced by thermal contraction. An inductor is placed between the sample and ground to ensure that there is no drop in the rf carrier signal across the sample; changes in sample resistance might otherwise cause spurious changes in the amplitude of the signal that is detected at the pickup electrode.

APPENDIX REFERENCES

1. M. Barmatz, H.J. Leamy and H.S. Chen, Rev. Sci. Instrum. 42, 885 (1971).

2. J.T. Tiedje, Ph.D. thesis, Univ. of British Columbia (1977).

3. J.T. Tiedje, R.R. Haering and W.N. Hardy, J. Acoust. Soc. Am. 65, 1171 (1979).

4. R.C. Lacoe, Ph.D. thesis, Univ. of California, Los Angeles (1983).

5. See, for example, P. Morse, "Vibration and Sound". 2nd ed., McGraw-Hill, New York (1948).

6. J.R. Barker, "Mechanical and Electrical Vibrations". Wiley, New York (1964).